Analysis of variations in characteristics of sand waves observed in the Dutch coastal zone: a field and model study

M.Sc dissertation thesis

Author: Jerker Menninga

Utrecht University, 2012

Supervisors

Prof. Dr. H.E. de Swart (UU)
Dr. T.A.G.P. van Dijk (Deltares)
Ir. B.W. Borsje (Deltares)
Prof. Dr. W.P.M. de Ruijter (UU)

Abstract

Sandy sea beds of coastal regions, like the shallow Dutch part of the North sea, are often characterised by distinct rhythmic morphological features, such as sand waves. Sand waves are often located in intensely used regions of critical depth, thus their dynamics may endanger human activities, such as shipping and offshore engineering. Parameters controlling sand wave dynamics, like growth and migration are often investigated by means of (non-)linear stability models. These studies however, are only able to investigate the behaviour of small scale bed perturbations. This study aims to identify the finite sand wave characteristics in the Dutch coastal zone and to relate these to local environmental conditions. Therefore, an empirical analysis is used to identify the sand wave characteristics, observed in the approach routes of the Dutch harbours of Rotterdam and IJmuiden, situated in the North sea, and to find empirical relations to environmental parameters. In addition, these parameters are tested with a numerical shallow water model (Delft3D), with which a realistic, finite sand wave field can be simulated. First of all, it was found that the Rotterdam sand waves are about 250 m long and about 3.5 m high. The IJmuiden sand waves are 400 m long and 2.5 m high. Furthermore, clear differences in migration rates are found between the sand wave crests and troughs for IJmuiden (~2.5 m/year and ~0 m/year, respectively), while the sand wave crests and troughs migrate with about the same rates at Rotterdam (~0.5 m/year). From a principal component regression analysis of field observation of environmental parameters, follows that the strength of the dominant tidal constituent, the relative phase shift between the M2 and M4 tide, the median grain size, the local water depth and the sand wave height are important in explaining the differences in sand wave migration rates. Model results, using a process based numerical model, reveal that sand wave migration behaviour is simulated in good qualitative agreement with the field observations. Moreover, in order to obtain a difference in crest and trough migration, a difference in suspended load and bed load sediment transport over the sand wave is required. Finally, the same qualitative relations between sand wave migration and the relative phase shift between the M2 and M4 tidal constituents, the median grain size and the water depth are obtained with the model as was obtained from the empirical analysis.

Contents

Chapter 1. Introduction

This study will focus on the morphology and evolution of tidal sand waves at the shipping approach routes of the Dutch harbours of Rotterdam and IJmuiden. The aim is to understand sand wave behaviour at both locations and to identify physical processes controlling the sand waves locally. This introduction will first present the most typical bed forms that are identified at the Dutch continental shelf and the dimensions typical for sand waves will be discussed. Furthermore, some of the practical incentives to study these features are presented. After that, a brief history about sand waves observation and model studies is discussed, followed by the most important physical mechanisms responsible for the formation and evolution of sand waves. Finally, the objectives and outline of this thesis are presented.

1.1 General

Sandy bottoms of coastal seas, such as the North Sea, are characterised by distinct rhythmic bed forms. The spatial scale of these bed forms range from several meters close to the shoreline to several kilometers on the continental shelf. Six different types of offshore rhythmic bed patterns are distinguished at the Dutch continental shelf (Dodd et al., 2003; Knaapen et al, 2005) (Table 1.1).

Sand banks are the largest bed type, with wavelength of several kilometers. They are near-static features and are formed due to tidal currents. It was shown by Huthnance (1982) and later by Besio et al. (2006) that on the Northern Hemisphere sand banks are always counter-clockwise rotated with respect to the major axis of the tidal ellipse of the dominant tidal constituent. The spatial scales of shoreface connected ridges are comparable to those of sand banks. However, they are formed in shallower waters and

Bed form	Length [m]	Height [m]	Migration speed [m/year]	Evolution time scale
Ripples	0.1 - 1	0.01 - 0.1	100 - 1000	Hours
Mega ripples	1 - 10	0.1 - 1	100 - 1000	Hours - days
Sand waves	100 - 1000	1 - 5	1 - 10	Decades
Long bed waves	1500	5	Unknown	Centuries
Shoreface connected ridges	5000 - 8000	1 - 5	1 - 10	Centuries
Tidal sand banks	5000 - 10000	1 - 5	-	Centuries

Table 1.1 Overview of bed forms located at the Dutch continental shelf. After Dodd et al. (2003), Knaapen et al. (2005) and Blondeaux et al. (2009).

start at the offshore end of the shoreface. As shown by, e.g., Trowbridge (1995) and Calvete (2001) they turn out to be driven by storm driven currents instead of tidal currents. Their orientation depends on the dominant direction of the storm driven current. The seaward end of the ridge is shifted upstream and makes angles of 20^0 to 35^0 with the shoreline. Furthermore, in contrast to sand banks, shoreface connected ridges are able to migrate. The smallest scale bed forms are ripples and mega ripples. They have lengths ranging between several centimeters to several meters. They are highly mobile and may migrate several meters per day. They are formed by tidal currents, but are also highly affected by (wind)waves and storms (Van Dijk & Kleinhans, 2005; Passchier & Kleinhans, 2005). Whether ripples or mega ripples are able to form is controlled by the bed roughness, which determines the resistance of the bed to the currents (Blondeaux, 1990; Blondeaux & Vittory, 1991).

Sand waves and long bed waves are intermediate bed form types. The latter features are relatively recently been observed by Knaapen et al. (2001) and are only observed in the North Sea at the approach route for the Rotterdam harbour. They mention typical wave lengths of 1500 m. Blondeaux et al. (2009) showed that these features may be rotated clockwise and anticlockwise with respect to the direction of the tidal current. Furthermore, they showed with a model study that long bed waves are formed in the case that tidal currents are relatively weak and elliptical. Sand waves are extensively studied; one of the first observations goes back to the early twentieth century (Van Veen, 1935). In general sand wave lengths may range from 100 m to 1000 m and heights of about 5 m. Sand waves migrate with migration rates up to 10 m/year (Van Dijk & Kleinhans, 2005). Formation is due to tidally driven flows and the orientation of the crests of sand waves is orthogonal to the principal axis of the tidal ellipse of the dominant tidal constituent (Fredsoe & Deigaard, 1992; Hulscher, 1993).

Coastal seas with pronounced sand wave fields are often intensively used for human activity. For instance, the busiest shipping routes in the world are located in the North Sea, with a number of the world's most important harbours situated at its coast. Furthermore, communication cables and pipelines transporting gas or oil are often situated at the bed of coastal seas. Finally, offshore wind farms become gradually more apparent. These activities may be endangered by dynamic bed forms, of which sand waves are clearly the largest. When sand waves become too high, they form a risk for the minimum depth for shipping. Migrating sand waves may result in the buckling or exposure of pipelines or cables and dynamic sand waves may form a risk for the stability of wind farms.

To monitor the sand wave field and to identify potential risks, extensive hydrographic survey programs are developed. The Netherlands Hydrographic Office of the Royal Netherlands Navy (NHLO) is responsible for the surveys of the Dutch continental shelf and the Dutch ministry of infrastructure and the environment (RWS) is responsible for the coastal zone and shipping approach routes of the Rotterdam and IJmuiden harbours. It is expected that understanding sand wave behaviour contributes to cost efficient planning of the survey programs.

1.2 Background

1.2.1 Observations

Sand waves are observed all over the world. For both the Atlantic and the Pacific coast of North America sand waves are studied by various authors (Bokuniewicz et al.,1977; Perillo & Ludwick, 1984; Xu et al., 2008; Sterlini et al., 2009). Also further south, off the coasts of Argentina, sand wave fields are observed (Aliotta & Perillo, 1987). In Asian waters sand waves are observed in the Taiwan streat, (Boggs Jr., 1974), the South China Sea, (Reeder et al., 2011) and in coastal waters of Japan (Ozasa, 1974; Ikehara & Kinoshita, 1994; Knaapen & Hulscher, 2002). Although sand waves are often observed in shallow seas, Xu et al. (2008) and Reeder et al (2011) show that sand waves may also be observed in seas with depths ranging between 100m and 600m.

Van Veen (1935) was one of the first to observe sand waves in the North Sea, which was extended by work of Stride (1970). They both observed symmetric sand waves in the southern part of the Dutch continental shelf, which become increasingly asymmetric northward. These early works only focussed on sand wave observations. McCave (1971) was one of the first who aimed to relate environmental conditions, like tidal current strength or sediment grain size, to the occurrence of sand waves. He showed that the occurrence of sand waves in the North Sea shows strong correlations to the size and direction of the sand transport vectors.
Despite the success of these early works, they were not able to identify the physical mechanism controlling the growth of sand waves.

1.2.2 Modelling

The conditions required for the formation and development of bed forms, such as sand waves, are investigated by use of models. In general two types of models can be considered: i) (non)linear stability models and ii) numerical morphodynamic models.

Stability models are able to determine the fastest growing modes and corresponding direction after a small perturbation of the sea bed. Huthnance (1982) was one of the first to develop a stability model. He simplified the depth-averaged shallow water equations and modelled sediment transport with a power-law sediment transport relation with the assumption of conservation of sediment. This model was later extended by Hulscher et al. (1993). These models were only able to predict the fastest growing modes related to sand banks, since they make use of depth averaged tidal flows. The development of sand waves however strongly depends on the vertical distribution of the tidal currents, which was shown by Hulscher (1996). She extended the previous model in the vertical, resulting in a full 3D solution of the flow. This linear model was able to predict the conditions which allow for the growth of modes corresponding to sand waves. Further improvements of the model concerned the increase in complexity of the viscosity parameter and the tidal flow, which were subsequently performed by Komarova & Hulscher (2000), Gerkema (2000) and Besio et al. (2003). These models only considered static sand waves. Németh et al. (2002) and Besio et al. (2004) were the first to develop models that allowed sand waves to migrate. These models were later extended by Besio et al. (2006). The previous models are all based on linear stability analysis, which investigates the growth rates after different perturbations of the bed. The fastest growing mode is assumed to prevail. As a consequence of linear stability analysis the models are limited to small amplitude sand waves. Nonlinear models for sand waves were developed by Németh et al. (2007), Sterlini et al. (2009) and Blondeaux & Vittori (2011). These models are able to model sand waves until their final amplitude.

The other type of models are numerical morphodynamic models. With these models one is able to incorporate complex physical processes like wind- and wave-driven currents, density gradients, turbulence models and complex initial bed forms. A drawback of these models is the long computation time, which becomes gradually manageable with improvements in computer technology. Therefore, only few studies are known that used these models (Tonnon et al., 2007; Borsje et al., 2011).

1.2.3 Physical processes

The studies in the previous section all have shown that sand waves are formed because of positive feedbacks between tidal currents and a sandy bed. Since a bed is never completely flat, these oscillating currents result in vertical recirculating cells, which transport sediment from the troughs to the crests. This section will describe the physical processes responsible for formation and migration of sand waves.

Sand wave formation - currents

The vertical structure of tidal currents over sand waves can be best understood by considering the qualitative description of headland eddies created by a tidal flow along a coastal promontory by Zimmerman (1981). The same mechanisms creating the headland eddies are responsible for the recirculating currents over sand waves (Figure 1.1). Over the sand wave crest the flow at a fixed level is accelerated, but due to friction the flow speed decreases towards the bed (size and direction of the current are indicated by the solid and dashed arrows). During flood tide (solid arrow), this results in the advection of negative vorticity to the right, while during ebb tide (dashed arrow), positive vorticity is advected to the left. So, the vorticity flux has the same sign during ebb and flood tide. When this is averaged over a tidal cycle, large residual recirculating cells are obtained, rotating in opposite direction.

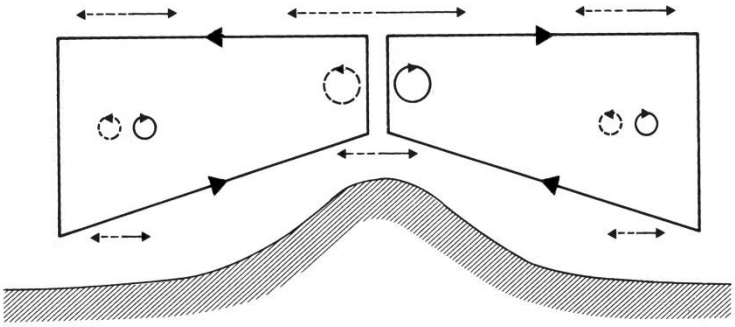

Figure 1.1 Representation of residual circulating currents excited by an oscillating flow over a sand wave. Tidal currents in the flood and ebb direction are represented by the black solid and dashed lines, respectively. The vorticity induced by the shear in the tidal flow is represented by the circles and the large solid cells represents the net residual circulation. (After Zimmerman, 1981)

Sand wave formation – sediment transport

Frictional forces exerted by the bed to the flow, produce shear in the flow. This shear results in a bed shear stress exerted by the fluid on the bed, which is able to transport the sediment. Sediment transport is only possible when the bed shear stress exceeds a certain critical value, which is determined by the sediment grain size and the flow velocity. The bed shear stress depends not only on the vertical velocity gradients, but also on the eddy viscosity, which, generally, is a function of the water depth, flow velocity and the bed roughness. The latter may be considered at two different scales; when the bed roughness is considered on the scale of the individual grains, which holds for sediment transport, the

bed shear stress is denoted with the skin friction; on a larger scale, the flow also experiences the resistance induced by bed forms like (mega)ripples. That latter part of the bed shear stress is denoted by the form drag.

Usually two types of sediment transport are considered; bed load transport and suspended load transport. Bed load transport occurs for coarse sediment and/or small shear stresses. The sediment grains are moved by rolling or saltation. Rolling occurs when stresses are very close to the critical bed shear stress. When the fluid drag is able to lift the grain from the bed, the grain may make a small jump in which the grain moves along a ballistic trajectory. In this case one may speak of saltation of the grain. The maximum height will not be higher than four grain diameters. After the jump the grain collides back to the bed, when it has sufficient inertia it may cause another grain to saltate. Generally, bed load transport occurs only in a thin layer above the bed (Dyer, 1986)).

When sediment grains are small enough and/or shear stresses are large enough, grains may get released from the bed and suspended load transport occurs. Lift forces generated by turbulent eddies have to be large enough to overcome gravitational forces, hence the friction velocity has to be larger than the settling velocity. Grains move almost always higher than two diameters from the bed (Bagnold, 1966; McCave, 1971). Using a numerical morphodynamic model, Borsje et al. (2011) showed that sand waves grow by means of bed load transport, while suspended load transport has a damping effect. Finally, when sand waves grow too high, their slopes may get too steep for grains to be transported uphill and, consequently, sediments will be transported downhill more easily because of gravitational effects. In modelling sand waves this processes is covered by the slope effect. So the slope effect will also suppress sand wave growth (Borsje et al., 2011).

Sand wave formation – currents and sediment transport

Figure 1.2 presents a schematisation of recirculation cells over a sinusoidal sand wave field. Thus, when the currents are strong enough, the grains may be eroded and transported by means of the bed shear stress. Now, considering Figure 1.2, a net sediment transport is induced the by recirculating currents, transporting sediment from the troughs to the crests. When the recirculating currents are strong enough they may be able to move sediment grains from the bed.

Considering the above, Van Santen et al. (2011), aimed to explain the distribution of wavelengths of sand waves observed on the Dutch continental shelf of the North Sea, with the most important measurable physical parameters, being the maximum strength of the dominant tidal constituent, ellipticity of the dominant tidal constituent, median grain

size of the sediment distribution and local water depth. From their observations they did not found strong correlations. However using these parameters in an extended version of the model of Besio et al. (2004), they showed that sand wave modes could develop for reasonable distributions of the chosen parameters. Note however that the bed resistance parameter turned out to be an important tuning tool in most of the linear stability models, which was also observed in other studies (e.g. Gerkema, 2000; Besio et al., 2004).

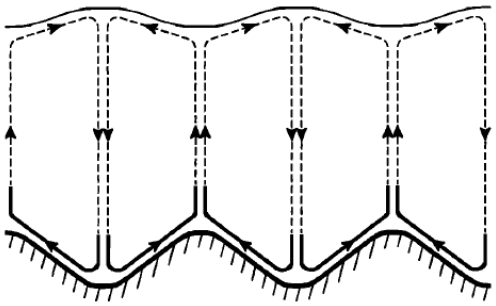

Figure 1.2 Sketch of recirculating currents over a sinusoidal bed (After Hulscher, 1996).

Sand wave migration

So far only sand wave formation is considered. Various emperical studies, however, showed that sand waves are able to migrate horizontally (Ludwick, 1972; Aliotta & Perillo, 1987; Besio, 2004; Barnard et al., 2006; Buijsman & Ridderinkhof, 2008a; Van Dijk et al., 2011). Although these studies were able to quantify migration rates, they were not able to correlate migration rates to environmental conditions. Németh et al. (2002) and Besio et al. (2004) developed a linear stability model with which they investigated the dependence of sand wave migration to asymmetries in the tidal flow. Considering Figure 1.2, where the recirculation cells and bottom profile showing a clear rhythmic pattern, a disruption of the tidal flow will result in an asymmetry between the recirculation cells and the bottom profile. They both found that the residual background flow, induced by e.g. wind or density gradients, is responsible for a disruption of the tidal flow, which resulted in sand wave migration in the direction of the residual current. From field observations however, Besio et al. (2004) also found that sand waves are able to migrate in the opposite direction of the residual background current. In an attempt to explain this, they incorporated the first higher harmonic of the semi-diurnal lunar tide, the M4 constituent, in their model. This showed that upstream migration is possible for an appropriate phase shift between the M2 and M4 tidal constituents. Hence, the asymmetries in the flow are not only imposed by the background residual current, but

also by higher order tidal constituents. In addition, Németh et al. (2002) showed that incorporating tidal asymmetries did not affect the sand wave length.

Besides the asymmetries in the oscillating flow, it is also expected that the height of the sand waves affects migration rates. Knaapen (2005) showed that the migration rates decrease for increasing sand wave heights. This might be counter intuitive, since higher sand waves will be more affected by the flow conditions. However, Schielen et al. (1993) showed that oscillating bed forms might be considered as a group of waves, travelling with a group velocity. Furthermore they showed that the phase velocity of the individual bed forms is lower than the group velocity, resulting in anormal dispersive waves. A general property of these types of waves is that the waves will move slower for increasing amplitudes.

Finally, using a numerical morphologic model, Tonnon et al. (2007) showed that surface waves generated by wind or swell may influence the migration and morphology of sand waves. When the local water depth is sufficiently shallow and when the surfaces waves are sufficiently active, the orbital motion of fluid particles in the water column, induced by the surface waves, will stir up sediments at the bed. Sediment will be transported as both bed load and in suspended load. Furthermore, Van Dijk & Kleinhans (2005) showed that it is expected that wave action is sufficient to stir up sediments at the bed for a considerable number of events per year for the IJmuiden area.

Sand waves and dredging

In shallow coastal seas it can be necessary to dredge sand wave fields in order to maintain a minimum navigation depth. This procedure is expensive, so understanding the regeneration mechanism of sand waves is essential in order to reduce costs. Katoh et al. (1998) and Knaapen & Hulscher (2002) conducted a study on the effects of dredging on sand wave development in the Bisanseto Sea, Japan. Both studies showed that sand waves regenerated in about 10 years. Furthermore, Katoh et al. (1998) argued that the regeneration process increased for increasing sediment inflow.

1.3 Specific aims

1.3.1 Objectives

As mentioned earlier in this chapter the general aim of this study is to understand natural sand wave behaviour in the shipping approach routes of the Dutch harbours of Rotterdam and IJmuiden and to identify physical processes controlling the sand waves locally. Furthermore, at the locations which are influenced by dredging activity, the effects of dredging on sand wave behaviour will be investigated. In order to do so the following specific objectives are formulated;

Objective 1:
A detailed analysis of overall sand wave characteristics in the Rotterdam and IJmuiden regions is conducted, as well as spatial variations and trends in these characteristics. From literature (e.g. Knaapen, 2005 or Dorst, 2009) it is expected that Rotterdam sand waves are shorter and higher than the IJmuiden sand waves. Furthermore, it is expected that the IJmuiden sand waves are more mobile.

Objective 2:
In order to identify the physical processes controlling the sand waves within the study areas, and hence to identify differences between the sites, variation in environmental parameters will be correlated to the sand wave length and sand wave migration. The selection of the environmental parameters that will be tested is based on the discussion presented in section 1.2.3 of this chapter. Therefore, sand wave length will be related to tidal current information of the dominant tidal constituent, median grain size and the local water depth. Since it is argued that sand wave migration rate may depend on several more parameters, the tidal current information of the M4 tidal constituent, the background residual current, the effects of surface waves and the sand wave height will be considered as well.

Objective 3:
Since the study areas are located in shallow coastal seas, it is expected that dredging is required to maintain nautical depth. At the locations where dredging takes place, the effects of dredging on sand wave behaviour will be investigated. Form Katoh et al. (1998) and Knaapen & Hulscher (2002) it is expected that sand waves will be regenerated in ten years. It will first be investigated if the data provides information about the natural bathymetry before dredging, after that dredging events are identified and, if possible, the regeneration characteristics will be quantified

Objective 4:
The ability of a process-based numerical model to simulate the observed sand wave fields is investigated. Such a model is used, instead of the more classical stability models, since one will be able to simulate complex physical processes better. It is expected that the simulated sand wave characteristics will be in good agreement with field observations. In addition, the controlling physical processes obtained from *objective 2*, will be compared with this model.

Objective 5:
When the model is able to simulate realistic natural sand wave behaviour, it will be tested whether the model is able to regenerate sand waves after dredged. After that, the regeneration rates obtained from the model will be compared to the results obtained from *objective 3*.

1.3.2 Outline

The five objectives are covered in two distinct parts. The first three objectives will be covered in part one (chapters 2 to 6), which will concern a detailed analysis of bathymetric data of the two research areas. First, in chapter 2 an overview of the available data and the specific location of the study areas will be presented. Chapter 3 then, will present the methods to quantify spatial sand wave characteristics, which will concern an analysis method developed by Van Dijk et al. (2008) and successfully applied by Van Dijk et al. (2011) and Van Santen et al. (2011). From these spatial sand wave characteristics, a method will be developed in order to quantify the sand wave mobility, which will also be covered in chapter 3. Finally, chapter 3 will present the methods to obtain the selected environmental parameters and the methods to correlate the spatial distribution of these parameters to the spatial distribution of sand wave length and migration rates. The results of these analyses will be presented in chapter 4, followed by a discussion (chapter 5) and a conclusion (chapter 6) on the data analysis part.

Part two will concern the modelling analysis, in which objectives four and five will be covered by use of the morphodynamic numerical model Delft3D. With this model, sand waves were first studied by Tonnon et al. (2007) and later by Borsje et al. (2011). This study will use the basic settings of the latter version, since it provides realistic simulations of natural sand waves, while Tonnon et al. (2007) study only one artificial sand wave. First, in chapter 7, the model setup and performed experiments will be presented, followed by the results in chapter 8. Chapter 9 discusses the interpretation of the model, which will be followed by the conclusion of the model analysis in chapter 10. Finally, a synthesis on the combined results of the empirical and the model study will be presented in chapter 11.

Part I

Data Analysis

Chapter 2. Available data

2.1 Bathymetric data

Bathymetric data is delivered by RWS. In general the point data was obtained using the Multi Beam Echo Sounding (MBES) method for all surveys, although some older sets were obtained with Single Beam Echo Sounding (SBES). The data was collected by sailing parallel to the tidal current, crossing marine bed forms normally. The MBES data were corrected for depth variations by tides and ship movement. This is not necessary for SBES data, because the beam width is sufficient to compensate for ship movement. The echo sounding data was converted to bathymetric data and delivered as *x, y, z,* t_{start}*,* t_{end} files, where *z* denotes the water depth at location *x,y* and t_{start}*,* t_{end} represent the surveys start and end date, respectively. The survey time depends on the location of a specific site and range from one day to a couple of months.

The resolution of the data sets strongly depends on the used echo sounding method. The MBES data are area covering and have a resolution increasing from about 6 m^2 per data point before the year 2000 to 2 m^2 per data point after 2000. The resolution of SBES data depends on the distance between points on a track line, which range from 5 m to 30 m, and on the distance between ship tracks, which range from 50 m to 125 m.

The data sets describe two areas. The IJmuiden area is located farthest North, with latitudinal coordinates (in UTM-WGS84) ranging from 5810100 to 5820200 and longitudinal coordinates range from 546500 to 604200. In total the IJmuiden area comprises 170 km^2. The area consists of two subareas; the approach route and the IJgeul. Based on the lateral survey extent, the approach route may be subdivided into the western approach route (IJAW) and the eastern approach route (IJAE) (Figure 2.1 left panel). The data for the two approach routes extend over 2006 to 2009, on a yearly basis (Table 2.1). As indicated in the figure, IJAE can be subdivided in a narrow and a wide part. This subdivision is based on the lateral extent of the surveys. The wide part was only surveyed in 2006, while the narrow part was surveyed from 2006 to 2009. To increase reliability of the IJmuiden analysis, additional data obtained in 1989, 1995, 1999 and 2005 is used from the NLHO, with the sets before 2000 being of SBES quality. Considering survey, frequency the IJgeul can be subdivided into two parts; the western part was surveyed once a year from 1991 to 2009, data sets of the eastern part span from 1994 to 2009, with an average frequency of 4 surveys per year.

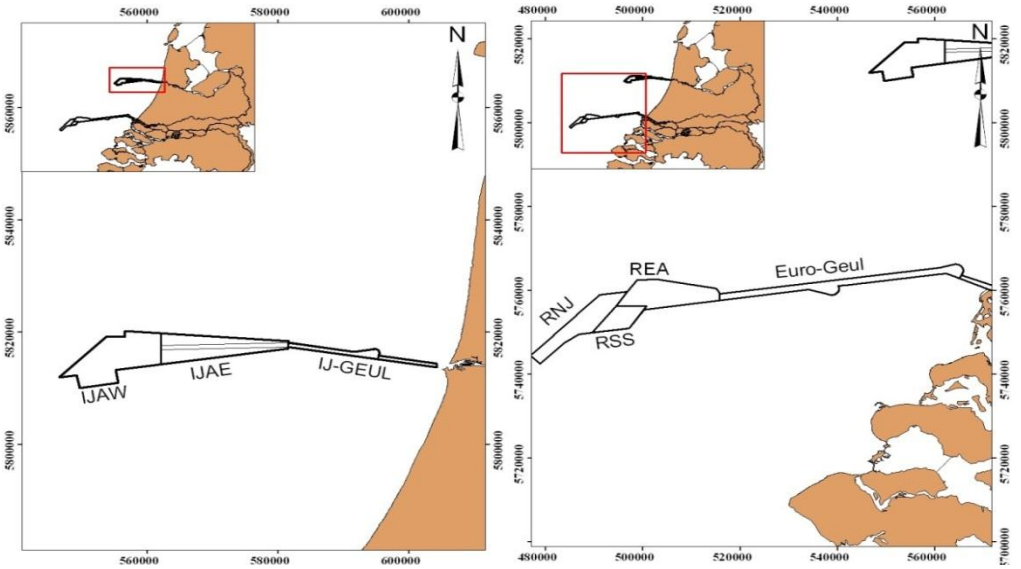

Figure 2.1 Contours of study areas. Left panel: The IJmuiden area. Right panel:Rotterdam. Note the narrow channel inside IJAE, which is only surveyed from 2007 to 2009.

Subarea	Timespan MBES+SBES	N sets	Timespan MBES	N sets
IJAW	1990-2009	8	2005-2009	5
IJAE	1990-2006	5	-	-
IJAE-channel	1990-2009	9	2005-2009	6
IJ-geul	-	-	1991-2009	29

Table 2.1 Table of used data sets for the IJmuiden area. Note that the number of data sets is based on the available data from RWS and NLHO.

The Rotterdam area is almost twice as large as the IJmuiden area, spanning 310 km^2, with with latitudinal coordinates (in UTM-WGS84) ranging from 5742600 to 5766300 and longitudinal coordinates between 476900 and 564300. For the Rotterdam approach route, three different areas are distinguished, the Nordhinder Junction (RNJ), the Short Stay anchor area (RSS) and the Eurogeul Approach route (REA) (Figure 2.1 right panel). All areas are surveyed once a year. The REA is measured from 1992 to 2009, while data for the RNJ and RSS range from 1990 to 2009 (Table 2.2). There is no data available for 1998 and 1999. The SBES method was used at RNJ before 1997 and at RSS before 1991, with an average data point density of 542 m^2/point.

The channel connecting the approach route to the shore is divided into the Euro-Geul and the Maasgeul. The Euro-Geul is surveyed every year from 1992 to 2009, some parts

however are surveyed more often up to 5 times per year. The Maasgeul connects the Euro-Geul to the shore and the available data span from 2001 to 2009 with a survey every month.

Subarea	Timespan SBES+MBES	N sets	Timespan MBES	N sets
RNJ	1990-2009	16	1997-2009	11
RSS	1993-2009	14	1994-2009	13
REA	-	-	1992-2009	16
Euro-Geul	-	-	1992-2009	17
Maasgeul	-	-	1996, 2001-2009	104

Table 2.2 Table of used data sets for the Rotterdam area.

2.2 Environmental data

2.2.1 Sediment grain sizes

Average grain sizes along the profiles are obtained from a grain size distribution map for the Dutch Continental Shelf created by research institutes TNO and Deltares. The map is constructed on a resolution of 200 m by Kriging interpolation of over 6000 grain size distributions in which the bathymetry is used as an external-drift variable (Figure 2.2) (Maljers & Gunnink, 2007).

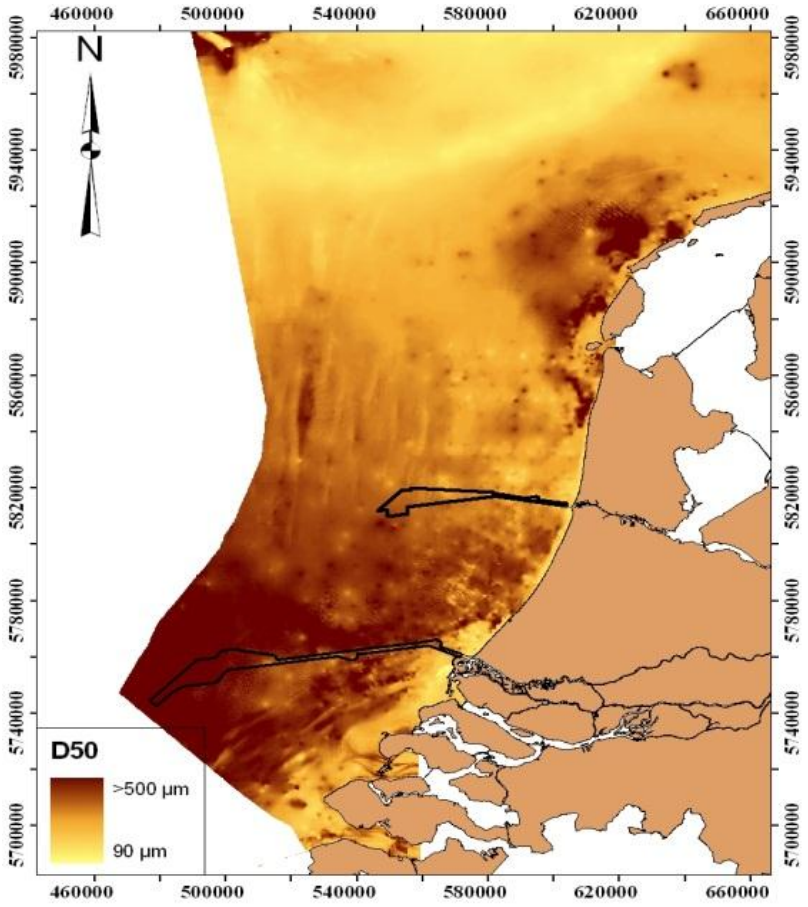

Figure 2.2 Median grain size of the sand fraction map for the entire Dutch continental shelf. TNO/Deltares

2.2.2 Tidal current information

As discussed earlier, sand waves are tide dominated features. Therefore, it is necessary to analyze the tidal behaviour for the Rotterdam and IJmuiden areas. The tidal information is extracted from the Multifunctional Access Tool foR Operational Oceandata Services (MATROOS) database. For the purpose of this research the 'hmnc_kustfijn' model provided the best resolution, spatially varying from 300 m to 800 m by 2.5 km at the edge of the model to more rectangular grid cells of 300 m to 400 m close to the coast and a temporal resolution of 1 minute (Rijkswaterstaat&Deltares, 2009). Since MATROOS provides only data of the last two years, no tidal data is available corresponding to the measurements times of the bathymetric data. Furthermore, since downloading current data from MATROOS is a time consuming procedure, data is downloaded over a timespan of two months; from 01-05-2011 to 01-07-2011, assuming that this timespan is sufficient to capture the most important tidal variations.

2.2.3 Surface wave information

To investigate the effects of surface waves on sand wave dynamics, the average height and period of the 1/3 highest waves in the 30 to 500 mHz wave spectrum are extracted from www.waterbase.nl from 1990 to 2010, with a measurement interval of 30 minutes (Figure 2.3). At both areas only one measurement location is available for the desired time extent. Therefore, it is assumed that the wave field does not change significantly in the areas. For IJmuiden the sensor of 'IJmuiden Munitiestortplaats' is used which is 36 km off the coast, whereas for Rotterdam 'Euro platform' is used at a distance of 58 km off the coast.

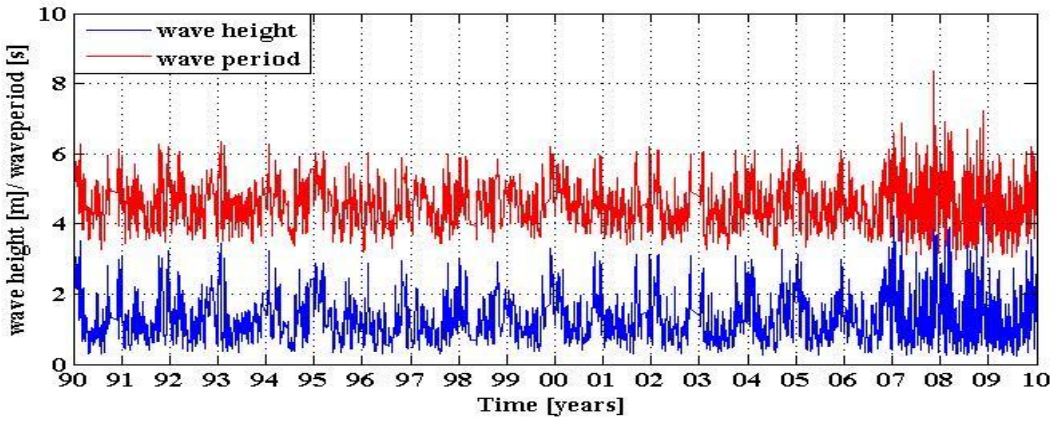

Figure 2.3 Example of wave height and wave period records for the IJmuiden area.

2.2.4 Dredging information

Information about dredging activity in the area of interest is delivered by RWS. The information consists of location, data and volume of extracted or nourished sand. A map of sand extraction sites is downloaded from the "Noordzeeloket" from RWS (www.noordzeeloket.nl; 2010).

Chapter 3. Methods

3.1 Digital elevation models

The data sets are interpolated to make Digital Elevation Models (DEMs). These are interpolated horizontal *xy*-grids, representing the sea bed surface elevation on an equidistance regular spaced grid. In contrast to the coordinates of point data, the *xy*-coordinates of the grid cells of the DEM's are similar for all data sets, by which an easy analysis of the sea bed evolution of the grid cells in time is possible.

Interpolation is done with the Inverse Distance Weighting (IDW) technique. This technique uses a user defined equidistant grid and a search radius which is equal for each grid point (Figure 3.1). A depth value is assigned to each grid point by taking the weighted average of all data points within the search radius, centered at the grid point. The weighting factor of each data point depends reciprocally on the distance between the data point to the grid point. The most suitable grid size and search radius depends on the data point density of the bathymetric data.

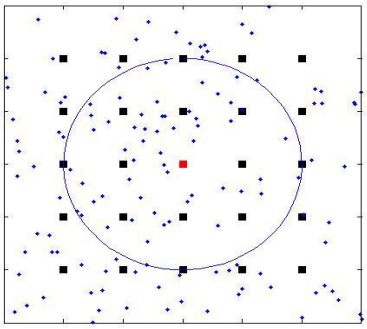

Figure 3.1 Example of IDW gridding technique. Squares denote grid point, the blue dotes the data points. The circle represents the search radius. Weighted averages of the de blue dots in the circle are assigned to the red square.

Because of the generally high point data density of the MBES sets, the IDW is performed on a uniform grid of 5 m by 5 m with a search radius of 25 m. This scheme does not perform well for the SBES data sets. For IJmuiden a grid of 10 m by 10 m with a search radius of 70 m, suits best for these sets. For the SBES sets of Rotterdam a grid of 25 m by 25 m, with a search radius of 50 m, performs best. Figure 3.2 and Figure 3.3 show the results for, respectively the IJmuiden bathymetry for 2006 and Rotterdam bathymetry for 2009.

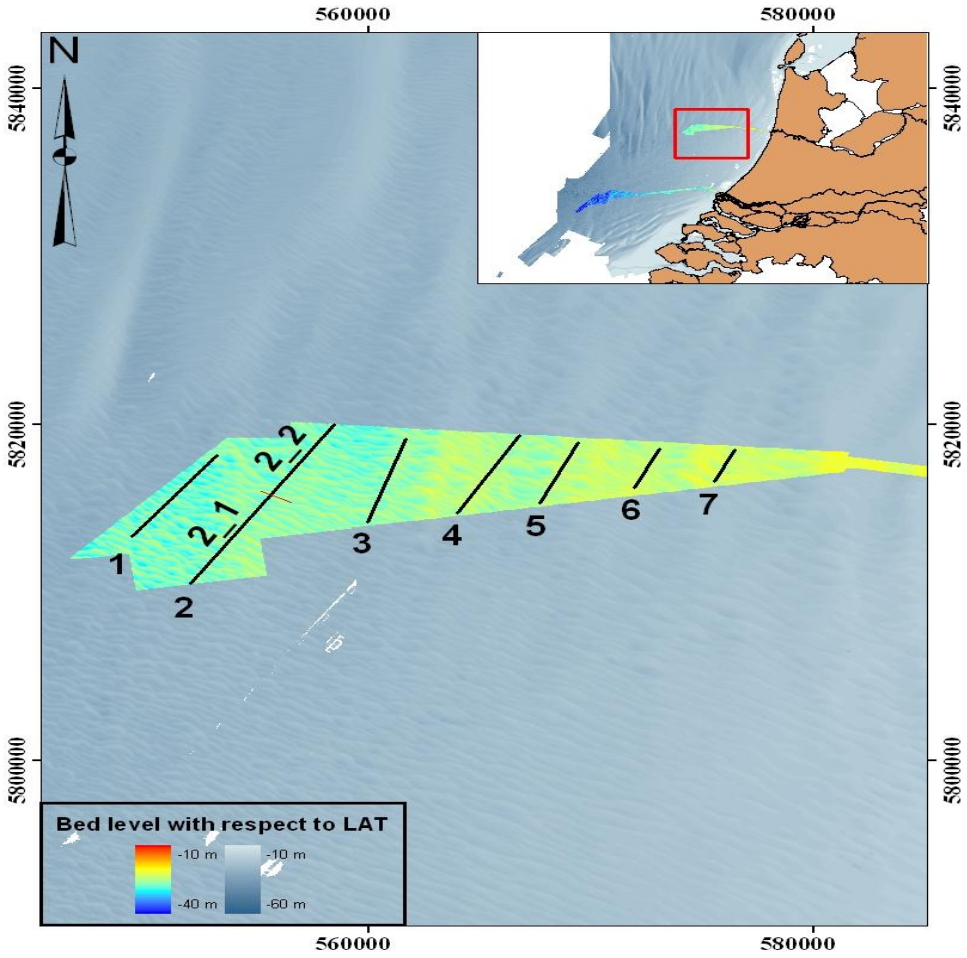

Figure 3.2 Bathymetry of the IJmuiden approach area. Bright colours are RWS data used in this study. Blueish shades are mosaic of most recent NLHO data, with a resolution of 25x25m. Black lines denote profiles, which will be explained in section 3.2.

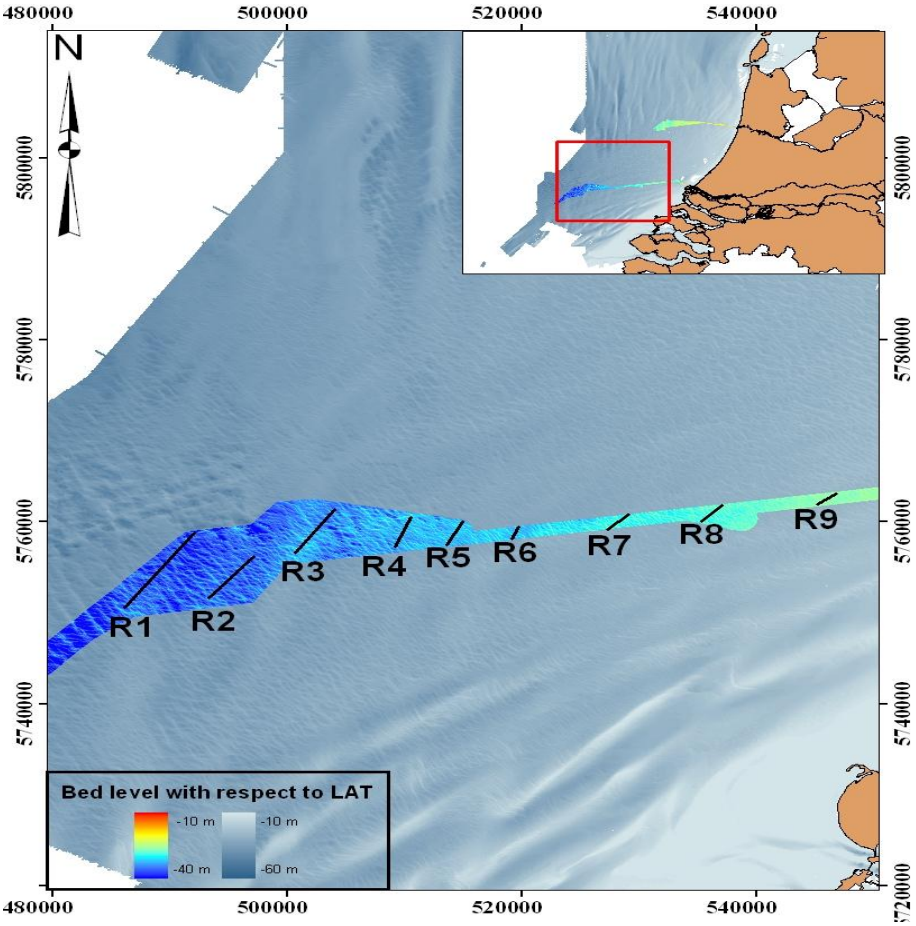

Figure 3.3 Bathymetry of the Rotterdam approach area. Bright colours are RWS data used in this study. Blueish shades are mosaic of most recent NLHO data, with a resolution of 25x25m. Black lines denote profiles, which will be explained section 3.2.

3.2 Bathymetry analysis

In nature, the sea bed consist of a superposition of several bed forms, this makes it difficult to identify the characteristics of individual bed forms directly from the DEM's. Separation of bed forms is accomplished with a method developed by Van Dijk et al. (2008), which uses a truncated Fourier analysis of a 1D profile through the bed elevation field. The profile is drawn perpendicular with respect to the dominant orientation of the sand waves in order to make correct calculations of the sand wave characteristics. Note that it is assumed that sand waves migrate perpendicular to their orientation.

3.2.1 Location selection

The first step in analysing the sand waves is to select appropriate analysis locations. This is accomplished by visual inspection of the bathymetric map. Profile locations are selected such that a profile only comprises one side of a large scale bed form. This is because small deviations in orientation between sand wave fields located at the crest or trough and the flank of a large scale bed form may occur. Furthermore it is hypothesised that migration is different over large bed forms. The number of profiles needed to fully describe the sites depends on the size of the areas, and the heterogeneity of the sand wave pattern. For IJmuiden seven locations are selected, whereas for Rotterdam nine profiles are chosen (Figures 3.2 and 3.3).

3.2.2 2-D Fourier analysis

In order to determine the dominant orientation of the sand wave field at the selected locations, a 2-D Fourier analysis is performed on small grids, cut from the DEM at the selected locations. Smaller grids are used, in order to analyse uniform and homogeneous bed patterns. The 2-D Fourier analysis results in a power spectral plot (Figure 3.4). The spectral power at a certain coordinate (k_x,k_y) determines the intensity of the Fourier component in the DEM. The coordinate corresponds to a wavenumber and an orientation by $k = \sqrt{k_x^2 + k_y^2}$ and $\theta = \arctan\left(\frac{k_y}{k_x}\right)$, respectively. Since the wavenumber relates to the wavelength λ by $k = 2\pi/\lambda$, one is able to find the dominant orientation of the sand waves in the DEM, by searching for the coordinate with the highest spectral power corresponding to wavelengths ranging from 100 m to 800 m. Although the example of Figure 3.4 implies a rather straightforward interpretation of the spectral plot, the large complexity of bed morphology may result in a large cloud of red cells, which represents a large variation in dominating modes. This makes interpretation difficult. To overcome

this problem, the chosen orientation might result from taking averages of minimum and maximum orientations.

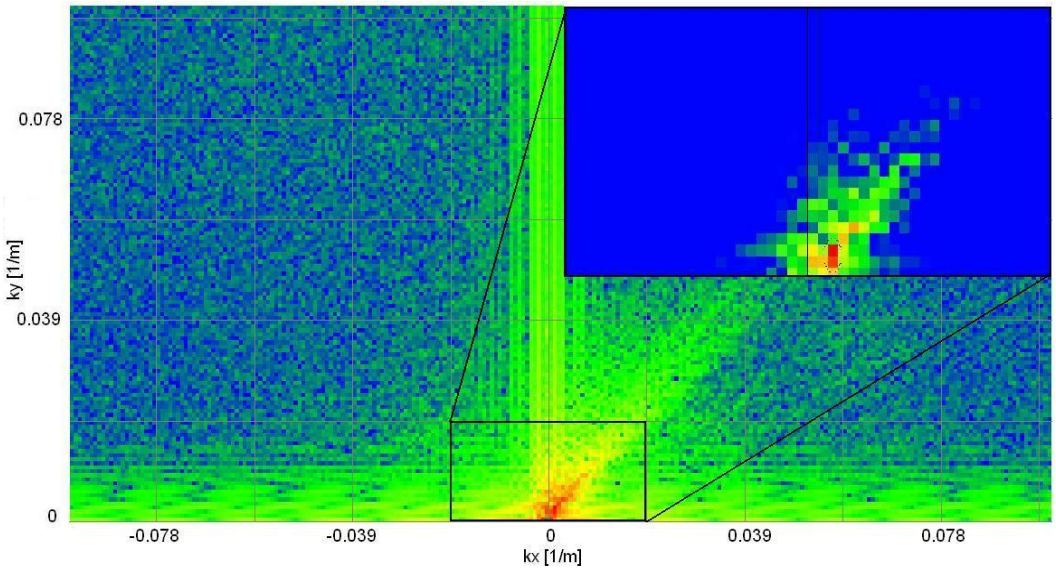

Figure 3.4 Example of a 2D spectral power plot for the dominant bed form modes. Red colours represent the most dominant modes; k_x and k_y are the directional wavenumbers. The orientation of the profile is determined by selecting the cell with the highest power. The line between the origin and that point defines the wave vector of the dominant mode and thus the orientation.

3.2.3 Cross sections

After determining the most appropriate direction profile, *xz* data is collected along the profile from the DEM, with a data point every meter. A 1-D Fourier analysis is now applied to the *xz* data, to separate sand waves from other bed forms, by discarding wavelengths that do not correspond to the sand wave length spectrum (usually between 100 m and 800 m). This leads to a smoothing of the sea bed, which may lead to a considerable underestimation of the height of sand waves. Therefore one has to be careful with the choice of wavelengths which has to be eliminated (Van Dijk et al., 2008). After eliminating all the bed forms but the sand waves, the crest and trough points (ct points) are selected. The 1-D Fourier approximation of the seabed may result in local minima or maxima, because of the superposition of waves with different wavelengths. These points are deselected manually (Figure 3.5).

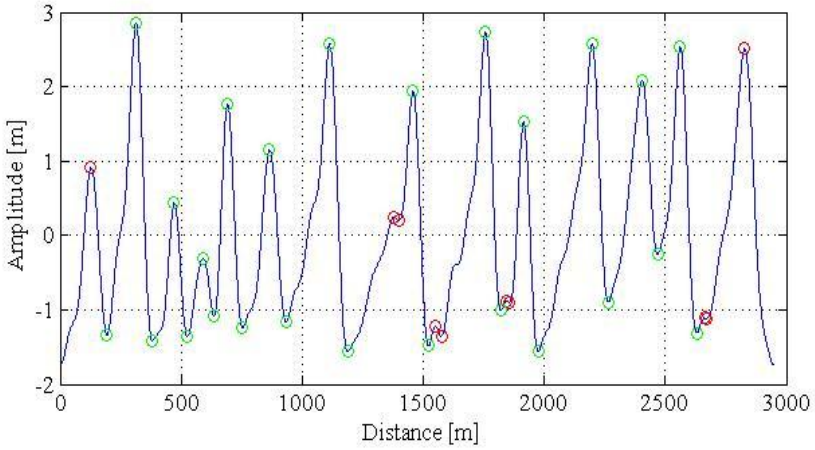

Figure 3.5 Example of a profile through the Rotterdam domain for the 2004 data set, after eliminating all small and large scale bed forms. Green circles represent selected crest and trough points. Red circles are manually discarded ct points.

3.2.4 Sand wave characteristics definitions

From the determination of the ct points along the profile one is able to calculate the minimum, maximum and average wavelength/ wave height. The wavelength is defined as the length of the base line segment connecting two consecutive troughs (Figure 3.6). The sand wave height is defined as the line perpendicular to the base line segment, connected to the selected crest point. The asymmetry index is defined as the ratio between the length of the stoss side and the lee side of the sand wave.

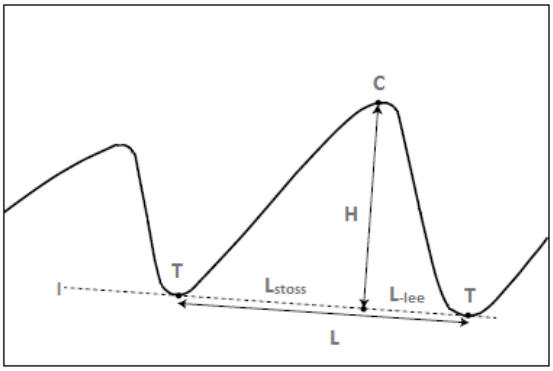

Figure 3.6 Definition of the sand wave length (L), sand wave height (H), stoss side of the sand wave (L_{stoss}), lee side of the sand wave (L_{lee}), crest points (C) and the trough points (T). (After Van Dijk et al. (2008)).

3.3 Sand wave migration rates

3.3.1 Method description

Analyzing sand waves at different times along the same profile allows for the opportunity to determine horizontal sand wave migrations rates. There are different methods to determine the migration rates.

The first method uses simple linear regression. The positions of the crests/troughs are plotted against the end date of each survey (also the start date or the average between start and end could be chosen here. This is an arbitrary choice, which does not affect the performance of the regression). A linear regression can now be applied to the crest/trough locations. The regression coefficient represents the average migration rate of each crest and trough.

Whether or not a trend is observed in the crest/trough positions along a profile is determined by the goodness of fit (R^2),

$$R^2 = 1 - \frac{\sum_i[(x_i - \hat{x}_\iota)^2]}{\sum_i[(x_i - \bar{x})^2]}. \quad 3.1$$

In this expression x_i determines a positions measurement of a certain crest/trough along a profile, $\bar{x}$ the average location of the crest/trough along a profile and $\hat{x}_\iota$ the predicted location of the crest/trough of interest and, finally, the subscript i determines the measurement number.

The accuracy of the linear regression model in predicting the crest/trough positions along a profile is determined by computing the error of estimate,

$$S_e = \frac{\sum|x_i - \hat{x}_i|}{n}. \quad 3.2$$

Here, x_i is the measured crest/trough position, $\hat{x}_i$ is the corresponding predicted value and n is the number of measurements in time of the crest/trough of interest. This measure determines to what extent a regression model is able to predict the measured values. When the differences between measured and predicted crest/trough positions for all

measurements of all crest/troughs along a profile are taken into account, a typical error of estimate for the profile of interest can be computed.

Figure 3.7 presents an example of the results for the linear regression method for individual crests (number 29 to 32, out of 38 crests) along Rotterdam profile R1 (see for profile definition Figures 3.2 and 3.3). The figure shows that a linear trend is observed in the position of the crests, which is also denoted by the goodness of fit (R^2~0.7). For almost all Rotterdam profiles the linear regression performs with similar accuracy for the crests positions (R^2~0.7, averaged over all Rotterdam profiles). The regression performs less well for the Rotterdam troughs, but is nevertheless acceptable (R^2~0.6, averaged over all Rotterdam profiles).

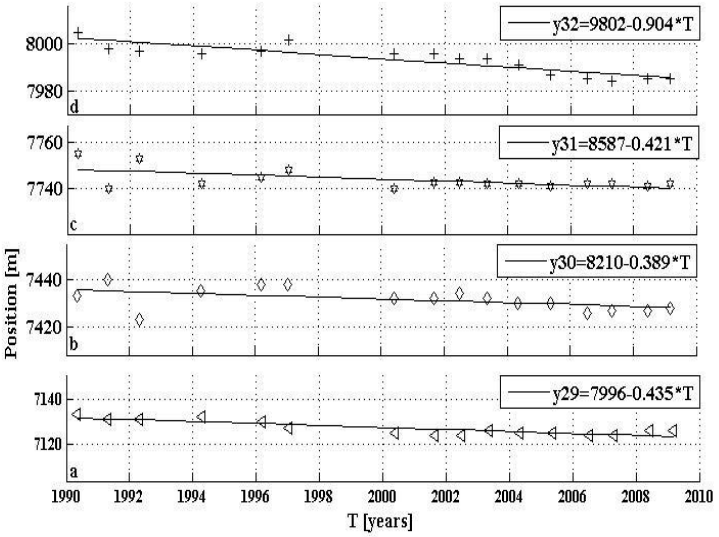

Figure 3.7 Example of a linear regression for Rotterdam profile R1. Every figure represents a crest. The vertical axis shows the absolute position of the crests along the profile. Horizontal axis shows the time in years. The regression coefficients in the formulas show the migration rates in m/year.

For IJmuiden clear linear trends are observed in the positions of the crests along the profiles (R^2~0.8, averaged over all IJmuiden profiles). The troughs for IJmuiden do not show clear trends in their positions (R^2~0.2, averaged over all IJmuiden profiles). This does not necessarily mean that linear regression is not allowed, but that there is little variation in time of the positions of the troughs along the profiles. In addition S_e = 4.6 m for the IJmuiden troughs, which implies that one is able to predict the position of the troughs in the IJmuiden area, using linear regression with a precision of 4.6 m.

Figure 3.7 also suggests that the fit is better for the surveys after 2000. This is probably because the SBES data sets (before 1996) are of poorer resolution than the MBES (1996 onwards) data sets. This difference in fit is especially recognized for all IJmuiden sets and for the Rotterdam sets for the RNJ and RSS areas. It will therefore be tested to what extent this poor fit biases the results of the linear regression.

A second migration rate calculation method calculates the sand wave migration rate between successive surveys. To do so, one has to take into account that the exact moment in time at which a specific data point is measured is not known, since only the survey's start and end date were provided with the bathymetric data. Therefore, each data set represents the sea bed morphology between the start and end date of a specific survey. When one wishes to calculate the sand wave migration rate between successive surveys, the time length of each survey has to be taken into account. Now, consider a crest in a specific profile that travels between two successive surveys from position x_1 to x_2. The maximum time this migration took is now the time difference between the start of the first survey and the end of the second survey, resulting in a maximum timespan, Δt_{max} (Figure 3.8). From this time interval a minimum migration rate, c_{min}, is calculated with,

$$c_{min} = \frac{x_2 - x_1}{\Delta t_{max}}. \tag{3.3}$$

The minimum timespan, Δt_{min}, is the time difference between the end of the first survey and the start of the second survey. This results in the maximum possible migration rate, c_{max}, between this surveys,

$$c_{max} = \frac{x_2 - x_1}{\Delta t_{min}}. \tag{3.4}$$

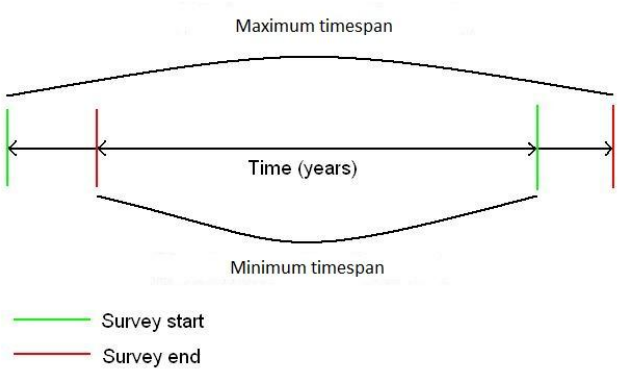

Figure 3.8 Example of minimum and maximum calculated migration rates.

The average of c_{min} and c_{max} provides the average migration rate between the surveys. For small survey timespans, the difference between the maximum and minimum migration rates should be close to zero. With this method one is able to determine migration rate variability within surveys. This variability may be natural or may be induced by inaccuracy of measurements.

An example of the interval method is presented in Figure 3.9, which shows the average migration rate, the maximum and minimum migration rates of individual crests and the maximum and minimum calculated migration rates due to maximum/minimum periods between successive surveys. In general, the differences due to the latter is rather small. Striking however are the large possible deviations of individual sand waves from the profile's averages, which in addition show both upstream migration (positive values) as well as downstream migration (negative values).

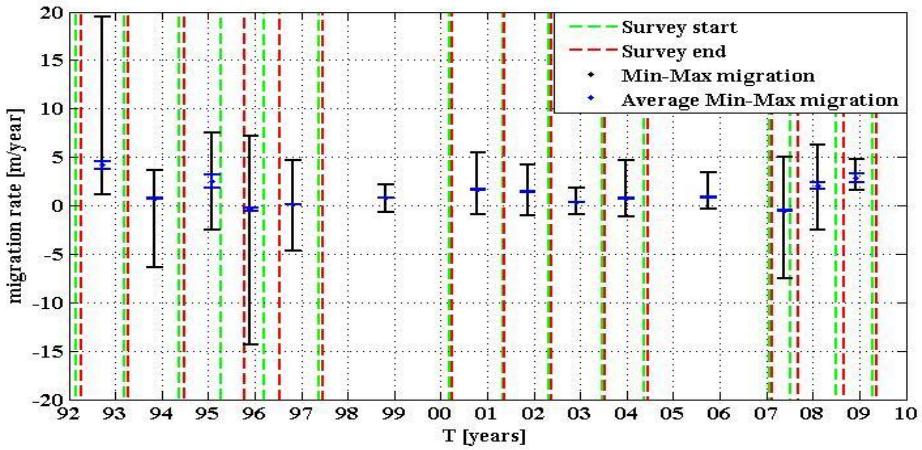

Figure 3.9 Example of the crest migration of the interval method along the Rotterdam profile R5. Migration rates are shown along the vertical axis, the time in years along the horizontal axis. Red/green dashed lines denote the start/end of a survey. Black bars indicate the minimum/maximum migration rate of an individual crest along the profile. The blue bars show the minimum/maximum migration rate based on the minimum/maximum interval between successive surveys.

3.3.2 Method selection

In order to select the best migration rate calculation method and to determine the influence of the data sounding method, first consider Figures 3.10 and 3.11. Figure 3.10 shows average migration rates along the profiles for the regression and interval method for the IJmuiden area. Both panels distinguish between crest migration and trough

migration and between resolution of the used data sets. Figure 3.11 shows the migration rate results for the Rotterdam area. For clarity of the figures, the crest and trough migration rates are presented in different figures in this case.

Overall, for profiles 3 to 9 for the Rotterdam area the interval method calculates migration rates of 0.25 to 0.5 m/year higher than the regression method. Exceptions are the crests along profile 9, where the regression method calculates the highest migration rates, and the troughs of profile 6 and 7 for which the two methods yield little difference.

For profiles 1 to 6 for IJmuiden the opposite occurs, with higher migration rates (up to 2.3 m/year) for both crests and troughs calculated with the regression method. Profile 7 shows completely different results, where the interval method calculates migration rates of 5 m/year lower for the crests and 4 m/year lower for the troughs than is obtained with the regression method. Figure 3.12 presents the linear regression applied to the positions of the crests along profile 7. The regression performs well with R^2 = 0.78, although S_e = 14.3 m. This large error and the figure show that there are large differences in the positions of the crests between successive survey. Thus, the interval method calculates large migration rates between surveys, which biases the average migration rate. The large possible outliers calculated with the interval method were also reflected in Figure 3.9. Therefore it is concluded that the regression method provides the most reliable average migration rates.

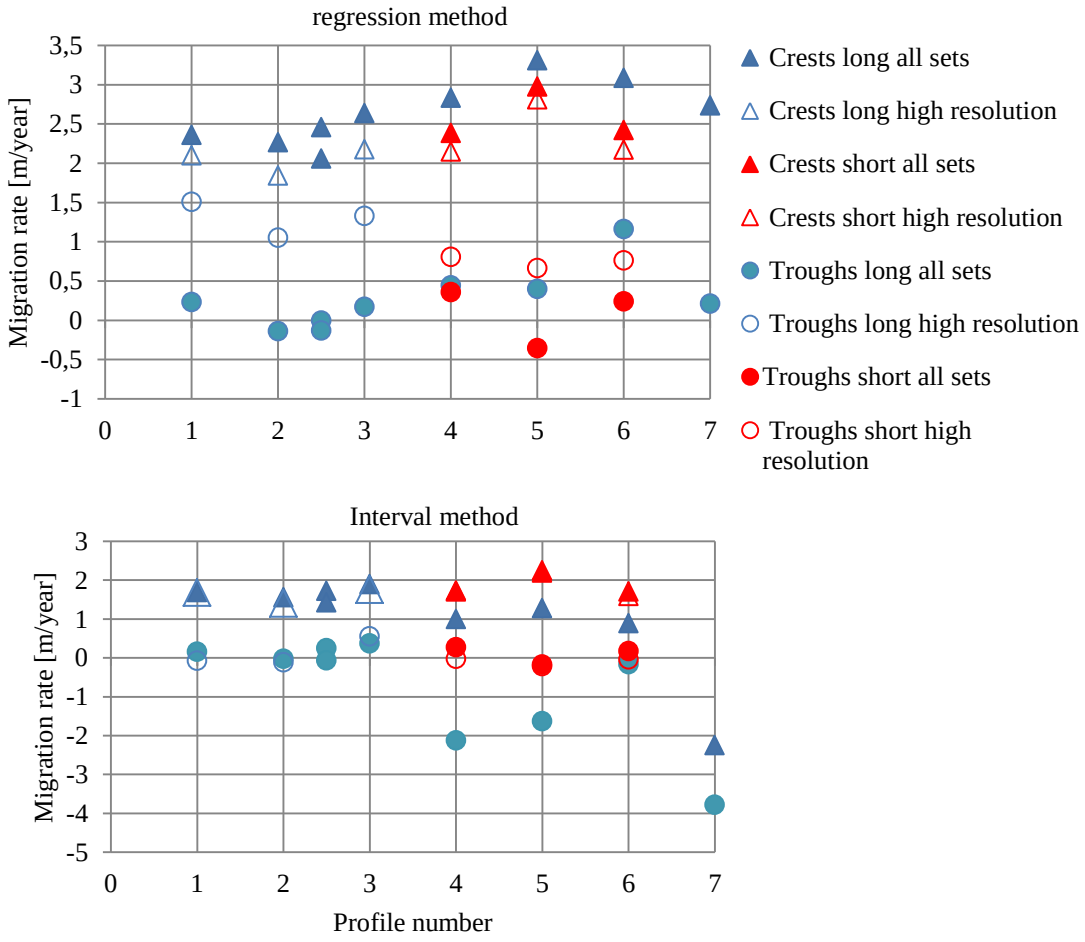

Figure 3.10 Migration rates for the IJmuiden area. The migration rates are averages for all crests/ troughs along a profile. Closed symbols denote migration rates calculated with all data sets, open symbols denote migration rates calculated with the high resolution sets only. Triangles represent crest migration, circles represent trough migration. Finally, blue colours denote the long profiles, red colours denote short profiles. The profile 2_1 and 2_2 are placed between profile number 2 and 3. Upper panel: Results of the regression method. Lower panel: Results of the interval method.

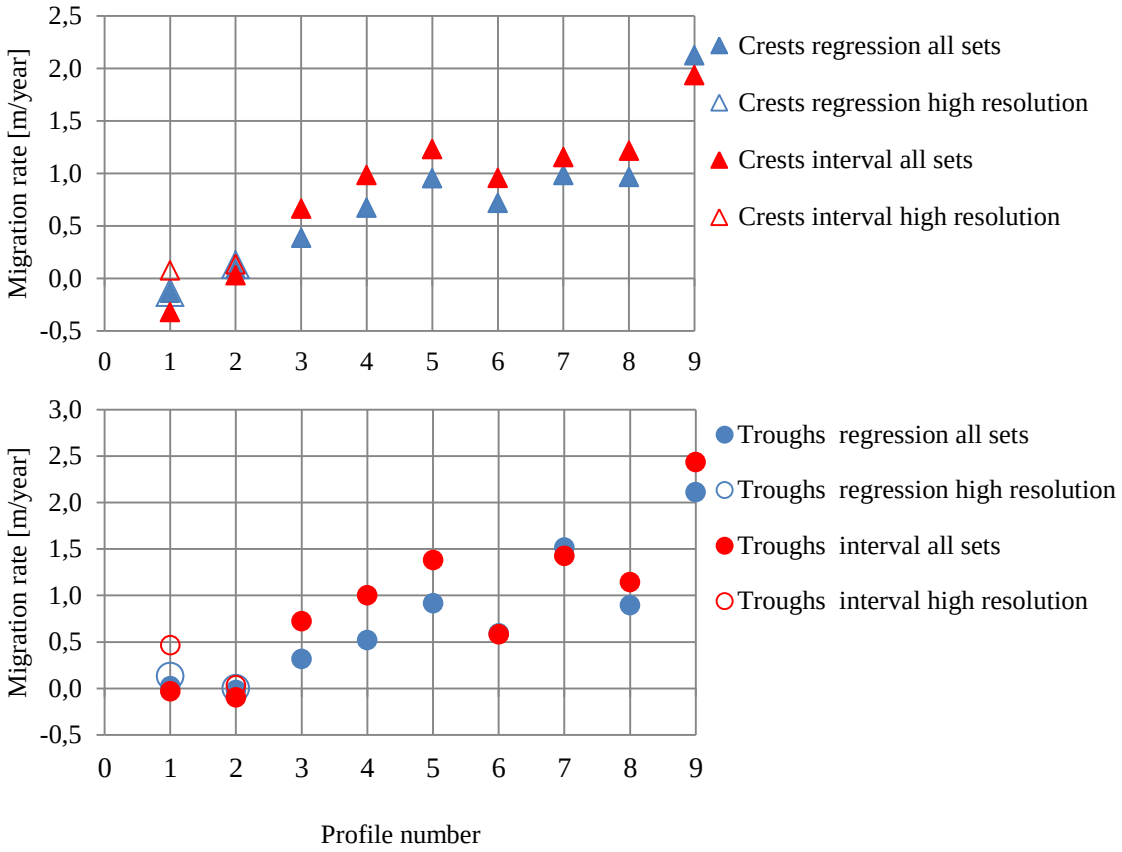

Figure 3.11 Profile averaged migration rates for the Rotterdam area. Closed symbols denote calculations based on all data sets. Open symbols denote calculation with only high resolution sets (profiles R1 and R2 only). Blue/ red colours denote regression/ interval method. Upper panel: Crest migration. Lower panel: Trough migration.

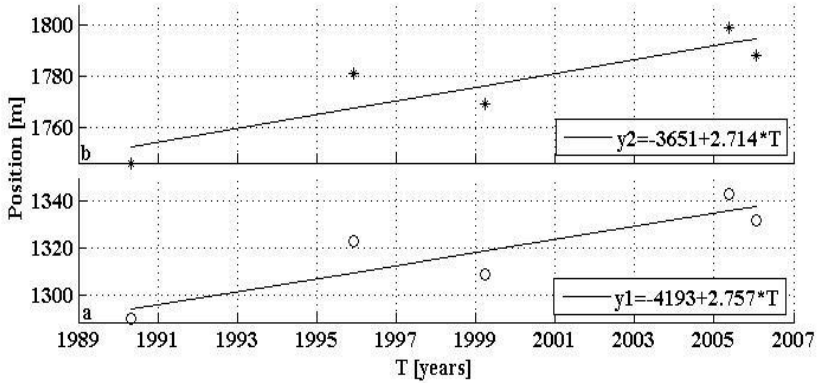

Figure 3.12 Example of linear regression through the crest positions along IJmuiden profile 7

Finally a decision has to be made whether the use of SBES in combination with MBES biases the results. For the IJmuiden area the regression calculations for the crest migration with MBES data sets only result in lower migration rates (up to 0.5 m/year) than when SBES+MBES data sets are used. This is also shown for the calculations with the interval method, although the difference is smaller (~0.1 m/year). For the Rotterdam area the opposite occurs, where the regression on the MBES datasets calculates slightly higher (~0.1 m/year) migration rates than when SBES+MBES datasets are used.

Calculations of the IJmuiden trough migration rates show clear differences between MBES and SBES+MBES for the regression method, where regression on the former data sets result in higher migration rates (up to 1.2 m/year) than regression on the latter data sets. For the interval method applied to the IJmuiden area this pattern is less pronounced, even though differences are calculated of about 0.2 m/year. Also for the Rotterdam area higher trough migration rates are calculated with the MBES data sets for both regression and interval methods, up to 0.1 m/year and 0.4 m/year, respectively.

Table 3.1 shows the goodness of fit for the regression method for calculations with the MBES+SBES data sets as well as for the MBES data sets only. Only the profiles for which this distinction was possible are presented (i.e. for IJmuiden profiles 1 to 3 and the short sections of profiles 4 to 6, and for Rotterdam the profiles R1 and R2). The presented values are averages over the profiles of interest. It shows that R^2 does not change considerably between MBES+SBES or MBES only. This indicates that in both cases linear trends are observed, which are more pronounced for the crests than for the troughs. The error of estimate however decreases with 0.5 m to 4.7 m when only MBES data sets are used. So the predictive ability of the linear regression model increases when the resolution of the bathymetric data is increased. Nevertheless, the increase in error is relatively small so, in the following, the presented migration rates are based on linear regression on the MBES+SBES data sets.

The final results and a more comprehensive interpretation are presented in chapter 4.

Profile	MBES+SBES		MBES	
	R^2 [-]	S_e [m]	R^2 [-]	S_e [m]
Crests R1+R2	0.37	2.0	0.41	1.5
Troughs R1+R2	0.35	3.1	0.37	2.5
Crests 1+2+3	0.78	4.7	0.79	1.4
Troughs 1+2+3	0.14	7.6	0.33	2.9
Crests 4Short+5Short+6Short	0.83	4.5	0.79	1.4
Troughs IJ4Short+IJ5Short+IJ6Short	0.17	5.9	0.22	2.1

Table 3.1 Table of goodness of fit and error of estimate for the linear regression method. The Rotterdam profiles are denoted with an 'R' prefix. The prefix 'Crests' or Troughs denote whether regression trough crest or trough points are considered. Only results are shown for the profiles for which both MBES as well as SBES data are available

3.4 Environmental parameters

This section describes how the environmental data obtained in chapter 2 are used for sand wave analysis. One of the objectives of this thesis is to find the dominating factors controlling sand wave behaviour in both the Rotterdam and IJmuiden areas. Selection on the most relevant parameters is based on the studies of Besio et al. (2004), Knaapen (2005) , Van Dijk & Kleinhans (2005) and Van Santen et al. (2011). When the controlling factors are known, possible differences between the sites could be explained. The environmental parameters that are investigated are: local water depth (which is here taken as the average depth along a profile), median sediment grain size, tidal characteristics and surface (wind) waves.

3.4.1 Sediment grain sizes along a profile

The grain size map is used in a Geographical Information System (GIS) and provides together with the chosen profiles averages of median grain sizes of the sand fraction along the cross sections. It should be noted that grain sizes may differ up to 30 micrometer between sand wave crests and troughs (Passchier & Kleinhans, 2005; Buijsman & Ridderinkhof, 2008; Van Oyen & Blondeaux, 2009). Taking averages with the described method ignores this effect.

3.4.2 Tidal analysis

The data obtained from MATROOS consist of current velocities decomposed in a longitudinal and latitudinal part. From these velocities the tidal constituents are obtained by harmonic decomposition of the data (for details see Van Santen (2009). From this harmonic analysis the following tidal characteristics will be determined: the maximum tidal velocity of the M2 and M4 constituents, which is determined by the length of the major axis of the tidal ellipse; the ellipticity of the M2 and M4 constituents, which is the ratio between the length of the minor axis and the major axis of the tidal ellipse; the relative phase shift between the M4 and M2 ($\phi_{\mathrm{M4\text{-}M2}}$) tidal constituents, which is calculates with

$$\phi_{\mathrm{M4-M2}} = \phi_{M4} - 2\phi_{M2}, \tag{3.5}$$

with ϕ_{M4} and ϕ_{M2} the phases of respectively the M4 and M2 constituents and finally *Z0* represents the steady residual background current

3.4.3 Sediment transport due to surface waves

Sediment transport is usually determined by the shear stress induced by tidal currents. However, short-period surface waves, generated by wind or swell, generate an orbital motion of fluid particles in the water column. When the waves are sufficiently long, this orbital motion may reach the seabed in shallow water (Soulsby, 1997). In addition, when the shear stress induced by the horizontal current generated by the orbital motion is large enough compared to the critical shear stress, the wave action is sufficient to stir up sediments. In this case, the total sediment transport is determined from the bed shear stress induced by tidal currents and the bed shear stress induced by surface waves. The contribution of bed shear stress induced by surface waves relative to the total bed shear stress is calculated by

$$\tau_{rel} = \frac{\tau_{w\,max}}{\tau_{c\_max} + \tau_{w\,max}}. \tag{3.6}$$

In this expression, τ_{rel} is the contribution of the bed shear stress induced by surface waves, relative to the total bed shear stress, $\tau_{w\,max}$ the bed shear stress induced by the surface waves and $\tau_{c\,max}$ the bed shear stress induced by the maximum tidal current. The latter parameter is calculated with

$$\tau_{c\,max} = \rho_w c_D u_{max}^2. \quad 3.7$$

Here, ρ_w is the water density (~1025 kg/m^3), c_D the drag coefficient ($\sim 2.5 \cdot 10^{-3}$) and u_{max} the maximum tidal current strength. The drag coefficient depends on the hydrodynamic conditions, bottom roughness and the reference roughness. For tidal currents this coefficient is often approximated by $2.5 \cdot 10^{-3}$ (Soulsby, 1997).

The bed shear stress induced by surface waves is calculated with (Soulsby, 1997)

$$\tau_{w\,max} = \frac{1}{2}\rho_w f_w u_{orb}^2. \quad 3.8$$

In this expression, f_w is the wave friction factor and u_{orb} the amplitude of the near-bed orbital motion. To compare the results from this analysis with literature, the White Colbrook equation of the skin friction discussed by Van Rijn (1993) and used by Van Dijk & Kleinhans (2005) is used, which uses the following expression for the wave friction factor

$$f_w = 2\exp[5.213\left(\frac{2.5D_{50}}{A_{orb}}\right)^{0,194} - 5.977], \quad 3.9$$

in which D_{50} is the median sediment grain size and A_{orb} the semi-orbital excursion. The latter is related to u_{orb} according to,

$$A_{orb} = \frac{u_{orb}T}{2\pi}, \quad 3.10$$

with T the wave period. The amplitude of the near-bed orbital motion (u_{orb}) follows directly from

$$u_{orb} = \frac{\omega H}{2\sinh(kh)}. \quad 3.11$$

Here, ω denotes the angular frequency, k the wavenumber and H the significant wave height. The angular frequency and the wavenumber can be calculated from the wave height and wave period records, which were obtained in section 2.2.3, by using linear wave theory (Soulsby, 1997). As a consequence, effects of having a range of waves with differing lengths and heights within a specified wave spectrum are neglected. Therefore, for each measurement interval only one wave type with the same height, length and period, is assumed. To simplify matters even more, daily averages of the wave height and

period are calculated. With these averages the wave number is calculated using the dispersion relation for linear free gravity waves

$$\omega^2 = gk \tanh(kh), \quad 3.12$$

with g the gravitational acceleration and h the water depth. Note that it is assumed that capillary waves no not play a role here, since there wavelengths are of $\mathcal{O}(cm)$, hence they will not reach the bottom.

By inserting the parameters $\xi = \frac{\omega^2 h}{g}$, $\eta = kh$ and $\omega = \frac{2\pi}{T}$, into (3.12) equation that is to be solved reduces to

$$\xi = \eta \tanh(\eta). \quad 3.13$$

This equation is solved iteratively using the Newton-Raphson iteration scheme (Soulsby, 1997)

$$x_{n+1} = x_n - \frac{f(x_n)}{f'(x_n)}, \quad 3.14$$

with $x_n = \eta$ and $f(x_n) = \xi - \eta \tanh(\eta)$ and n the number of iteration steps.
The iteration is stopped when the difference between x_{n+1} and x_n is smaller than 0.000001.

When the skin friction is known, the Shields parameter at the bed can be calculated

$$\theta_w = \frac{\tau_w}{(\rho_s - \rho_w) g D_{50}}. \quad 3.15$$

Here, ρ_s is the grain density (~2650 kg/m^3). Sediment transport due to surface waves is only possible when the Shields parameter exerts a certain threshold. Van Dijk & Kleinhans (2005) use a range between 0.03 and 0.06, this study however uses a grain size dependable approximation of Soulsby (1997)

$$\theta_{cr} = \frac{0.30}{1 + 1.2 D_*} + 0.055[1 - \exp(-0.020 D_*). \quad 3.16$$

In this expression, D_* is the dimensionless grain size which is calculated by

$$D_* = \left[\frac{g\left(\frac{\rho_s}{\rho_w} - 1\right)}{\upsilon^2}\right]^{1/3} D_{50}. \qquad 3.17$$

Here, and υ the kinematic viscosity ($\sim 1.36 \cdot 10^{-6} m^2 s^{-1}$). Note that (3.18) only determines the Shields parameter for motion due to surface waves.

This model calculates for each measurement-day whether the combination of wave height and period is sufficient to exert the threshold described by (3.18). This results in the number of days over the twenty year record for which the threshold is exerted. Since every profile has its own unique combination of grain size and water depth, unique measures for every profile are obtained. These measures are converted to a relative quantity in the order of percentage.

3.4.5 Analysis of the dredging data

The methods described in section 3.2 will also be used to analyse the dredged parts of the area. It should however be noted that these methods are only applicable when one is able to identify the bed forms using the 2D spectral analysis. Therefore, dredging should only increase the entire water level, while the natural bed forms are retained. When the natural bed forms are destroyed, it is expected that the 2D spectral analysis will not be able to identify the sand wave modes. In this case the orientation of the sand waves expected at the dredged areas will be determined by analyzing bathymetric maps in the vicinity of the areas of interest. It is assumed that the sand wave orientation of these areas can be extrapolated to the dredged sites.

3.5 Factor analysis

With a factor analysis one aims to find relations between a set variables (the so called 'input variables') that are considered to explain the behaviour of a second set of variables (the so called 'output variables'). The most simple factor analysis is to plot and correlate all input variables (in this study the environmental parameters) with respect to the output variables (in this study the sand wave migration rate and the sand wave length). From inspection of the plots one may get insight into the (lack off) correlation of the output variables with the input variables. To analyse the linear dependence of the output variables on each of the input variables one may perform a multivariate regression between the input data and the output data. Problems however, arise when the input variables are mutually correlated. These correlations can not directly be identified from the simple plots, but are expected in this study. For instance, the calculation of the bed shear stress induced by surface waves directly depends on depth and grain size distribution, while the latter two variables may also depend on each other (Varfaillie et al., 2006). Thus, in order to be able to use a multivariate linear regression to identify the controlling input variables, a new set of independent input variables has to be obtained. When the variables in this new set are linear combinations of the original set of input variables, the regression coefficients, resulting from the multivariate linear regression, still provide information about the relative importance of the each of the original input variables in explaining the behaviour of the output variables.

The principles of the Principal Component Analysis (PCA) are used to create a set of independent variables. After that a multivariate linear regression is performed on the new input variables, which is known as a Principal Component Regression (PCR).

3.5.1 Principal Component Analysis

Jolliffe (2002) describes the basic rule of the PCA as follows:

" The central idea of principal component analysis is to reduce the dimensionality of a data set in which there are a large number of interrelated variables, while retaining as much as possible of the variation present in the data set."

This means that the input variables are transformed to a new set of uncorrelated variables, the principal components (PCs). In addition, this new set of variables are ordered in such a way that all variability present in the original variables is retained in the first few

principal components. To obtain independent variables, the PCA uses eigenvalue and eigenvector manipulations on the variance-covariance matrix of the input data.

The first step is to stack the input data in a $[n \times p]$ matrix **x** whose (*i*,*j*)th element is a value of the *j*th input variable for the *i*th observation. Note that the input variables are measured/calculated in different units and are distributed around different means. In order to compare the variability in the input variables it is convenient to distribute them around zero means. In addition, to make them independent of measurement units, the zero mean distributions are divided by their standard deviation. This procedure is called standardisation and is schematically represented by

$$\mathrm{X_{ij}} = \frac{x_{\mathrm{ij}} - f_j}{s_j}. \qquad 3.18$$

Here, $\mathrm{X_{ij}}$ are elements of the standardised input variable matrix **X**; x_{ij} are elements of the original input matrix **x**; f_j and s_j are the mean and the standard deviation of the *j*th input variable, respectively.

The next step is to create an orthogonal vector space of *p*-dimensions, with which the matrix **X** will be uncorrelated. One of the most important properties of this vector space is that the variance present in the matrix **X** is retained along the vectors. To achieve this, an eigenvalue and eigenvector analysis is applied to the covariance matrix **R** (Haan, 1977; Davis, 1986; Jolliffe, 2002),

$$\mathbf{R} = \frac{\mathbf{X}' \cdot \mathbf{X}}{n-1}, \qquad 3.19$$

where *n* is the number of observations. The *(i*,*j)*th element of **R** is the covariance between the *i*th and *j*th element of **X**, when $i \neq j$. The covariance determines the joined variation of two input variables about their common mean. When $i = j$, the *(i*,*j)*th element of **R** is the variance between the *j*th element of **X**, which is the squared standard deviation of the *j*th standardised input variables (Davis, 1986).

Now, the eigenvalues and eigenvectors are calculated with,

$$(\mathbf{R} - \lambda \mathbf{I})a = 0. \qquad 3.20$$

This equation yields a total of *p* eigenvalues (λ), corresponding to a total of *p* eigenvectors (*a*), **I** is the identity matrix. The matrix with the eigenvalues on the diagonal

and zeros otherwise is written as $[\lambda_j] = \mathbf{D}_{\boldsymbol{\lambda}}$, with $j = 1, \ldots p$. Furthermore the eigenvectors a_j (with $j = 1, \ldots p$) are the columns of the eigenvector matrix **A**.

Finally, in order to obtain the set of uncorrelated variables, the standardised input variables, **X**, are spanned along the orthogonal vector space **A**. The resulting uncorrelated variables are the PCs (**Z)**

$$\mathbf{Z} = \mathbf{X} \cdot \mathbf{A}. \qquad 3.21$$

So, each element Z_{ij} of **Z** is a linear combination of the *i*th observation of all *p* standardised input variables and the *j*th eigenvector.

Finally, since **R** consist of the covariances of the elements of matrix **X**, the size of eigenvalue λ_j is the variance of the *j*th principal component.

3.5.2 Interpretation of the principal components

The next step is to reduce the dimensionality of the obtained dataset **Z**, in order to make the PCs suitable for analysis purposes**.** This is possible, because some of the original input variables depend very strongly on each other and therefore their covariances will be similar. The eigenvector/ eigenvalue calculations from **R** will then result in some eigenvectors which are related to almost zero valued eigenvalues. Calculating PCs from such a set of eigenvectors will result in some PCs that do not represent any of the variation of the input data. Most of the variance present in the original data is retained along the first few PCs. Thus, for analysis purposes, the dimensionality of **Z** is reduced by choosing a subset $\hat{\mathbf{Z}}$ from **Z**, that consist of the first *m* PCs, with $m < p$. This study uses the traditional method of choosing the size of *m* (Jolliffe, 2002). This method uses a cumulative percentage of the total variation which is desired to be retained in the selected principal components. Recall that each PC corresponds to an eigenvalue, determining the variance of the particular PC. The ratio of the eigenvalues to the sum of all eigenvalues determines to which level the total variance in the data is explained by a particular PC (i.e. eigenvector) corresponding to a particular eigenvalue. For example, the ratio of eigenvalue *j* to the sum of all eigenvalues is 70%. This means that the *j*th principal component explains 70% of the total variance. This study will test thresholds for which 80% and 90% of the variance is retained along the eigenvectors.

3.5.3 Principal component regression

The basic model for a multivariate regression reads

$$y_i = \sum_{j=1}^{p} \beta_j x_{ij} + \varepsilon, \qquad 3.22$$

with y_i the *i*th observation of the original output variable out of the output variable array **y**; β_j the regression coefficient corresponding to the *j*th input variable, x_{ij} an element of the original input variable matrix **x** and ε an error coefficient (Jolliffe, 2002). The regression coefficients array $\boldsymbol{\beta}$ is then estimated by

$$\boldsymbol{\beta} = (\mathbf{x}'\mathbf{x})^{-1}\mathbf{x}'\mathbf{y}. \qquad 3.23$$

This expression holds only when no multicollinearities exists. This is not likely in the presented analysis. Therefore it is more convenient to calculate the regression coefficients directly from the reduced set of PCs, $\hat{\mathbf{Z}}$, since the principal components are uncorrelated. This is done by following the procedure of Jolliffe (2002), which starts by rewriting (3.23),

$$\mathbf{X}\hat{\mathbf{A}}\hat{\mathbf{A}}'\boldsymbol{\beta} = \hat{\mathbf{Z}}\boldsymbol{\gamma}, \qquad 3.24$$

In which $\hat{\mathbf{A}}$ and $\hat{\mathbf{Z}}$ denote the reduced sets of eigenvectors and PCs, respectively, $\boldsymbol{\beta}$ is now the regression coefficient array corresponding to the standardised input variables and $\boldsymbol{\gamma} = \hat{\mathbf{A}}'\boldsymbol{\beta}$. From this (3.24) is written as,

$$\mathbf{Y} = \hat{\mathbf{Z}}\boldsymbol{\gamma} + \boldsymbol{\varepsilon}. \qquad 3.25$$

With **Y** the array of standardised output variables.
Since the principal components are orthogonal, a least square method is now allowed to use in order to obtain $\boldsymbol{\gamma}$,

$$\boldsymbol{\gamma} = \left(\hat{\mathbf{Z}}'\hat{\mathbf{Z}}\right)^{-1}\hat{\mathbf{Z}}'\mathbf{Y}. \qquad 3.26$$

The regression coefficients in terms of the standardized input data follow from,

$$\boldsymbol{\beta} = \hat{\mathbf{A}}\boldsymbol{\gamma} \qquad 3.27$$

This procedure is equivalent to equations (3.24) and (3.25), but possible difficulties caused by multicollinearities are avoided by using multiple regression on the principle components.

Several methods are used to test the performance of the PCR. First, the R^2, as defined in section 3.3.1, is used to test the goodness of fit of the regression. Second, the sensitivity of regression coefficients from the PCR to the used observations will be tested. For this, a cross validation is used. With this method one observation is retained from the total set of n observations. Then, the regression coefficients are calculated with the PCR with the remaining n-1 observations. This procedure is repeated for all n observations, in which every observation is used once as a test observation. This procedure will result in a $[p \times n]$ matrix of regression coefficients, in which p is the number of regression coefficients and n the number of observations. When this matrix is averaged over all n observations an average regression coefficients array of size p is obtained. The standard deviations will then denote the accuracy with which the regression coefficients are calculated. Large standard deviations denote a large variability between cross validation runs, hence low accuracy, while low standard deviations denote the opposite.

Third, synthetic data will be generated by calculating new observations from the original observations by using the expected error margin for each variable, to test the sensitivity of the analysis to the total size of the data set. The synthetic observations are calculated within this margin, in which patterns observed in the original data are taken into account. The errors are intuitively chosen, being +/- 20% for the sand wave migration, +/- 10% for the tidal current information, +/- 20% for the sand wave height, +/- 20% for the surface waves, +/- 50μm for the sediment grain size and +/- 20 cm for the local water depth. With this method the number of observation are increased by a factor three.

Fourth, the dependency on the number of input variables will be tested. For this, calculations are performed in which the number of input variables are reduced by discarding all constrained input variables (e.g. the M2 and M4 ellipticity), since problems due to normality may occur by these type of variables.

Finally, the obtained average regression coefficients are used to predict the sand wave length and migration for two additional observations for each area. All environmental parameters that are concerned for the regression model will also be measured/calculated for the additional observations. Then, the sand wave length and migration rate will be calculated with the regression model. Comparing this result with the sand wave length and migration rate, directly determined from the data, will indicate the predictability of the regression model.

The results of these tests will be presented in chapter 4, since it uses the results for the sand wave migration rate, sand wave length and the environmental parameters, which will be presented in their final form in section 4.1, 4.2 and 4.3, respectively.

Chapter 4. Results

4.1 Sand wave morphology

Visual inspection of the DEMs (like Figures 3.2 and 3.3) reveals that in both the IJmuiden and the Rotterdam area a variety of different bed forms occur, from shoreface-connected ridges to mega ripples. At IJmuiden, sand waves show relatively regular patterns, with a southwest northeast dominating direction. Sand waves patterns for Rotterdam are more irregular with a large number of bifurcations. Nevertheless also for the Rotterdam sand waves a dominating direction from southwest to northeast can be distinguished.

The results for sand wave length and height are presented in Table 4.1 (IJmuiden) and Table 4.2 (Rotterdam). Sand waves for the IJmuiden area are generally about 420 m long, with a minimum wavelength of 175 m and a maximum of 740 m and a standard deviation of 84 m. These sand waves have an average height of 2.8 m, with a standard deviation of 0.6 m. The table shows that along profile 7 the longest sand waves are found. This result is probably biased, since only 2 sand waves are located along this profile. Comparing the results of the long and short profiles also indicates that the calculated average sand wave length may be biased by the number of sand waves taken into account. The sand wave height seems to be less dependent on the number of sand waves. Finally, sand waves along the northern part of profile 2 (profile 2_2) are about 65 meter longer than the southern part (profile 2_1). The average height is almost consistent for the three profiles (=2, 2_1, 2_2), although the minimum measured height for the northern part is higher than the minimum height for the southern part.

Rotterdam sand waves have an average length of 250 m, with a minimum of 100 m and a maximum of 480 m and a standard deviation of 36 m. These sand waves have an average height of 3.4 m, with standard deviation of 0.7 m. Inspection of the table indicates that sand wave lengths do not change towards the coast, while sand wave heights tend to decrease.

Profile	Profile length[m]	N sand waves	Average length [m]	Min-max length [m]	Average height [m]	Min-Max height [m]
1	6200	16	380	175 – 740	3.4	1.9 – 5.0
2	10000	24	395	185 – 670	3.3	1.8 – 4.9
2_1	5000	12	365	185 – 635	3.2	1.8 – 4.9
2_2	5000	11	430	220 – 685	3.4	2.5 – 4.7
3	5300	11	450	255 – 760	3.4	2.0 – 4.6
4	5000	11	428	175 – 740	2.6	1.2 – 3.6
4 short	787	2	260	230 – 300	1.9	1.0 – 2.8
5	4000	9	395	210 – 560	2.3	1.0 – 3.4
5 short	740	1	400	-	2.5	-
6	2600	7	310	210 – 365	1.5	0.9 – 2.2
6 short	746	2	245	205 – 285	1.7	1.7 – 1.8
7	2100	2	615	470 – 755	2.8	2.8 – 2.9
Average			418 (σ=84)		2.5 (σ=0.6)	

Table 4.1 Average and ranges of sand wave lengths and heights for the IJmuiden area. Also averages for the total area are shown, with their standard deviations, *σ*.

Profile	Profile length[m]	N sand waves	Average length [m]	Min-max length [m]	Average height [m]	Min-Max height [m]
R1	10200	38	315	185 – 440	4.0	1.5 – 7.5
R2	6000	27	200	100 – 355	3.2	1.1 – 6.1
R3	5800	21	270	125 – 480	4.1	1.3 – 7.6
R4	3500	15	220	100 – 365	3.5	1.7 – 6.5
R5	2950	12	205	105 – 330	3.1	1.0 – 4.3
R6	1450	5	225	145 – 345	3.3	2.6 – 4.2
R7	2450	8	245	175 – 375	3.6	1.8 – 4.9
R8	2150	8	250	170 – 335	3.3	2.2 – 4.0
R9	2000	6	315	185 – 440	2.1	1.7 – 2.7
Average			249 (σ=36)		3.4 (σ=0.7)	

Table 4.2 Average and ranges of sand wave lengths and heights for the Rotterdam area. Also averages for the total area are shown, with their standard deviations, *σ*.

4.2 Crest/trough migration

Results of the migration rates for the crests and troughs, determined using the regression method, are presented in Table 4.3 (IJmuiden) and 4.4 (Rotterdam). Table 4.3 shows that the crests of the IJmuiden sand waves migrate in the southwest to northeast direction, with average rates between 2.1 m/year to 3.3 m/year, with extremes ranging from 1.8 m/year to 4.9 m/year. Crest migration rates are slightly lower along the short sections of profile 4 to 6, than is calculated for the long sections of these profiles. The average goodness of fit varies between 0.70 and 0.86, while the error of estimate ranges from 4.2 m to 9.4 m. This shows that the positions of the crest points are migrating along a clear trend. Migration rates for the IJmuiden troughs show rather different results. Average migration rates for the troughs vary between -0.1 m/year (which is in the northeast southwest, or upstream direction) and 1.2 m/year and extremes ranging from -1.3 m/year to 3.5 m/year. Moreover, the goodness of fit is rather low with averages between 0.03 and 0.29 and the average error of estimate ranging from 5.3 to 14.3. The low goodness of fit shows that the trough points are not migrating steadily, but are migrating back and forth around a certain average location. Since the crests are all migrating in the same direction, the present analysis reveals that the sand waves in IJmuiden are becoming increasingly asymmetric.

Average migration rates of profiles 1 to 3 of the Rotterdam sand wave crests (Table 4.4) are close to zero, with extremes between -0.9 m/year and 1.5 m/year and an average goodness of fit increasing from 0.33 for profile 1 to 0.57 for profile 3. This indicates that the crests for these profiles migrate around an average position. The crests for the other profiles migrate with average rates between 0.7 m/year and 2.1 m/year and show steady migration with an average goodness of fit ranging from 0.69 to 0.92. The Rotterdam troughs show similar results; low migration rates with low goodness of for the profiles farthest offshore and increasing migration rates with increasing goodness of fit for the profiles closer to the shore. This shows that the mobility of the Rotterdam sand waves increases towards the shore.

profile	Migr. crest [m/yr]		av. R^2 [-]	av. S_e [m]	Migr. troughs [m/yr]		av. R^2 [-]	av. S_e [m]
	av.	*min-max*			*av.*	*Min-max*		
1	2.4	1.8 – 3.0	0.81	4.8	0.2	-1.3 – 1.4	0.21	7.7
2	2.3	1.3 – 2.8	0.83	4.8	-0.1	-1.3 – 1.3	0.14	7.3
2_1	2.5	2.1 – 2.8	0.81	5.0	0.0	-1.3 – 1.4	0.16	7.7
2_2	2.1	1.3 – 2.5	0.84	4.2	-0.1	-0.7 – 1.8	0.13	7.5
3	2.6	1.9 – 3.6	0.86	4.5	0.2	-0.6 – 1.8	0.13	7.7
4	2.8	2.6 – 3.8	0.77	6.9	0.4	-0.6 – 1.7	0.13	11.1
4 short	2.4	2.0 – 2.8	0.80	4.4	0.4	-0.3 – 1.3	0.16	6.2
5	3.3	2.2 – 4.9	0.80	7.9	0.4	-0.9 – 3.5	0.11	12.4
5 short	3.0	-	0.88	4.3	-0.4	-1.1 – 0.4	0.29	5.3
6	3.1	2.6 – 3.5	0.70	9.4	1.2	0.6 – 2.1	0.21	11.2
6 short	2.4	2.4 – 2.5	0.80	4.8	0.2	-0.2 – 0.6	0.06	6.1
7	2.7	2.7 – 2.8	0.78	8.0	0.2	-0.4 – 0.9	0.03	14.3

Table 4.3 Average and minimum/maximum migration rate results for the IJmuiden profiles for the crests and troughs points. Results are calculated with the linear regression method. Also shown are the average goodness of fit and error of estimate, which are averaged over all crest/trough points along a profile.

profile	Migr. crest [m/yr]		av. R^2 [-]	av. S_e [m]	Migr. troughs [m/yr]		av. R^2 [-]	av. S_e [m]
	av.	*min-max*			*av.*	*Min-max*		
R1	-0.1	-0.9 – 0.6	0.33	2.4	0.0	-1.3 – 1.9	0.30	4.2
R2	0.1	-0.9 – 1.5	0.43	1.5	0.0	-1.1 – 1.8	0.40	2.0
R3	0.4	-1.0 – 1.4	0.57	1.7	0.3	-0.8 – 1.3	0.44	2.4
R4	0.7	0.0 – 1.2	0.81	1.1	0.5	-2.0 – 1.2	0.68	1.9
R5	1.0	0.7 – 2.1	0.89	1.3	0.9	-0.5 – 1.3	0.72	2.6
R6	0.7	0.5 – 0.9	0.85	1.2	0.6	-0.2 – 0.9	0.55	2.3
R7	1.0	0.1 – 2.0	0.69	1.7	1.5	0.8 – 5.0	0.87	2.4
R8	1.0	0.1 – 1.3	0.80	1.4	0.9	0.2 – 1.8	0.71	2.0
R9	2.1	1.5 – 3.1	0.92	2.4	2.1	1.4 – 3.2	0.89	2.4

Table 4.4 Average and minimum/maximum migration rate results for the Rotterdam profiles for the crest and trough points. Results are calculated with the linear regression method. Also shown are the average goodness of fit and error of estimate, which are average over all crest/trough points along a profile.

4.3 Environmental parameters

The environmental parameters per profile are shown in Table 4.5 and Table 4.6, respectively. The tables show that the environmental conditions for Rotterdam vary to a greater extent than for IJmuiden. For example, the difference between the deepest and shallowest profile in Rotterdam is about 10 meter, while for IJmuiden this difference is just over 3 m. The same conclusion holds for the median grain size. In Rotterdam the maximum value is 445 μm and the minimum value is 301 μm. In IJmuiden these values range between 317 μm and 266 μm.

4.3.1 Tides

Table and Table 4.6 also present the result from the harmonic decomposition of the current velocity field at the Rotterdam and IJmuiden areas. Clearly, the M2 current is stronger for Rotterdam than for IJmuiden, with a maximum of 0.79 m/s in Rotterdam versus 0.66 m/s in IJmuiden. For both sites the M2 current decreases shoreward, but in the Rotterdam area the decrease is stronger than in the IJmuiden area, with a minimum of 0.67 m/s versus 0.63 m/s, respectively.

The M2 tides for both sites are almost unidirectional, although this is more pronounced for IJmuiden than for Rotterdam, where the ellipticity may reach 0.12. The ellipses in the IJmuiden area are almost parallel, with inclination angles varying between 65^{o} and 67^{o} (not shown in the table). In contrast, in the Rotterdam area the ellipses rotate clockwise shoreward, from an angle of 64^{o} for profile 1 to 51^{o} for profile 9.

The M4 constituent shows larger differences between the two sites, especially for the ellipticity and the inclination angle. In IJmuiden the ellipticity reaches values up to 0.76, while in Rotterdam the ellipticity does not exceed 0.27. In addition the inclination angle varies between 13^{o} and 20^{o} for Rotterdam. In IJmuiden this variation is larger; 116^{o} to 144^{o}.

The relative phases between the M2 and M4 tidal constituent of both sides differs about 200^{o}. For IJmuiden the phase shift range from about 340^{o} farthest offshore to about 360^{o} closest to the coast. For Rotterdam the phase shift range from 130^{o} for profile R2 to 102^{o} for profile R9, indicating that the phase shift decreases towards the coast. However, note that for profile R1a phase shift of 115^{o} is obtained, which does not agree with the overall trend of the phase shifts for Rotterdam.

Profile	Depth [m]	U_{max} M2 [m/s]	ε M2 []	U_{max} M4 [m/s]	ε M4 []	ϕ_{M4-M2} [°]	Z0 [m/s]	D_{50} [µm]	$\theta_w > \theta_{cr}$ [%]
1	27.0	0.66	0.018	0.047	0.51	339	0.019	309	3.0
2	26.5	0.66	0.009	0.047	0.54	342	0.018	308	3.4
2_1	26.5	0.66	0.006	0.046	0.55	338	0.019	317	3.4
2_2	26.6	0.65	0.012	0.047	0.54	345	0.018	300	3.3
3	26.0	0.65	0.001	0.046	0.58	346	0.019	288	3.8
4	24.5	0.64	0.006	0.046	0.62	352	0.018	278	6.0
5	24.3	0.64	0.011	0.045	0.64	355	0.017	268	6.2
6	23.8	0.63	0.012	0.043	0.67	354	0.022	271	7.0
7	23.6	0.63	0.005	0.041	0.76	0.84	0.029	266	7.3
σ	1.4	0.011	0.0049	0.0018	0.080	7.8	0.0036	20	1.8

Table 4.5 Environmental parameters for IJmuiden averaged over a profile, parameters shown are: Depth, Amplitude M2 (U_{max} M2), M2 ellipticity (ε M2), Amplitude M4 (U_{max} M4), M4 ellipticity (ε M4), relative phase M4-M2 tide (ϕ_{M4-M2}), residual background current (Z0), grain size (D_{50}) and the relative influence of the surface waves on the sediment transport (θ_{cr}). Also shown is the standard deviation per parameter for all profiles.

Profile	Depth [m]	U_{max} M2 [m/s]	ε M2 []	U_{max} M4 [m/s]	ε M4 []	ϕ_{M4-M2} [°]	Z0 [m/s]	D_{50} [µm]	$\theta_w > \theta_{cr}$ [%]
R1	36.0	0.79	0.11	0.060	0.07	115	0.019	445	0.1
R2	35.4	0.73	0.11	0.053	0.09	130	0.040	421	0.1
R3	33.3	0.71	0.10	0.054	0.11	124	0.044	398	0.0
R4	32.6	0.73	0.11	0.057	0.16	122	0.041	372	0.1
R5	31.8	0.72	0.11	0.056	0.19	121	0.039	317	0.1
R6	32.0	0.72	0.12	0.057	0.21	120	0.039	332	0.1
R7	29.0	0.71	0.12	0.057	0.25	116	0.039	306	0.4
R8	28.4	0.69	0.12	0.058	0.27	110	0.034	336	0.5
R9	26.6	0.67	0.11	0.059	0.27	102	0.034	301	1.3
σ	3.2	0.032	0.0059	0.0021	0.078	8.3	0.0074	53	0.4

Table 4.6 Environmental parameters for Rotterdam averaged over a profile, parameters shown are: Depth, Amplitude M2 (U_{max} M2), M2 ellipticity (ε M2), Amplitude M4 (U_{max} M4), M4 ellipticity (ε M4), relative phase M4-M2 tide (ϕ_{M4-M2}), residual background current (Z0), grain size (D_{50}) and the relative influence of the surface waves on the sediment transport (θ_{cr}). Also shown is the standard deviation per parameter for all profiles.

4.3.2 Surface waves

The surface waves reach average heights of about 1.3 m for both locations, with a period of 4.6 s for IJmuiden and 4.4 s for Rotterdam, which agrees well with Van Dijk & Kleinhans (2005). For both locations 3 to 4 iterations are needed to calculate the wavelength, which reaches averages of 33 m for IJmuiden and 31 m for Rotterdam. Since depth and grain sizes differ for both sites, the largest differences are found for the orbital velocity and amplitude of fluid particles at the bottom.

The orbital velocity for IJmuiden have averages between 0.02 m/s (profile 1) and 0.03 m/s (profile 7) with maxima of 0.24 m/s to 0.35 m/s. Finally, the orbital amplitude have averages between 0.02 m and 0.03 m and maxima between 0.28 m to 0.34 m. The range of these parameters for Rotterdam is larger, but the minima are decreased. The average orbital velocities range from 0.003 m/s (profile R1) to 0.01 m/s (profile R9), with maxima of 0.15 m/s (profile R1) to 0.33 m/s (profile R9). The average amplitudes of the particle trajectories range from 0.002 m to 0.01 m, with maxima ranging from 0.16 m to 0.36 m, for profile R1 and profile R9, respectively.

Whether the surface wave action is sufficient to induce a bed shear stress additional to the bed shear stress induced by the maximum tidal current, is calculated with equation (3.6). Averaged for each study area and over all events of sufficient wave action (hence, when $\theta_w > \theta_{cr}$) , it is calculated that surface waves may increase the total bed shear stress with 26% for IJmuiden and with 23% for Rotterdam, with τ_{c_max} ~ 0.9 Nm^{-2} and τ_{c_max} ~ 1.25 Nm^{-2}, respectively.

The relative number of events over the twenty year record for which the Shields wave parameter exceeds the critical Shields parameter for waves is presented in Table 4.5 and 4.6. This shows that for IJmuiden surface wave action is sufficient to stir sediment at the bed for about one twentieth of the time. In contrast, for Rotterdam currents induced by surface waves reach the bottom rarely, thus the critical Shields parameter is exceeded very occasionally.

4.3.3 Dredging

Figure 4.1 shows the dredged areas for the IJmuiden and Rotterdam areas. Inspection of the of bathymetric maps shows that the natural bed forms are completely destroyed by dredging activity. Therefore, the expected orientation of the sand waves are determined as described in section 4.3.5. The location of the chosen profiles are also shown in Figure 4.1.

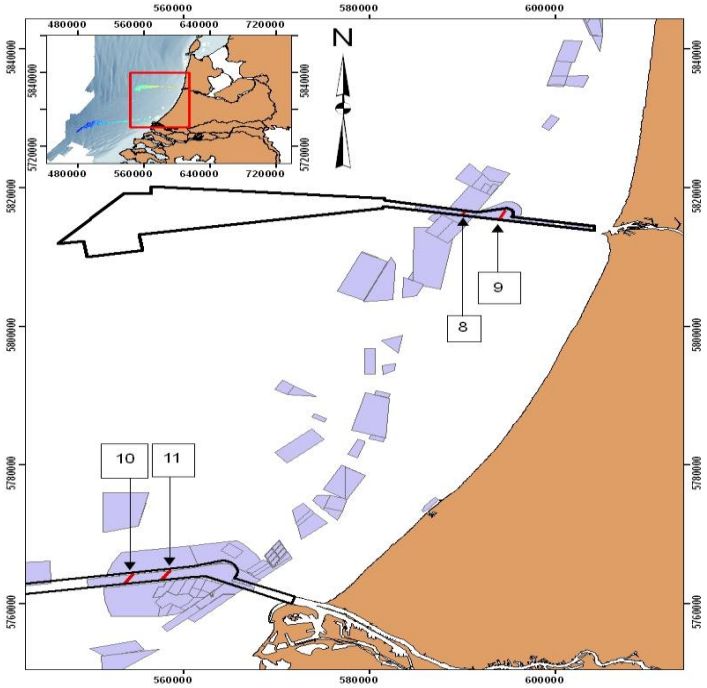

Figure 4.1 Sand extraction sites for Rotterdam and IJmuiden. The blue areas are frequently dredged. Also shown are the additional profiles through the dredged areas.

The *xz*-profiles are shown in Figure a-d. Along all profiles the sand wave field is clearly destroyed and no natural sand wave patterns can be distinguished. For Figure 4.2a information about dredging activity was delivered for the years 1998 to 2003. However, between 1991 and 1995 and between 1995 and 1996 also a clear increase in water depth is visible. The same holds for Figure 4.2b, where dredging information was delivered for the years 2000 to 2003 and where an increase in water depth occurs between 1994 and 2000. For the Rotterdam profiles (Figure 4.2 c-d) dredging information was delivered for the years 1997 and 2008. Again, an increase in water depth is shown between 1991 and 1995. Thus, not all dredging information was delivered, which makes it difficult to study the effect of dredging on sand wave characteristics, since it is not known which pattern is natural and which is anthropogenic. Furthermore, since the sand wave pattern is completely destroyed, the method used in this study to determine ct-points and migration rates can not be used for the dredged parts and will thus not be presented in this study. Outside the regions for which the dredging information was delivered, one sand wave at the IJmuiden area was observed (by inspection of dredging tracks in the bathymetric maps) for which the crest was removed (Appendix Figure A.1). After the dredging

activity, no additional dredging events could be identified in the bathymetric map. The figures in the appendix show that no sedimentation is identified by the depth evolution of a single point at the dredged area, in the short time span of available data sets after the dredging event (Appendix, Figure A.2). In addition, a cross section is drawn through this sand wave field (Appendix, Figure A.3). This clearly shows the dredging event between the 2006 measurements, resulting in an increase of the water depth by about 1.2 m. However, to the right of the sand wave crest, the water depth has been decreased by about 40 cm. Furthermore, between the 2006 and 2007 measurements some peaks are removed, but also some local lows are filled (see the spiky pattern between the 100 m and 300 m distance point in Figure A.3)

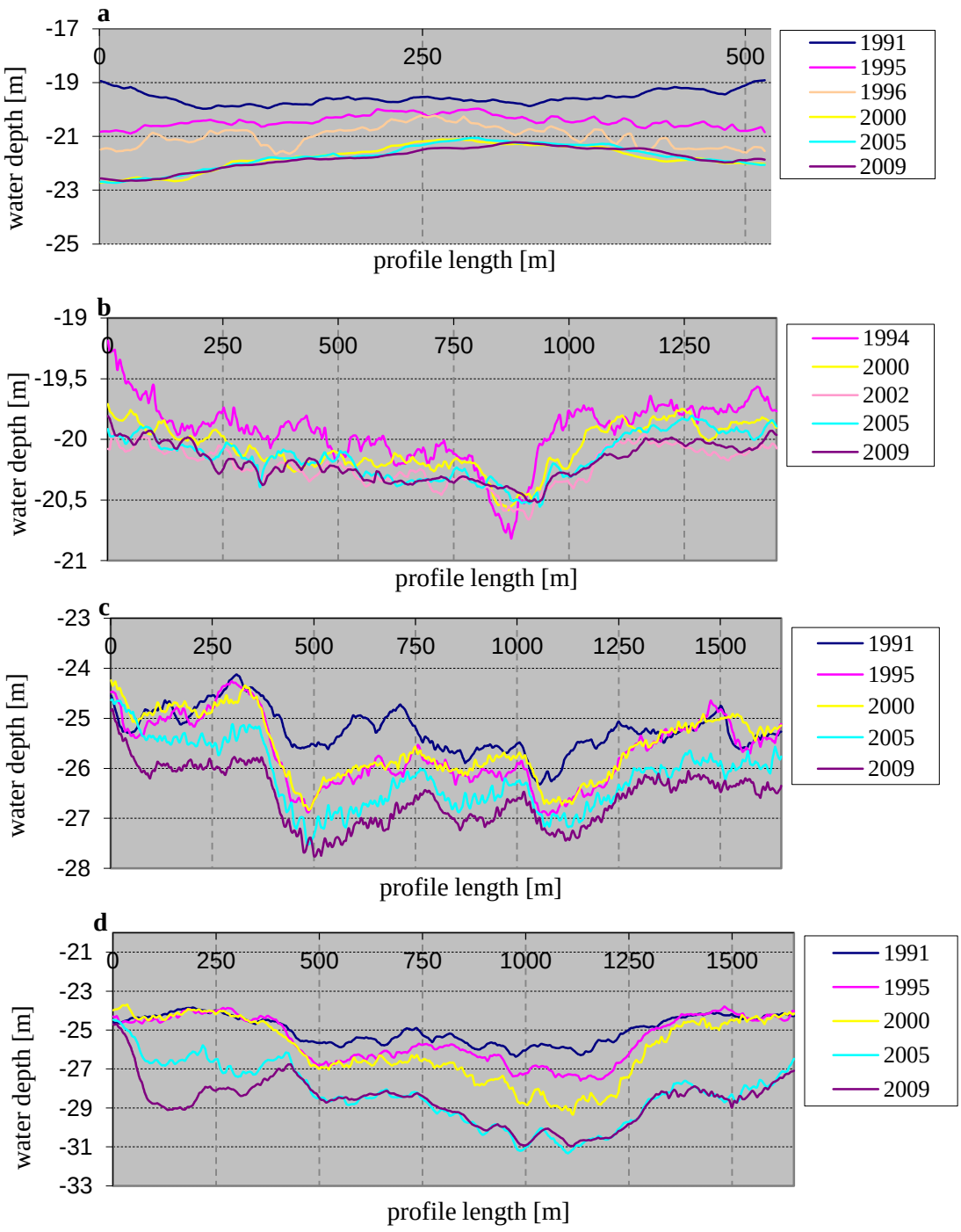

Figure 4.2 Results for dredged cross sections a) IJmuiden profile 8; b) IJmuiden profile 9; c) Rotterdam profile 10; d) Rotterdam profile 11. For convenience not every data set is shown. The presented data sets clearly show a destroyed sand wave field. Furthermore, clear deepening of the channels over time is shown.

4.4 Factor analysis

4.4.1 Simple correlations

In Figure 4.3 sand wave length is plotted against the environmental parameters. Likewise in Figure 4.4 this is done for the migration rate.

A larger number of environmental parameters are analyzed for sand wave migration. Since it was not possible to discriminate between crests and troughs for a number of environmental parameters, averages over all trough and crest migration rates along a profile are taken, resulting in typical sand wave migration rates for the profile of interest. It is already shown that sand waves migrate faster in the IJmuiden area than in the Rotterdam area. However, the figure shows that the migration rates for Rotterdam show a larger distribution than the migration rates for IJmuiden. At first sight the simple plots indicate correlations between the migration rates and some environmental parameters. The sand waves tend to move slower for increasing M2 amplitude, increasing D_{50}, increasing sand wave height and increasing water depth. Clusters discriminating between Rotterdam and IJmuiden are visible for the M4 amplitude, M2 and M4 ellipticity, and the phase shift.

Clearly these simple plots can not be decisive in determining the controlling factors for sand wave length or migration rate.

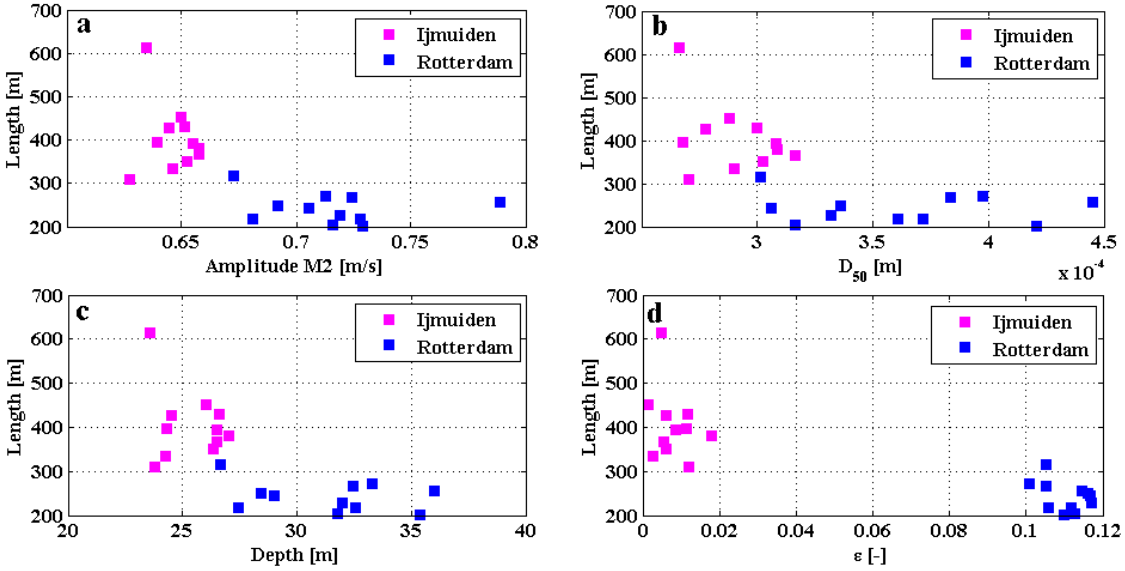

Figure 4.3 Sand wave length versus a) the M2 amplitude; b) grain size; c) water depth; d M2 ellipticity.

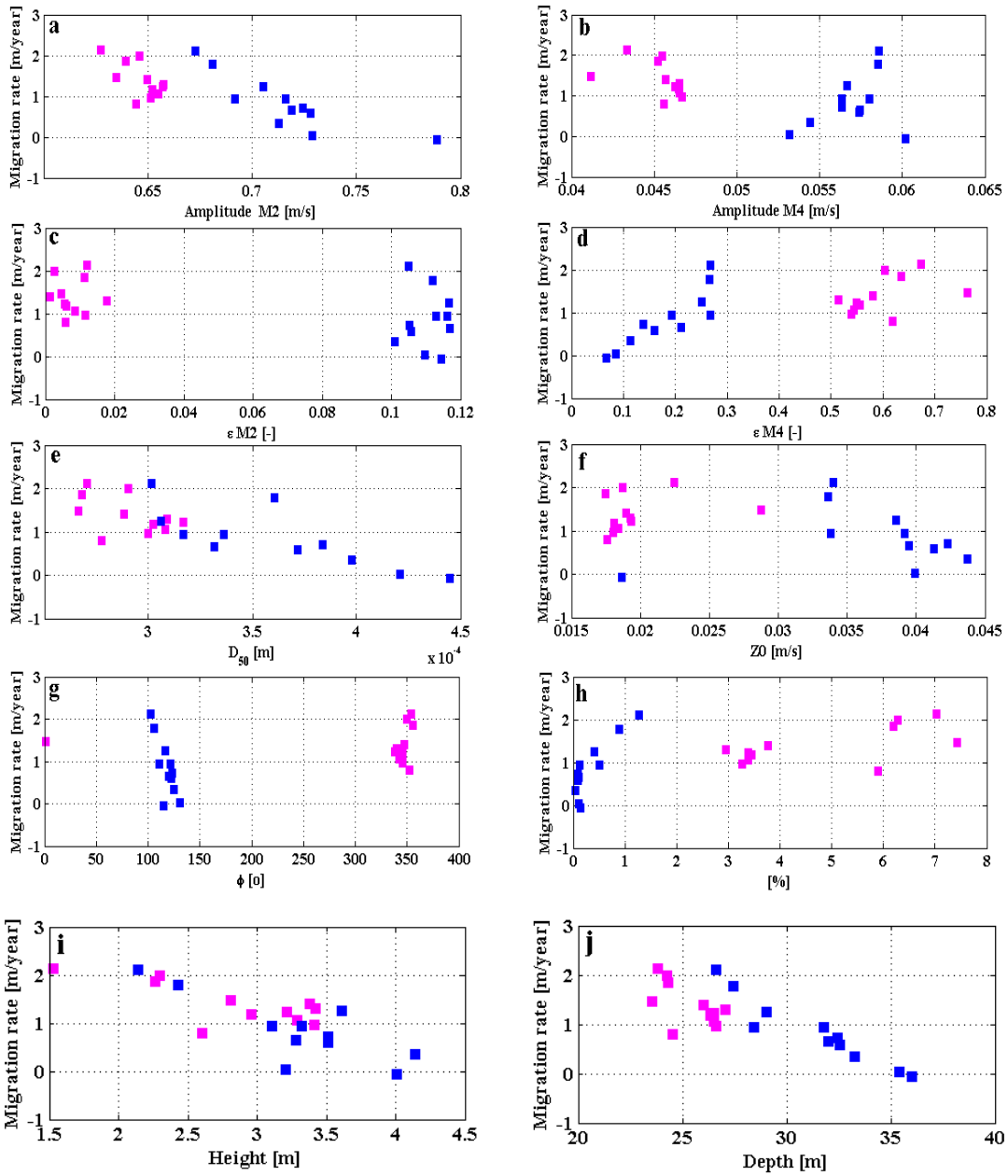

Figure 4.4 Sand wave migration versus all environmental parameters from Tables 3.5 and 3.6

4.4.2 Principal component regression results

Threshold selection

Table 4.7 presents the PCR results in which the environmental parameters selected for sand wave migration rates are used as input variables and the migration rates are used as output variables, for 9 observation at the IJmuiden area. The presented results follow directly from equation 3.29, hence the regression coefficients resulting from the PCR in terms of the original standardised input variables. The table shows that in order to retain 80% of the original variance in the new dataset only 2 PCs are needed, while 3 PCs are needed when 90% of the variance is required. In general, the goodness of fit of the PCR increases from 0.46 to 0.52. Considering the size of the regression coefficients two remarkable changes are shown when the explained variance is increased from 80% to 90%. The first is the increase of the coefficients of the M2 ellipticity from 0.08 to 0.30. This indicates that the ellipticity is dominantly explained by the third PC. The second is a significant decrease for $\phi_{M4\text{-}M2}$. These differences indicate that the choice of the threshold of minimum variance is rather important and that information might be lost when the chosen threshold is too low. The choice of 90% explained variance along the PCs provides the best result, this threshold will be used in the following.

Parameter	**Coefficients variance >80% n PC's=2**	**Coefficients variance >90% n PC's=3**
Constant	0.00	0.00
Water depth	-0.12	-0.09
$U_{max\ M2}$	-0.14	-0.15
ε_{M2}	0.08	0.30
$U_{max\ M4}$	-0.02	-0.06
ε_{M4}	0.05	0.05
$\phi_{M4\text{-}M2}$	0.10	0.05
Z_0	-0.06	0.02
D_{50}	-0.13	-0.09
θ_{cr}	0.11	0.09
Sand wave height	-0.20	-0.20
R^2	0.46	0.52

Table 4.7 Results of the regression coefficients for two thresholds for minimum explained variance by the PCA. The first column shows the environmental parameters, the second column shows the coefficients when at least 80% of the variance is explained; the third column shows the coefficients when at least 90% of the variance is explained. Finally R^2 is the goodness of fit

Sensitivity analysis

To test the sensitivity of the PCR analysis to the size of the input data, the PCR for the sand wave migration rates for the combined sites, is considered (Table 4.8). The table shows the results when one analysis is performed on all observations (which result in 18 observation for the combination), when a cross validation is used, hence 18 runs, and when a cross validation is performed on a data set with additional synthetic data, hence 54 runs. Comparing the regression coefficients of the single run and the averages of the coefficients from the 18 cross validation runs, shows that the size of some coefficients may change significantly between runs. This is especially shown for $\varepsilon_{M2,}$ $U_{max\ M4}$, ε_{M4}, $\phi_{M4\text{-}M2}$ and Z_0, for which the standard deviations show that between cross validation runs, the regression coefficients may be calculated within a range of 30% to 80% around their mean. This indicates that the PCR does not perform well in calculating the coefficients of these variables. These coefficients are however of minor importance, compared to the coefficients of the local water depth, sediment median grain size and the sand wave height.

Adding synthetic data increases the importance of ε_{M4}, $\phi_{M4\text{-}M2}$ and Z_0 with a factor 3, while the importance of $U_{max\ M2}$ and the sand wave height is decreased with almost 50%. Considering the relatively high standard deviations of ε_{M4}, $\phi_{M4\text{-}M2}$ and Z_0 for the $n=18$ cross validation, it is suggested that generating synthetic data for these variables inflates the errors, which may have biased the calculations of the coefficients for $U_{max\ M2}$ and sand wave height. In addition, the size of coefficients with low standard deviations for the n=18 cross validation run does not change for the n=54 cross validation run, which is especially true for the coefficients of local water depth, median grain size, influence of surface waves and sand wave height. It is therefore concluded that the regression coefficients averaged over all cross validation run for the original observations provides the best result for the PCR; relatively large coefficients with low standard deviations are more important than small coefficients with large standard deviations. Comparable results are obtained for tests on the individual data sets of the Rotterdam and IJmuiden areas. These results are shown in the Appendix.

Finally, Table 4.9 presents the results for the test when the constrained variables are discarded from the PCR analysis. It is shown that the PCR is relatively robust, since the coefficients are comparable to the results of Table 4.8.

Parameter	*n=18*	Cross validation *n=18*		Cross validation *n*=54	
		av. β	σ	av. β	σ
Constant	0.00	0.00	0.00	0.00	0.000
Depth	-0.19	-0.18	0.01	-0.21	0.008
$U_{max\ M2}$	-0.15	-0.14	0.02	-0.03	0.015
ε_{M2}	0.07	0.08	0.03	-0.02	0.007
$U_{max\ M4}$	0.03	0.07	0.04	-0.02	0.006
ε_{M4}	0.07	0.04	0.02	0.16	0.002
$\phi_{M4\text{-}M2}$	-0.07	0.00	0.03	-0.11	0.009
Z_0	0.12	0.08	0.03	0.13	0.013
D_{50}	-0.25	-0.23	0.02	-0.25	0.005
$\theta_w > \theta_{cr}$	0.11	0.08	0.02	0.17	0.005
Height	-0.41	-0.45	0.06	-0.25	0.006
R^2	0.80	0.79		0.70	

Table 4.8 Results for the PCR with the sand wave migration rates as ouptut variables for the combination of Rotterdam and IJmuiden; *n* denote the number of observations, av. β denote the average of the regression coefficients, which are averaged over *n* cross validation runs and σ is the correspondin standard deviations, Finally R^2 is the goodness of fit.

Parameter	Cross validation *n=18*		Cross validation *n*=54	
	av. β	σ	av. β	σ
Constant	0.00	0.00	0.00	0.00
Depth	-0.20	0.01	-0.31	0.004
$\boldsymbol{U_{max\ M2}}$	-0.17	0.03	-0.12	0.01
$\boldsymbol{U_{max\ M4}}$	0.01	0.04	-0.09	0.01
$\boldsymbol{Z_0}$	0.12	0.04	0.14	0.01
$\boldsymbol{D_{50}}$	-0.25	0.02	-0.34	0.003
Height	-0.43	0.08	-0.32	0.01
$\boldsymbol{R^2}$	0.79		0.76	

Table 4.9 Results for the PCR when the constrained variables are discarded, with the sand wave migration rates as ouptut variables for the combination of Rotterdam and IJmuiden; *n* denote the number of observations, av. β denote the average of the regression coefficients, which are averaged over *n* cross validation runs and σ is the corresponding standard deviations, finally R^2 is the goodness of fit.

Final results sand wave migration

Based on the results of the sensitivity tests the final results for the PCR are calculated with the cross validation based on the original observations. The results for the migration rates are shown in Table 4.10. The table shows that the standard deviations of the coefficients for the IJmuiden area are relatively high. The variation in the results for the regression coefficients between runs of the cross validation is larger than 100% for some variables, especially for of ε_{M2}, $U_{max\ M4}$ and Z_0. The coefficients for local water depth, $U_{max\ M2}$, D_{50}, influence of surface waves and sand wave height show standard deviations lower than 30% relative to their mean and are therefore considered to be reasonably robust. It is suggested that the latter five parameters are dominant in explaining the variation in migration rates for IJmuiden, although the error margins for calculating the coefficients are relatively large.

For the Rotterdam area the standard deviations are considerably smaller with respect to the mean of the regression coefficients then for the IJmuiden area. So, the analysis for Rotterdam is more robust. Only $U_{max\ M4}$ and Z_0 show large error margins with respect to their mean and are considered to be not important in explaining sand wave migration. The

coefficients for the other parameters are of equally size and their error margins are lower than 30%. So these parameters are of equal importance in explaining the variation in sand wave migration over the Rotterdam area. It is remarkable that the Therefore it is suggested that differences in sand wave migration rates occur due to differences between the M2 and M4 tidal constituents.

Combining the two sites indicates that the local water depth, $U_{max\ M2}$, the median grain size, the influence of surface waves and the sand wave height explain the variation in sand wave migration the best.

Location / **Parameter**	**IJmuiden** *n*=9		**Rotterdam** *n*=9		**Combined** *n*=18	
	av. β	σ	av. β	σ	av. β	σ
Constant	0.00	0.00	0.00	0.00	0.00	0.00
Depth	-0.09	0.04	-0.17	0.02	-0.18	0.01
$U_{max\ M2}$	-0.15	0.04	-0.17	0.01	-0.14	0.02
ε_{M2}	0.25	0.13	-0.07	0.04	0.08	0.03
$U_{max\ M4}$	-0.07	0.05	0.04	0.04	0.07	0.04
ε_{M4}	0.05	0.01	0.14	0.02	0.04	0.02
$\phi_{M4\text{-}M2}$	0.05	0.07	-0.14	0.02	0.00	0.03
Z_0	0.05	0.12	0.03	0.04	0.08	0.03
D_{50}	-0.09	0.06	-0.13	0.02	-0.23	0.02
$\theta_w > \theta_{cr}$	0.10	0.03	0.17	0.02	0.08	0.02
Height	-0.19	0.06	-0.13	0.06	-0.45	0.06
R^2	0.54		0.94		0.79	

Table 4.10 Results for the PCR for all areas, with the sand wave migration rate as output variable; *n* denote the number of observations, av. β denote the average of the regression coefficients, which are averaged over *n* cross validation runs and σ is the corresponding standard deviations, finally R^2 is the goodness of fit.

Final results sand wave length

Table 4.11shows the results of the PCR for the sand wave length for IJmuiden, Rotterdam and for the two areas combined, when a cross validation is used on the original

observations. For IJmuiden and Rotterdam the regression does not perform well with R^2 of 0.34 and 0.35 respectively. The performance of the regression increases when the both sites are considered together (R^2=0.72). The analysis indicates that sand wave lengths at IJmuiden are controlled by the M2 ellipticity, while for Rotterdam all variables may be considered of having equal importance. Finally, considering the two sites, the M2 ellipticity is the most dominating factor.

Location / **Parameter**	**IJmuiden** *n=9*		**Rotterdam** *n=9*		**Combined** *n=18*	
	av. β	σ	av. β	σ	av. β	σ
Constant	0.00	0.00	0.00	0.00	0.00	0.00
Depth	-0.10	0.08	-0.20	0.11	-0.13	0.01
$\boldsymbol{U_{max\ M2}}$	-0.02	0.09	-0.34	0.15	-0.23	0.02
$\boldsymbol{\varepsilon_{M2}}$	-0.46	0.10	-0.25	0.19	-0.59	0.05
$\boldsymbol{D_{50}}$	-0.08	0.08	0.14	0.27	0.08	0.02
$\boldsymbol{R^2}$	0.34		0.35		0.72	

Table 4.11 Results for the PCR for all areas, with the sand wave length as output variable; *n* denote the number of observations, av. β denote the average of the regression coefficients, which are averaged over *n* cross validation runs and σ is the corresponding standard deviations, finally R^2 is the goodness of fit.

Predictability of the model

The predictability of the obtained models is tested for four additional profiles, equally divided over the sites. For IJmuiden the control profiles are drawn between profiles 2 and 3 and between profiles 3 and 4. For Rotterdam this is done between profiles 3 and 4 and between profiles 8 and 9 (the red squares and crosses in Figure 4.5. The data obtained for the original profiles is also obtained for the control profiles. However this data is not used in the analysis, thereby enabling the opportunity to test the model in predicting sand wave lengths/ migration rates comparable to the measured lengths/ migration rates. The migration rate plot shows that the model is able to predict the measured migration reasonable well, for both the analyzed profiles as well as for the predicted profiles. The largest difference between predicted and measured is shown for IJmuiden profile 4. The model obtained for sand wave length is also able to predict the measured lengths, although the differences for the IJmuiden control profiles are rather large.

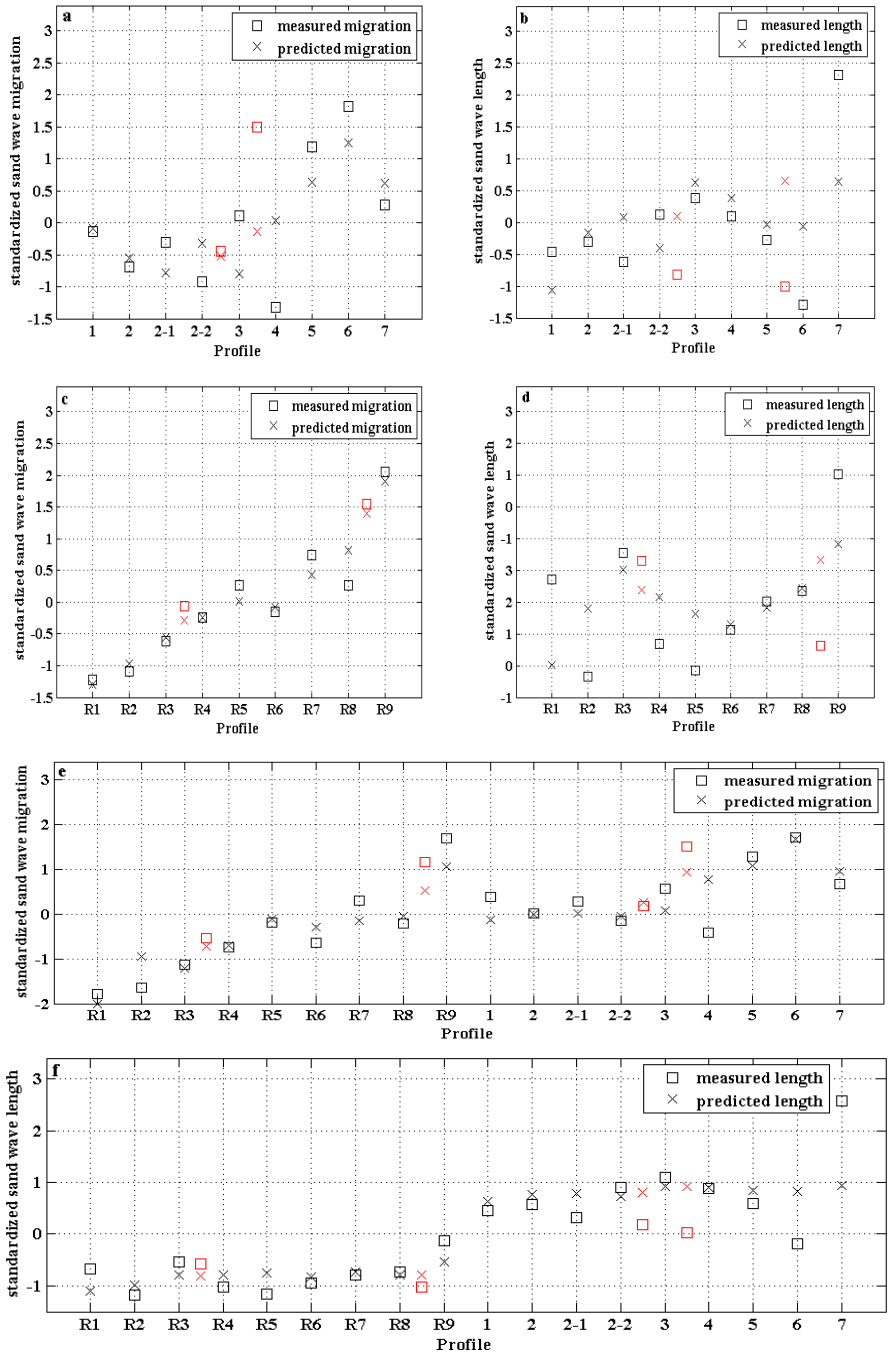

Figure 4.5 predictability plots of the PCR for both sand wave length and migration. Profiles are plotted along the horizontal axis. The normalized and standardized migration rates/ lengths are plotted on the vertical axis. a) IJmuiden sand wave migration; b) IJmuiden sand wave length; c) Rotterdam sand wave migration; d) Rotterdam sand wave length; e) sand wave migration for combined sites (prefix R denote Rotterdam profiles); f) length for combined sites.

Chapter 5. Discussion

5.1 Sand wave height and length

The sand wave height and length obtained by this study are compared with the literature (Table 5.1). Knaapen (2005), Dorst (2009) and Van Dijk et al. (2011) all report results of the spatial characteristics of sand waves at the Rotterdam and IJmuiden area. The analysis method used by Van Dijk et al. (2011) and this study is comparable to that of Knaapen (2005) in the sense that it selects the position of crests and troughs after eliminating noise from (mega)ripples. Dorst (2009) selects the position of crests and troughs using a statistical deformation analysis. This approach aims to reduce the errors in positioning and depth. The used analysis seems to be important in selecting the sand wave crests and troughs. The results obtained by Dorst (2009) are especially different for the profiles of the RNJ and RSS areas. This may result from the complex bed forms at these locations (Knaapen et al., 2001). The methods used by Knaapen (2005), Van Dijk et al. (2011) and this study are able to differentiate between different bed forms, resulting in the analysis of only the sand wave signal. The results obtained by Van Dijk et al. (2011) and Knaapen (2005) compare well with the results of this study. However, Knaapen (2005) under-predicts the sand wave height compared to this study and Van Dijk et al (2011) with 1 m to 2 m. A possible explanation can be that Knaapen (2005) uses a low-pass filter in which all wavelengths smaller than 30 m are removed, while in this study all wavelengths smaller than 100 m are removed.

Considering the relation between the environmental parameters and the sand wave length (figure 4.3), reveals that the sand wave length tend to decrease for increasing values of the parameters. Comparing these results with a data analysis from Van Santen et al. (2011) show a similar relation between the M2 amplitude and the sand wave length. Unfortunately Van Santen et al. (2011) were not able to correlate the other controlling parameters to the sand wave length with a data analysis. Field data of various authors gathered by Blondeaux & Vittori (2011) show that the sand wave length increases with increasing water depth, which contradicts the results of this study. In addition, from a number of modelling studies (Van Santen et al., 2011 and Borsje et al., 2009) it is expected that sand wave lengths also increase for increasing sediment grain size, which is also not observed for the presented study areas. Furthermore Van Santen et al. (2011) presented a relation between the tidal ellipticity of the dominating tidal constituent and the sand wave length. Their relation is, however, only valid for ellipticities of $0.1 < \varepsilon < 1$.

In the present study the ellipticity is in general close to or smaller than 0.1, so it is not likely that in the considered areas the sand wave length depend on the tidal ellipticity. In addition, since the relation between the sand wave length and the M2 maximum tidal current presented in this study compare well with literature, whereas the relations of local water depth and sediment grain size with the sand wave length do not, it is suggested that, for the areas of interest, the influences of these parameters on sand wave length subordinate to the influence of the M2 amplitude.

	Profile name	**L [m]**	**Height [m]**	**Mig [m/y]**
RNJ				
Knaapen (2005)	North Hinder 2	224.6	2.4	-0.2
Dorst (2009)	*average*	300 - 900	-	0
Van Dijk et al. (2009)	-	-	-	-
This study	R1	256	4.0	-0.06
RSS				
Knaapen (2005)	Short stay	235.5	2.2	0.1
Dorst (2009)	*average*	400 - 600	-	0
Van Dijk et al. (2009)	4	203	3.3	0.66
This study	R2	200	3.2	0.03
EAR				
Knaapen (2005)	Approach CH. 1	230.3	2.5	0.14
Dorst (2009)	*average*	200 - 500	-	0
Van Dijk et al. (2009)	-	-	-	-
This study	R4	218	3.5	0.6
IJAW				
Knaapen (2005)	-	-	-	-
Dorst (2009)	*average*	400	-	-3 - 7
Van Dijk et al. (2009)	WIJ12-pr1	398	2.9	2.2
This study	2	393	3.3	1.1

Table 5.1 Sand wave characteristics comparison found by three other studies. The abbreviations of the areas are presented in Figure 2.1.

5.2 Sand wave migration

The differences in migration rates resulting from the tested calculation methods may be caused by a natural back and forth migration from the crests and troughs, which is distinguishable with the interval method. However, since usually the troughs are more smooth than the crests, the method of selecting ct points may have difficulties in selecting the correct position, especially when the trough is relatively flat and shows low mobility. The method then may select the trough position around a certain average, which may result in the calculation of back and forth migration, while in reality the trough has not travelled. This effect may also explain the large migrations rates which are found by the interval method. Although less pronounced, this effect may finally also bias the migration rates of the crests. The average migration rate along a profile calculated with the interval method may therefore be biased to great extent by these outliers. The regression method on the other hand, is much more stable and is hardly effected by outliers. Yet, the regression method may be biased by the resolution of the data sets and misses the specific information on fluctuations in migration rates. However when one is dealing with a large number of data sets of the same location, it is suggested that migration rates should be estimated using a linear regression method.

Similar to the length and height of the sand waves, the migration rates are compared with literature (Table 4.3). Dorst (2009) was not able to determine migration rates for Rotterdam, since the errors for depth and positioning are in the range of the confidence interval. The methods used by Knaapen (2005), Van Dijk et al. (2011) and this study do not consider confidence intervals and are able to indicate migration rates. Migration rates found by Knaapen (2005) compare well with this study, whereas the migration rates calculated by Van Dijk et. al. (2011) are quite different. This is especially remarkable for the IJmuiden profile, since this profile is drawn at exactly the same location for both studies. Van Dijk et al. (2011) calculated the migration rates based on the interval method, while the presented migration rates for this study are obtained using the linear regression method. Besides, the difference may result from the resolution of the used data sets. For their analysis Van Dijk et al. (2011) use five data sets, with two being of MBES quality. For the same profile this study uses eight data sets, with five MBES sets. For IJmuiden it is shown that the SBES data sets may increase the average migration rates. Thus, the resolution of the used data sets may be very important in comparing the results with other studies.

A novelty of this study is the obtained difference in migration rates between crests and troughs for the IJmuiden area. No earlier studies report this contrast for the IJmuiden area. This contrast suggests that the asymmetry for the IJmuiden sand wave increase,

which implies an unstable sand wave field. Although remarkable, this phenomenon is not further analyzed, because the distinction between troughs and crests could not be made for the majority of the environmental parameters.

5.3 Environmental parameters

Some important remarks should be made about these parameters. First, in creating the sediment grain size distribution map it was a priori assumed that the distribution of the grain sizes depends on depth. As a consequence the results do not necessarily reflect the natural variability. Second, it is assumed that taking a two month current speed record is sufficient in determining the average tidal characteristics, which are assumed to be constant during the time length of the bathymetric data. It is therefore not possible to related possible variation in the currents to the sand wave behaviour Third, the tidal currents are depth averages and therefore also the characteristics of the tidal ellipses are depth averages. Prandle (1982) and Van der Giessen (1990) however show that the characteristics of the tidal ellipses may differ significantly with depth.

The results of the surface waves obtained by this study compare well to the results of Van Dijk & Kleinhans (2005). They also show that the critical Shields parameter is exceeded more frequently at shallow sites with small grain sizes than at deep sites with large grain sizes. It is shown that for IJmuiden the critical shields parameter is exceeded one twentieth of the time, whereas for Rotterdam the shields parameter is exceeded rarely. For the events that the critical Shields parameter is exceeded, the currents induced by surface waves increase the bottom shear stress with about 25%. Considering the small number of events for which surface waves effects reach the bed for Rotterdam, it is concluded that sediment transport for Rotterdam is only occasionally effected by surface waves, whereas for IJmuiden surface waves may have a considerably larger effect. An important difference with Van Dijk & Kleinhans (2005) is the used value of the critical Shields parameter. use an interval between 0.03 and 0.06 and only when the calculated shear stress agrees this interval sediment transport is allowed. This study however calculates a typical critical shear stress for every profile and sediment transport due to surface waves is allowed when this minimum is exceeded. This sediment transport is not limited by a maximum critical value.

This study hypothesized that the effects of dredging on sand wave dynamics could be analyzed from the provided data sets, using the method of Van Dijk et al. (2008). However it is shown that at frequently dredges locations the sand wave field is completely destroyed. The bed forms that can be distinguished in the cross sections are

very likely the result of human intervention. Hence, it is not possible to study the effect of dredging on sand wave behaviour using the provided data sets. Nevertheless at one individual location at the IJmuiden area a sand wave is identified from which in one year time the complete crest was removed (Appendix Figures A.1 to A.3) However, at this location no information is available about the exact dredging events. In the cross section and by following the elevation of a single point at the bed at this location, a clear increase in the water depth is identified, which is considered to be a result from dredging, in the year 2006. However, between the years 2006 and 2007, the spiky pattern visible between the 100 m and 300 m distance points was removed, but it can not be concluded that this is natural or forced behaviour. It could be that the local flow removed the spiky pattern, but this can also be the result of dredging events. Furthermore, to the right of the sand wave crest, the water depth decreased by 40 cm. It could be that dredged material was deposited here (forced behaviour), but it is also possible that natural sedimentation takes place. Therefore, it is concluded that exact information about dredging activity is necessary to clearly study the effect of dredging on sand wave behaviour. Finally, from Appendix Figure A.2, it is indicated that sedimentation rates are very low after dredging. Although only a view measurements are available after the dredging event, it is indicated that sand waves will not recover in ten years, which was hypothesised from observations in the Bisanseto sea, Japan, in chapter 1. (Katoh et al., 1998; Knaapen&Hulscher, 2002). Since the water depth at that location is comparable to the studied locations, it is suggested that this difference results from differences in the flow structure and the sediment grain size (Katoh et al., 1998). Since no clear answer can be provide to study the effects of dredging to sand wave behaviour, it is suggested to perform a modelling study.

5.4 Factor analysis

5.4.1 General remarks

A principal component regression technique is used to discriminate between the controlling parameters of sand wave migration. There are some important remarks about the used method. First of all the principal component regression will always provide a result, regardless the input parameters. The physical relevance and the reliability of the results therefore strongly depend on the chosen control parameters. Second, discarding parameters based on the PCR does not imply that these parameters do not have a physical relation to the sand wave length or migration. It does however imply that the particular parameter can not be considered explanatory in the distribution of the sand wave length or migration rate over the area of interest. Third, the stability of the analysis depends on the size of the input data set. For this study nine input locations are selected for both IJmuiden and Rotterdam, resulting in eighteen locations for the combination of both sides. It is noted that these data sets are small and that the number of environmental parameters is large. Therefore the obtained results can only be used in the context of the analyzed areas and can not be extended to other regions.
The stability of the analysis is tested by using a cross validation, by increasing the number of observations with synthetic data and by discarding the constrained input parameters. By doing so, it is shown that the analysis may be sensitive to the size of the number of observations. The standard deviations of the average regression coefficients, averaged over the number of cross validation runs, indicate the accuracy of calculating the regression coefficients between cross validation runs. Increasing the size of the dataset by adding synthetic observations should increase the robustness of the analysis. It is however indicated that this also may inflate some of the inaccuracies. Thus, the results of the PCR is obtained by using a cross validation on the original observations.

In principle, PCR is a powerful tool in selecting the input variables that control the behaviour of the output variables. However some important improvements are suggested for future analysis. In order to increase reliability it is suggested that the number of observations within the Rotterdam and IJmuiden areas are increased. Furthermore an increase in generality could be accomplished when the number of study areas are increased. Improvements can also be accomplished by incorporating non-linearity for the input variables that are not expected to be linear related to the output variables. Despite all of these points the analysis will always depend on the chosen input variables. So one has to know a priori the physical relevance of how the input variables are expected to be related to the output variables.

These discussion points are summarised in a Strengths, Weaknesses, Opportunities and Threats (SWOT) diagram (Table 5.2)

SWOT	
Strengths	**Weaknesses**
- Predictability of regression model - Determination of control parameters	- Size input data sets - Arbitrary selection procedure - Generality - Dependence on chosen input parameters
Opportunities	**Threats**
- Larger data sets - Incorporate nonlinear functions in regression model - Increase regions	- Physical relevance of selected parameters - Dependence reliability on distribution output data

Table 5.2 SWOT (Strengths, Weaknesses, Opportunities and Threats) analysis for applying PCR on sand wave behaviour.

5.4.2 Remarks on results for PCR and sand wave migration

The PCR performs best in explaining the migration rates distribution for Rotterdam. This is because the migration rate for Rotterdam shows a larger distribution than for IJmuiden (Figure 4.4). For Rotterdam it was shown that the distribution of migration rates is explained by seven factors, all equally weighted, being the local water depth, U_{maxM2}, ε_{M2}, ε_{M4}, $\phi_{\text{M4-M2}}$, D_{50}, influence surface waves and sand wave height. It is suggested that sand wave migration over Rotterdam is affected by variations in the interaction between the M2 and M4 tidal constituent. The importance of the relative phase shift compare well with the conclusions from Besio et al. (2004). They show that an upstream migration is possible when $\phi_{m4\text{-}m2}$ is in the range of 30^{o} to 180^{o} degrees. Although no upstream migration is reported for Rotterdam, the migration rates of profiles 1 to 3 are close to zero and can therefore very well be explained by this process since the phase shifts for all Rotterdam profiles are in the specified range. However, the Rotterdam profiles closer to the coast show considerable downstream. Therefore it is too drastic to conclude that the

migration behaviour for Rotterdam is only explained by the phase shift. The morphological parameters (water depth, D_{50}, sand wave heigth) may be relatively important in explaining the migration rate distribution. It should be noted that the PCR indicates that the variation of surface waves may have a considerable influence on sand wave migration at Rotterdam. However, it is questionable whether this result is physically realistic, since the events of surface wave action, sufficient to reach the bed, are rare.

The PCR is less robust for the IJmuiden area, which is indicated by the relatively high standard deviations resulting from the cross validation test (Table 4.10). Five parameters (local water depth, $U_{max\ M2}$, D_{50}, influence of surface waves and sand wave height) were considered to be explanatory for the distribution of sand wave migration at this area. In contrast to Rotterdam, the distribution of the M4 tidal constituent (both strength as well as ellipticity) and the relative phase shift are not sufficient to affect the migration rates. So, the morphological parameters control the sand wave migration for this area. The surface waves may have an additional influence, since its coefficient is comparable to the other important parameters and, physically, they may reach the bed about once in twenty days, which is line with the morphological timescale.

Comparing Rotterdam and IJmuiden, it is indicated that the largest difference in important parameters between the sites is the relative phase shift. So, relative to the other parameters, this parameter varies considerably within the Rotterdam site, in contrast to Rotterdam.

5.4.3 Remarks on results for PCR and sand wave length

In section 4.4.2 it was shown that the sand wave length depends on the M2 ellipticity. Model results from Van Santen et al. (2011) however indicates that the M2 ellipticity only influences sand wave length when the ellipticity is larger than 0.1. For IJmuiden the ellipticity is close to zero, while for Rotterdam the ellipticity is about 0.1. Considering the model results it is therefore not realistic that the sand wave length is affected by the ellipticity at the study areas, although Van Santen et al. (2011) were not able to test their results with field observations. In addition, earlier in this study it was suggested that there may be a correlation between tidal current strength and sand wave length. This correlation is however not represented in the PCR model, instead it is considered of being of lowest importance. This result however may not reflect the physical reality, since this study assumes a linear relation between the environmental parameters and the depended variables. However, Van Santen et al. (2011) show that the relation between the tidal current strength has a rather exponential shape instead of a linear shape, which is also reflected in Figure 4.3. Therefore it is suggested that a considerable improvement of the analysis can be provided by incorporating nonlinear functions into the regression model.

Chapter 6. Conclusions on data analysis

The data analysis part of this study aims to quantify empirical sand wave characteristics for the IJmuiden and Rotterdam shipping approach routes from datasets provided by RWS. Datasets from the Royal Netherlands Navy are added to the IJmuiden sets, because of the limited temporal extent of the RWS sets. All datasets are interpolated to a regular grid using an inverse distance weighting technique and the sand wave characteristics are subtracted using the method of Van Dijk et al. (2008). Three objectives were considered in this part.

Objective 1
What are the differences in sand wave length, sand wave height and sand wave migration for the IJmuiden and Rotterdam areas?

Clear differences between the Rotterdam and IJmuiden sites could be distinguished. At IJmuiden sand waves are about 420 m (σ = 84 m) long and show an average height of 2.5 m (σ = 0.6 m). A clear difference in migration rate is shown between the crests and troughs. The crests migrate about 2.6 m/yr (σ = 0.3 m/year), while the troughs show low mobility. This indicates that the sand waves at IJmuiden are unstable and become progressively more asymmetric. In general the characteristics for the IJmuiden sand waves do not show large spatial variations.
The Rotterdam sand waves are about 250 m (σ = 36 m) long and 3.4 m (σ = 0.7 m) high, which is almost consistent over the area. The migration rates for Rotterdam show a large distribution, from 0 m/yr at the RNJ up to 2.0 m/yr closest to the coast. No difference between crest and trough migration is found, indicating a stable sand wave field.

Objective 2
Which environmental parameters control the obtained sand wave characteristics for the regions of interest?

To identify environmental parameters explaining sand wave behaviour differences between the sites a principal component regression is performed between the environmental parameters and sand wave length and migration. The choice of the environmental parameter is based on modelling studies of Besio et al. (2004) Knaapen (2005), Van Dijk & Kleinhans (2005) and Van Santen et al (2011).

In general it is concluded that the PCR is performed on too few locations, which enhances the instability and the lack of generality of the obtained model. However using a cross validation on the original data invokes the opportunity in selecting the variables for which the regression coefficients could be calculated accurately. From this it can be concluded that the variation in sand wave migration rates, within Rotterdam is controlled by the local water depth, U_{maxM2}, ε_{M2}, ε_{M4}, $\phi_{M4\text{-}M2}$, D_{50}, influence surface waves and sand wave height. For IJmuiden the distribution of sand wave migration rates is controlled by the local water depth, $U_{max\ M2}$, D_{50}, influence of surface waves and sand wave height. Considering the combination of the areas, indicates that variations in the local water depth, U_{maxM2}, D_{50} and sand wave height are most important.

Although the variation in migration rates could reasonable well be explained using the PCR, the analysis failed for the sand wave length. It is suggested that this is because of a lack of measurement locations, but also because non-linear terms are used in the model that assumes variables to be linear. Therefore it is suggested that increasing the measurement locations and incorporating nonlinear functions will increase the models predictability.

Objective 3
What is the effect of dredging on sand wave behaviour?

Because of a lack of available information about dredging event no clear answer can be provided to this question. Nevertheless, it is indicated that after dredging of a single sand wave crest no or very low sedimentation takes places, which indicates that the sand wave will not be regenerated. Of other more intensively dredged areas, the sand wave field was completely destroyed. Therefore it was not possible to identify sand waves here, hence it was not possible to study the effect of dredging on sand wave behaviour.

Part II

Model analysis

Chapter 7. Methods

This chapter describes the methods for the model analysis, with which the sand wave fields obtained in part I will be simulated (see objectives 4 and 5 in chapter 1). First the model equations (based on the Lesser et al.,2004 and Borsje et al., 2011) and most important assumptions are presented, after that, the experiments performed with the model are discussed.

7.1 Model equations

This section describes the used model configurations. In the first two section the used expressions and the appropriate boundary conditions for the hydrodynamics and the bed evolution are presented. After that the numerical solution procedure will be discussed.

7.1.1 Hydrodynamics

The used model consist of the solutions of the momentum equations, a continuity equation, a turbulence closure model, sediment transport equations and a sediment continuity equations. To simplify the model and to reduce calculation time, a 2DV approach is used. This implies that the equations are solved for only one horizontal dimension (*x*-direction) and for the vertical dimension (*z*-direction). Therefore, zero flow and uniformity are assumed in the *y*-direction. Furthermore, sigma layering is used to solve the equations in the vertical, where the σ coordinate is defined as

$$\sigma = \frac{z - \zeta}{H + \zeta}. \tag{7.1}$$

Here, z is the vertical coordinate in the x,z coordinate system and H and ζ are the water depth below the reference plane and the free surface, respectively. (Figure 7.1).

The set of hydrostatic equations in respectively the horizontal and vertical is described by

$$\frac{\partial u}{\partial t} + u\frac{\partial u}{\partial x} + \frac{\omega}{H+\zeta}\frac{\partial u}{\partial \sigma} = -\frac{1}{\rho_w}\frac{\partial P}{\partial x} + F_u + \frac{1}{(H+\zeta)^2}\frac{\partial}{\partial \sigma}\left(\nu_v \frac{\partial u}{\partial \sigma}\right), \tag{7.2}$$

$$\frac{\partial \omega}{\partial \sigma} = -\frac{\partial \zeta}{\partial t} - \frac{\partial[(H+\zeta)u]}{\partial x}, \tag{7.3}$$

$$\frac{\partial P}{\partial \sigma} = -g\rho(H + \zeta). \qquad 7.4$$

Here, u is the horizontal velocity, ω the vertical velocity relative to the moving vertical σ-plane, which is computed from the continuity equation (7.3), ρ_w the water density, P pressure, F_u a horizontal stress term and υ_v the vertical eddy viscosity. The terms on the left hand side in 7.2 describe the total time derivative of the horizontal current, which is controlled by the terms on the right hand side, which are from left to right the hydrostatic pressure, the horizontal friction and the vertical friction. The equation shows that the vertical eddy viscosity is not assumed to be constant in the vertical, which is convenient since the eddy viscosity increases towards the viscous boundary layer and decreases again from the boundary layer to the bed (Rodi, 1984). Furthermore the vertical momentum equation is described by the hydrostatic balance (7.4), thus a shallow water system is considered.

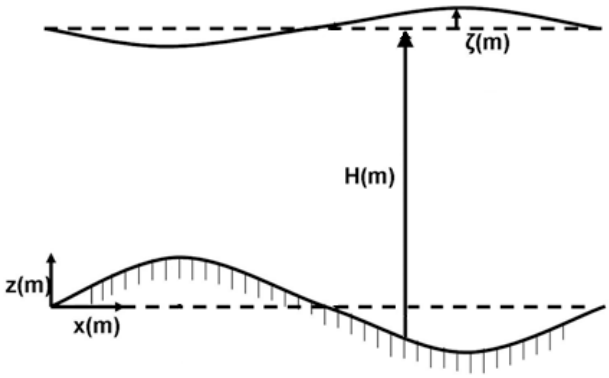

Figure 7.1 Situation sketch.

Borsje et al. (2011) show that the best resemblance of the modelled sand wave lengths with field data is obtained when a space and time dependent vertical eddy viscosity model is used, which is described by the k-ε turbulence enclosure model (Rodi, 1984)

$$\nu_v = c_\mu \frac{k^2}{\varepsilon}. \qquad 7.5$$

In this equation, k is the turbulent energy and ε the dissipation, which are described by production terms representing shear stresses at the bottom, bed and in the flow and are calculated in each grid cell by transport equations (Lesser et al.,2004). Furthermore, c_μ is a constant of 0.09 (Rodi, 1984).

To solve these equations a number of boundary conditions are used. At the free surface, no wind conditions and zero vertical velocity is assumed

$$\frac{\rho_w \upsilon_v}{H+\zeta}\frac{\partial u}{\partial \sigma} = 0\,, \quad \omega = 0; \quad \sigma = 0. \tag{7.6}$$

At the bed the boundary conditions read

$$\tau_b = \rho_w u_* |u_*|\,, \quad \omega = 0\,; \quad \sigma = -1. \tag{7.7}$$

The friction at the bed, τ_b, is related to the shear velocity, u_*, and the water density. The shear velocity is a function of the velocity just above the bed, while a logarithmic velocity profile is assumed,

$$u_* = \frac{\kappa}{\ln\left(1+\frac{\Delta z_b}{2z_0}\right)}\, u_b. \tag{7.8}$$

In this equation, u_b is the horizontal velocity just above the bed, Δz_b the distance to the bed, z_0 the roughness height and κ the Von Kármán constant (~0.41). Furthermore, the vertical velocity is set to zero at the bed. Tidal current information is incorporated into the model using the Riemann boundary conditions at lateral boundaries, which represents a tidal wave entering the domain at the open lateral boundaries (Verboom&Slob, 1984). The advantage of this boundary condition is that the outgoing waves will not be reflected back to the computational domain at the open boundary. Using this approximation allows for the use of multiple tidal constituents. The model uses information about the maximum current strength of the tidal constituent and its relative phase. Relative phase shifts between e.g. the M2 and M4 constituents are incorporated by applying a phase difference between the constituents at each boundary.

7.1.2 Bed evolution

The bed evolution is modelled by the sediment continuity equation. This equation states that the time evolution of the bed depends on the spatial variation of the suspended sediment transport and the bed load transport rates. Furthermore it is assumed that there is no gain or loss of sediment within the modelled area, so the sediment can only be redistributed over the domain. The sediment continuity equation reads

$$\left(1-\varepsilon_p\right)\frac{\partial z_b}{\partial t}+\frac{\partial(S_b+S_s)}{\partial x}=0. \tag{7.9}$$

Here, z_b is the position of the seabed, ε_p the bed porosity, S_b the bed load transport and S_s the suspended load transport. This equation is solved be incorporating expressions for the bed load transport and the suspended sediment transport. For a more physical description of these transport mechanisms the reader is referred to section 1.2.3.

First, the bed load transport is modelled by using Van Rijn (2004), which is a Delft3D default setting (Deltares, 2012)

$$|S_b| = 0.006\alpha_s\rho_s D_{50} w_s M^{0.5} M_e^{0.7}. \tag{7.10}$$

Here, ρ_s is the sediment specific density and D_{50} is the median sediment grain size. Variables M and M_e are the sediment mobility number and the excess mobility number and describe the ability of the sediment to be transported by the current, respectively. They are described by

$$M = \frac{v_r}{(s-1)gD_{50}}, \tag{7.11}$$

$$M_e = \frac{(v_r - v_{cr})^2}{(s-1)gD_{50}}. \tag{7.12}$$

In this equation, s is the relative density ($s = \rho_s/\rho_w$), v_r is a depth average velocity computed from the velocity in the grid cell closest to the bed, assuming a logarithmic velocity profile, v_{cr} is the critical depth averaged velocity for the initiation of bed motion. Since a wavy sea bed will be considered, grains may glide, role or saltate downhill by means of gravity, furthermore gravity will hinder uphill bedload transport. This effect is incorporated into (7.10) by means of α_s

$$\alpha_s = \lambda_s\left[\frac{\tan\varphi}{\cos(\tan^{-1}\beta)\ (\tan\varphi-\beta)}-1\right]. \tag{7.13}$$

Here, λ_s is a user defined slope parameter (= 2.5, which is a Delft3D default setting), β the slope of the sea bed and φ the angle of repose, which is defined as the critical angle at which grains can be piled up on each other.

The suspended sediment concentration is calculated by

$$S_s = \int_a^{H+\zeta} \left(uc - \varepsilon_{s,z} \frac{\partial c}{\partial x} \right) dz. \qquad 7.14$$

To appreciate this formulation, first note that it is assumed that suspended sediment only occurs above a reference height, *a*, located just above the bed. So, sediment is allowed to be transported in suspension between this height and the surface, while between the bed and the reference height, sediments can only be transported as bed load. The reference height depends on the bed roughness and is here determined by $a = 0.01H$ (Van Rijn, 2007; Borsje et al., 2011), where *H* is described in (7.1). According to Fresdøe&Deigaard (1992) there is a phase lag for suspended load between erosion and deposition of sediments. So, it is possible that more sediment is eroded from the bed then deposited, which increased the total suspended sediment concentration in the water column, or vice versa. Therefore, (7.14) depends on the suspended sediment concentration, *c*, which is calculated by solving the advection-diffusion equation, using a 2DV approach, which reads in the σ-coordinate system

$$\frac{\partial [hc]}{\partial t} + \frac{\partial [huc]}{\partial x} + \frac{\partial \left((\omega - w_s)c \right)}{\partial \sigma} = h \left[\frac{\partial}{\partial x} \left(\varepsilon_{s,x} \frac{\partial c}{\partial x} \right) \right] + \frac{1}{h} \frac{\partial}{\partial \sigma} \left[\varepsilon_{s,z} \frac{\partial c}{\partial \sigma} \right]. \qquad 7.15$$

Here, *h* is the flow depth, *c* the mass concentration of the sediment fraction, w_s the settling velocity of suspended sediment, $\varepsilon_{s,x}$ and $\varepsilon_{s,z}$ the horizontal and vertical eddy diffusivity in the *x*- and *z*-direction, respectively. The last two terms are taken equally to the horizontal and vertical eddy viscosity. Since the suspended sediment concentration is calculated from a reference height, the suspended sediment concentration above this height is not determined by the available sediment at the bed, but from a reference suspended sediment concentration, c_a, at height *a* (Van Rijn, 2007; Borsje et al., 2011)

$$c_a = 0.015 \rho_s \frac{D_{50} T_a^{1.5}}{a D_*^{0.3}}. \qquad 7.16$$

Here, D_* is the dimensionless grain size, which was defined in section 3.4.3 and T_a the dimensionless shear stress, which is defined by (Van Rijn, 2007; Borsje et al., 2011)

$$T_a = \frac{\mu_c \tau_c - \tau_{cr}}{\tau_{cr}}. \qquad 7.17$$

Here, μ_c is the grain related efficiency factor, which is defined as the ratio between the grain-related friction coefficient and the current-related friction coefficient (Van Rijn, 2007), τ_c the current related effective bed shear stress and τ_{cr} the critical bed shear stress.

Finally, note that the vertical diffusive fluxes are set to zero at the free surface and that no suspended sediment transport is imposed at the open later boundaries, so no background suspended sediment transport is imposed initially.

7.1.3 Solution

To solve the physical relation, a 2DV staggered grid is used (Lesser, 2004; Borsje, 2011). In the vertical 20 layers are used , where the spacing between the layers decrease towards the sea bed, allowing more accurate calculations near the sea bed, which is required for the k-ε turbulence enclosure model. In the horizontal, a domain length of 50 km is chosen, with a wavy bed pattern, with a total length of 5 km, imposed at the centre. Doing so, instability problems at the lateral boundaries, because of interactions between the flow and the bed pattern, are avoided. In order to reduce computation time and because only the bed evolution in the centre of the domain is of interest, the horizontal spacing of the horizontal grid cells is allowed to decrease from 1500 m at the lateral boundaries to 10 m in the centre. The depth points are located at the grid nodes, while the velocity components are perpendicular to the grid cell faces, where the positive flood direction is directed from left to right in the 2DV plane (Figure 7.2). Furthermore, the shear velocity (7.8) is solved in the centre of the first grid cell above the bed.

Since the typical times scale for changes in the flow is shorter than the morphological timescale, the bed evolution is accelerated. This is accomplished by using a morphological upscaling factor, MORFAC, which is applied after each time step. When 100 minutes computation time is chosen, with MORFAC = 100, the resulting bed pattern after 100 minutes is considered to be the bed pattern after 10,000 minutes modelling with MORFAC = 1. This study will initially investigate 10 years of bed evolution. With a MORFAC of 60, this results in 61 computing days, which corresponds to about 117 tidal cycles with a tidal period of 12h26m. For all experiments a 30 second time step is applied.

7.2 Experiments setup

The bed pattern at the centre of the domain is imposed by a sinusoidal wave pattern incorporated into an envelope, which ensures a smooth transition to the sand wave field. Rapid transitions enhance the possibility of flow instabilities (Figure 7.2). The morphology of the initial sand wave field is based on the morphological parameters for Rotterdam and IJmuiden sand wave fields at the approach routes. For each area one profile is chosen for which the sand wave and environmental conditions are considered to be typical for the concerned area. Therefore, the IJmuiden profile 3 and Rotterdam profile 4 are used (Table 7.1). Note that the sand wave height for the IJmuiden profile is higher than the average sand wave height for the IJmuiden area. However, compared to the other profiles, the values of the other parameters are closest to the typical IJmuiden values.

The relative influence of the above parameters will be tested with the model by varying one variable and fixing the others. Note that the model does not contain the effects of surface waves and that a unidirectional tide is considered. Therefore, the effects of surface waves and the effects of the tidal ellipse on the sand wave evolution, could not be investigated by the model.

To investigate the effects of dredging, the crest of the centre sand wave will be cut. After that it is investigated whether the model is able to regenerate the dredged sand wave to the size of the surrounding sand waves.

Profile	Depth [m]	Length [m]	Height [m]	$U_{max,M2}$ [m/s]	$U_{max,M4}$ [m/s]	*Z0* [m/s]	ϕ_{M2} [°]	ϕ_{M4} [°]	ϕ_{M4-M2} [°]	*D50* [μm]
3	26	430	3.4	0.65	0.046	0.019	298	223	346	288
R4	32.6	220	3.5	0.73	0.057	0.041	317	36	122	372

Table 7.1 Initial parameters for the IJmuiden and Rotterdam simulations. For the settings for IJmuiden profile 3 and for Rotterdam profile R4 are used. Depth denote water depth; Length, sand wave length; Height, sand wave height; $U_{max,M2}$, the maximum M2 tidal current strength; $\grave{U}_{max,M4}$, the maximum M4 tidal current strength; *Z0*, the residual background current; ϕ_{M2}, the phase of the M2 tidal constituent; ϕ_{M4}, the phase of the M4 tidal constituent; ϕ_{M4-M2}, the relative phase shift between the M2 and M4 tidal constituents; *D50*, the median grain size.

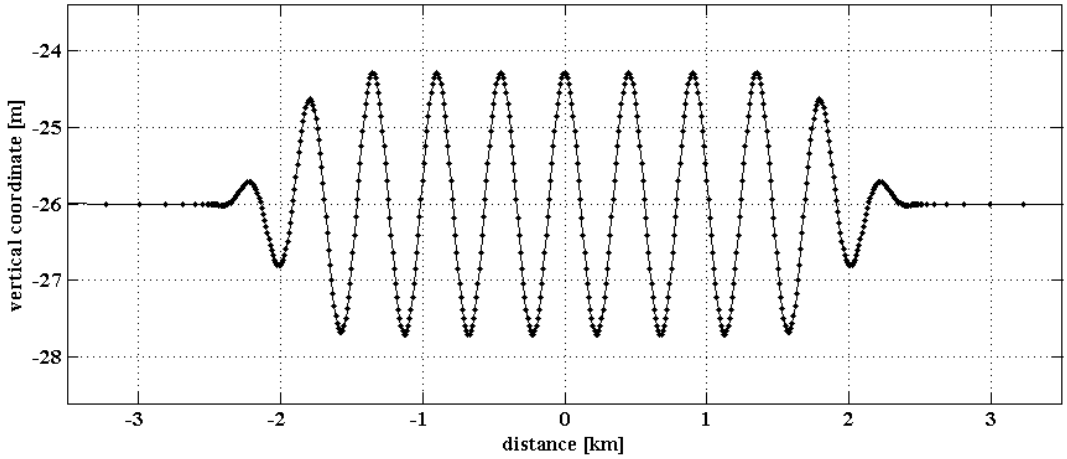

Figure 7.2 Example of initial bed level for the IJmuiden situation. So, depth is 26 m, sand wave height is 3.4 m and sand wave length is 430 m.

Chapter 8. Results

This chapter presents the results from the model and experiment setup presented in the chapter 7. The studied sites will be treated separately. For each site, the model sensitivity to the environmental parameter will be presented first, followed by a comparison between the model and results and the empirical results from parts I. The results of the dredging analysis are treated in the last section. The interpretation of the results will be presented in chapter 9.

8.1 IJmuiden area

8.1.1 Model sensitivity

Figure 8.1 presents the results for the tests considering the relative influences of the different tidal constituents for the IJmuiden profile 3. For the initial conditions of , the figure shows clear migrating sand waves, with migration rates of 9 m/year for the crests and 4 m/year for the troughs. Migration rates decrease when individual constituents are turned off. When no M4 tide is considered, the sand wave crests migrate with 5 m/year and the troughs with 2 m/year. In addition, when no residual background current is considered, the crests migrate with 6 m/year and the troughs with 3 m/year. For these tests the total height of the sand waves increased from 3.4 m to about 3.5 m, but also the water depth increased, since both the crests and troughs get deeper. So, in general, the sand waves get higher and deeper. Considering the difference in crest and trough migrations, the initially symmetric sand waves become asymmetric after ten years of modelling. For the initial conditions the stoss side is 280 m long, while the lee site is 170 m long. For the tests without a M4 constituent or without a Z0 background current, the stoss side becomes 260 m, while the lee side becomes 190 m, which is less asymmetric than for the initial conditions. Note that for none of the simulations the total sand wave length changes. No bed evolution is obtained when the flow is excited without the M2 tidal constituent. When the magnitude of this constituent decreased with only 0.1 m/year, the migration rates for both crests and the troughs decreases to 4 m/year and 3 m/year respectively, hence the sand waves become less asymmetric. In addition, the sand waves show larger growth.

The tests for the influence of the relative phase shifts between the M2 and M4 tidal constituents, reveal that this parameter affects sand wave migration rates considerably (Figure 8.2). Relative phase shifts between $\phi_{M4\text{-}M2} = 0^o$ and $\phi_{M4\text{-}M2} = 90^o$ contribute to

migrating sand waves in the direction of the background residual current, whereas relative phase shifts between ϕ_{M4-M2} = 90° and ϕ_{M4-M2} = 180° induce sand wave migration in upstream direction. The relative phase shift also influences the asymmetry. Symmetric sand waves are obtained for the simulation with ϕ_{M4-M2} = 120°.

When D_{50} is increased with 100 μm (Figure 8.3), sand waves grow with 60 cm over ten years. These sand waves migrate slightly slower with respect to the initial conditions, with a crest migration rate of 8 m/year and 3 m/year for the troughs. Furthermore, the asymmetry is comparable to the asymmetry obtained from the initial conditions. Increasing the water depth results in a crest migration of 6 m/year and a trough migration of 4 m/year, hence both the migration as well as the obtained asymmetry are less pronounced for increasing water depth. Furthermore, the sand wave height hardly changes in time. When the sand wave height is increased to 6 m (hence an amplitude of 3 m), the crest migrate slightly faster with a rate of 10 m/year, while the troughs migrate with a rate of 3 m/year. So the ratio between crest and trough migration increased from about 1:2 for the initial conditions to about 1:3, when the sand waves height is increased. Furthermore the asymmetry increases considerably, with a stoss side length of 300 m and a lee side length of 150 m.

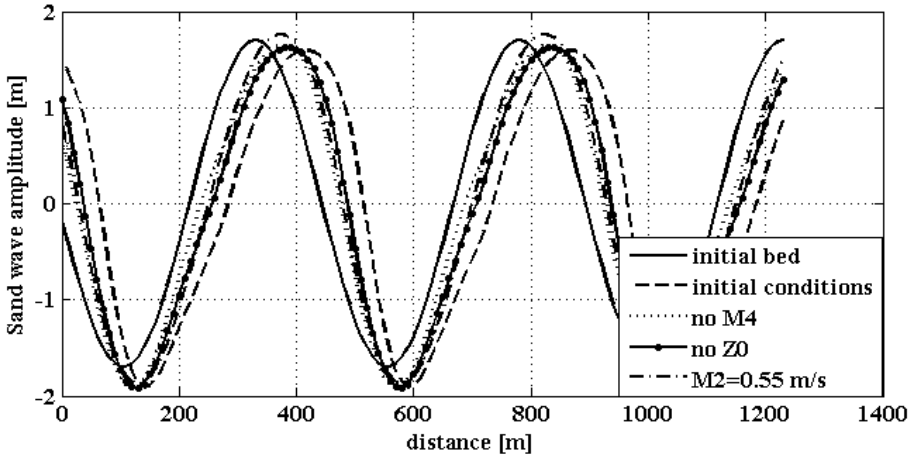

Figure 8.1 Model results after 10 morphological years for the IJmuiden conditions, when the initial conditions of Table 7.1 are used, without the M4 constituent, without the Z0 current and when the strength of the M2 tidal current is decreased with 0.10 m/s.

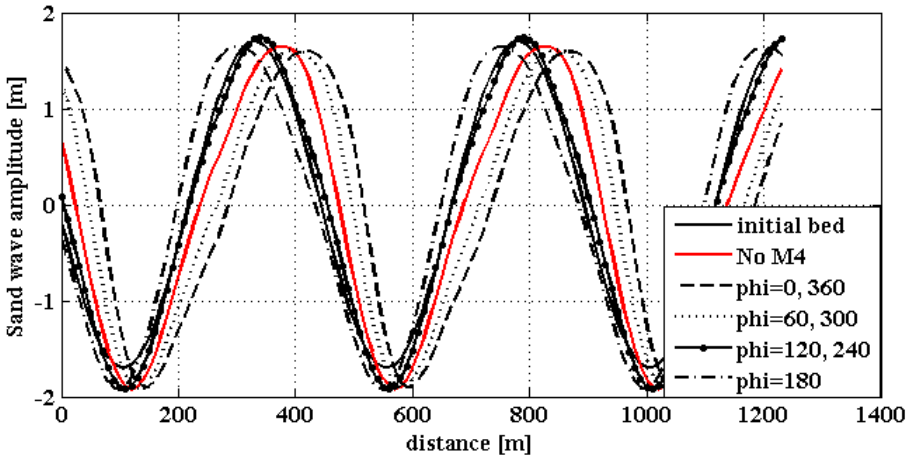

Figure 8.2 Model results after 10 morphological years for IJmuiden conditions, when the relative phase shift between the M4 and M2 tidal constituents is changed. To appreciate the relative influence of the Z0 current, also the simulation without the M4 constituent is shown.

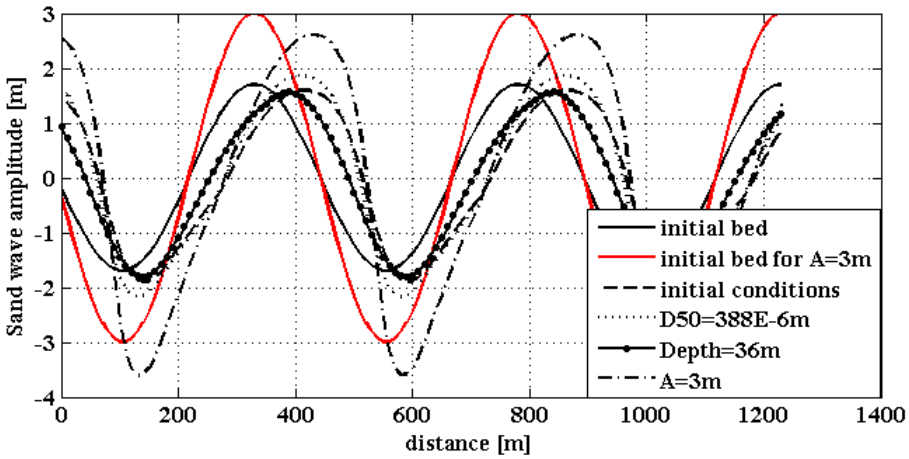

Figure 8.3 Model results after 10 morphological years for the IJmuiden conditions, when the sediment grain size, the water depth and the sand wave height is changed. Note that also the initial bed for the a sand wave height of 6 m is shown, as well as the model results for the initial conditions.

8.1.2 Model comparison with field results

The above model results for the initial conditions are in good qualitative agreement with field observations. In part I it was shown that sand waves at the IJmuiden area are asymmetric and that there is a distinguishable difference in migration rate between sand wave crests and troughs. Nevertheless, the modelled results are about a factor 4 too high, since field observations show crest migration rates of about 2 m/year to 3 m/year and trough migration rates of about 0 m/year. Buijsman & Ridderinkhof (2007) argue that the residual background current may be seasonal dependent. Since this study uses a two month average tidal current record (from May 2011 to July 2011), it is possible that the Z0 current is estimated too high, which may result in an overestimation of the sand wave migration rates. However, Figure 8.1 shows that turning off the residual background current completely, does not result in realistic migration rates. Decreasing $U_{max,M4}$ with a factor 4, which is the factor with which the migration rates are overestimated, results in migration rates of 3 m/year and 1 m/year for the crests and troughs, respectively, which is more realistic. However, no seasonal dependency of $U_{max,M4}$ is reported yet. Therefore, the mechanism that influences the overestimation of the sand wave migration in the model remains unclear.

Comparing results of the numerical model, while varying its parameters, with the results of the PCR analysis from part I, results in the following. In part I, variations in the local water depth, maximum tidal current of the M2 constituent, median grain size and sand wave height, were considered to be important to explain the behaviour of sand wave migration for the IJmuiden area. The data analysis and the model analysis showed comparable results for the influence of the local water depth and the median sediment grain size on sand wave migration rates. The data analysis indicated that increasing these two parameters should decrease migration rates, a result that is also found with the model (Figure 8.3). Note however, that the influence of the median grain size on the sand wave migration rate is considerably smaller in the model than was suggested from the data analysis. Contradictory results are obtained for increasing the tidal current strength and increasing the sand wave height, which should result in decreasing sand wave migration, according to the data analysis.

8.2 Rotterdam area

8.2.1 Model sensitivity

When the initial conditions of for the Rotterdam area are considered, the sand wave migration rates for both the crests and the troughs are 4 m/year (Figure 8.4). Migration rates increase when the M4 tidal constituent is turned off. Then, the crests and troughs migrate with 7 m/year. This implies that the residual background current affects migration in the flood direction and the M4 constituent affects migration in the ebb direction. This is confirmed by the simulation when the Z0 constituent is turned off. In that case, the sand waves migrate in ebb direction, with rates of -1 m/year for crests and troughs. Similar to the IJmuiden results, no bed evolution is simulated when the M2 tidal constituent is turned off (not shown in the figure), but decreasing sand wave migration is simulated when the M2 constituent is decreased with 0.1 m/s.

The direction of the sand wave migration is determined by the relative phase shift between the M2 and M4 tidal constituent (Figure 8.5), which is comparable to the model results obtained for the IJmuiden area. The figure shows that the same patterns are simulated for Rotterdam; migration in the positive direction for phase shifts between 0^o and 90^o and upstream migration for phase shifts between 90^o and 180^o.

Changing the local water depth and the sand wave height all show a small influence on sand wave migration. Increasing the water depth with 10 m, causes the migration rates of the crests to increase to 6 m/year and those of the troughs to 5 m/year, hence the sand waves get slightly more asymmetric (Figure 8.6). This is also observed when the sand wave height is increased, then the crests migrate with 4 m/year and the troughs with

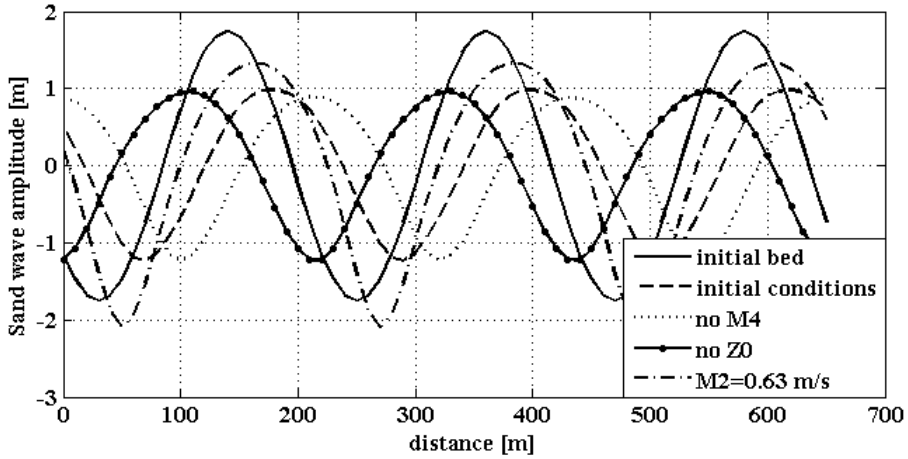

Figure 8.4 Model results after 10 morphological years for the Rotterdam conditions, when the initial conditions of Table 7.1 are used, without the M4 constituent, without the Z0 current and when the strength of the M2 tidal current is decreased with 0.10 m/s.

3 m/year. No change in sand wave migration is obtained when the median grain size is increased, however the grain size has a considerable influence on sand wave growth. For all other simulations considerable sand wave damping is obtained. Damping is also modelled for increasing median grainsize, but this is less pronounced.

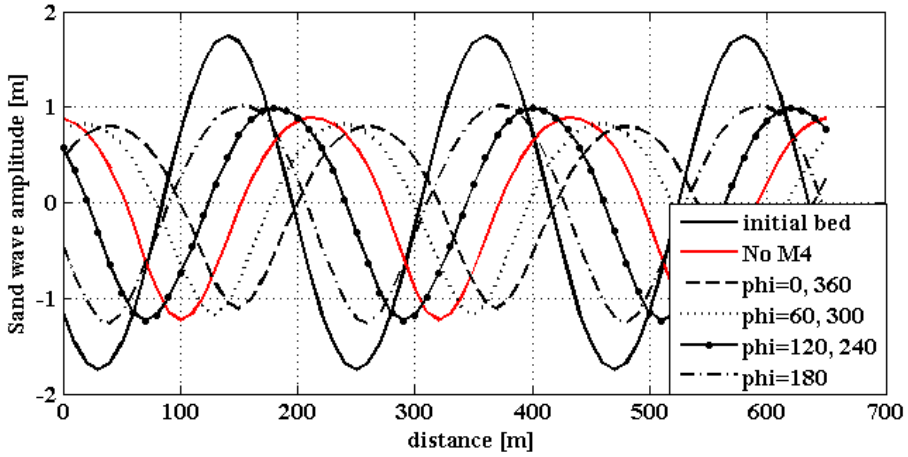

Figure 8.5 Model results after 10 morphological years for the Rotterdam conditions, when the relative phase shift between the M4 and M2 tidal constituents is changed. To appreciate the relative influence of the Z0 current, also the simulation without the M4 constituent is shown.

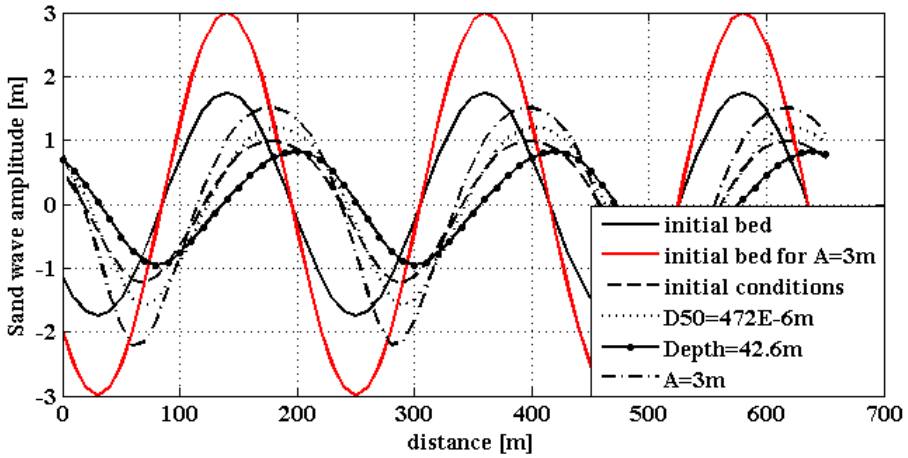

Figure 8.6 Model results after 10 morphological years for the Rotterdam conditions, when the sediment grain size, the water depth and the sand wave height are changed. Note that also the initial bed for the a sand wave height of 6 m is shown, as well as the model results for the initial conditions.

8.2.2 Model comparison with field data

Similar to the IJmuiden results, the sand wave migration obtained from the model are in reasonable qualitative agreement with the observations from part I, for example crests and troughs migrate with the same rate, which enhances symmetric sand waves. However, quantitatively the modelled migration rates are, again, overestimated with about a factor 4. In contrast to the IJmuiden simulations, the Z0 component counteracts the upstream migration effects caused by the relative phase shift, resulting in a net downstream migration. So, considering the possibility of a seasonal dependent Z0 component (Buijsman & Ridderinkhof, 2007), realistic migrating sand waves might be obtained by tuning the Z0 parameter. Figure 8.7 shows the results when the strength of Z0 is decreased with a factor 4. This factor is based on the size of the overestimation of the sand wave migration rates. This results in a crest and trough migration of -1 m/year, which is more realistic, compared to part I.

Although, the modelled sand wave migration is in qualitative agreement with the sand wave migration observed in the field, the field observations did not show damping of sand waves. Borsje et al. (2011) indicate that the model will return negative growth rates for short sand waves (wavelength < 200 m). In addition, the modelled sand waves for the IJmuiden conditions did not show damping. Therefore, it is suggested that the sand wave length of the Rotterdam sand waves influences the obtained damping. This is tested by increasing the initial sand wave length for Rotterdam with a factor 2, while the other parameters are unchanged. It is expected that this results in growing or stationary sand waves. In addition, it is tested whether damping sand waves can be obtained for the IJmuiden conditions, when the sand wave length of the initial sand wave field is decreased with a factor 2. The results are shown in Figures 8.8 and 8.9. For the Rotterdam situation the sand waves start to grow, while damping sand waves are simulated for the IJmuiden situation. Remarkably, also the difference between crest and trough migration changed, compared to the initial bed. For Rotterdam the longer sand waves migrate with 4 m/year and 2 m/year for crests and troughs, respectively, whereas for IJmuiden, the shorter sand waves migrate with 7 m/year and 6 m/year, respectively.

From the data analysis in part I, it was suggested that sand wave migration for Rotterdam is controlled by the local water depth, $U_{max,M2}$, ε_{M2}, ε_{M4}, $\phi_{\text{M4-M2}}$, D_{50}, influence of surface waves and sand wave height. Again, since the model does not provide information about all these environmental parameters, only the local water depth, $U_{max,M2}$, $\phi_{\text{M4-M2}}$, D_{50}, and sand wave height are considered here. It is shown that the median grain size and the sand wave height does not affect the modelled migration rates so much. Increasing the local water depth results in increasing migration rates in the model, while the opposite relation

was obtained from part I. This result is also obtained for varying $Umax_{,M2}$ (Figure 8.4). The relation between the relative phase shift and the migration rates, obtained from the model, show strong resemblance with part I. Table 4.6 showed that the relative phase shift for Rotterdam decreased shoreward from about 120° offshore to 100° close to the shore. Furthermore it was shown that migration rates for the Rotterdam sand waves increases towards the shore. This is in good agreement with the model, since it is shown that the upstream migrating effects get less pronounced when the phase shift is decreased from 120° to 100°, hence downstream migration rates will increase.

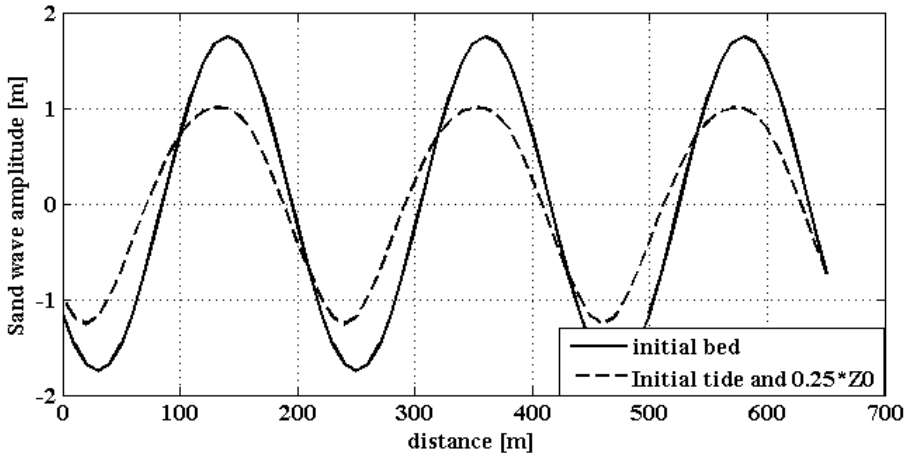

Figure 8.7 Model results after 10 morphological years for the Rotterdam conditions, when the Z0 current is decreased with a factor 4. The other parameter values are set to their initial settings.

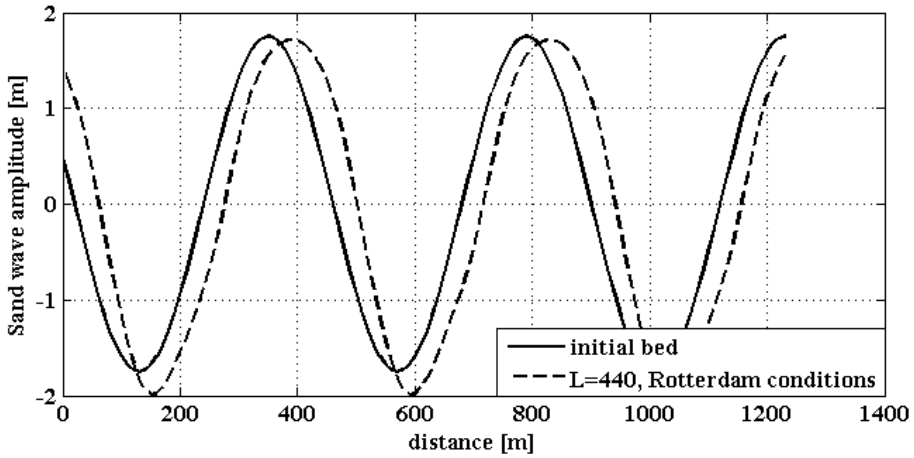

Figure 8.8 Model results after 10 morphological years for the Rotterdam conditions, when the sand wave length is doubled compared to the initial setting. The other parameter values are set to their initial settings.

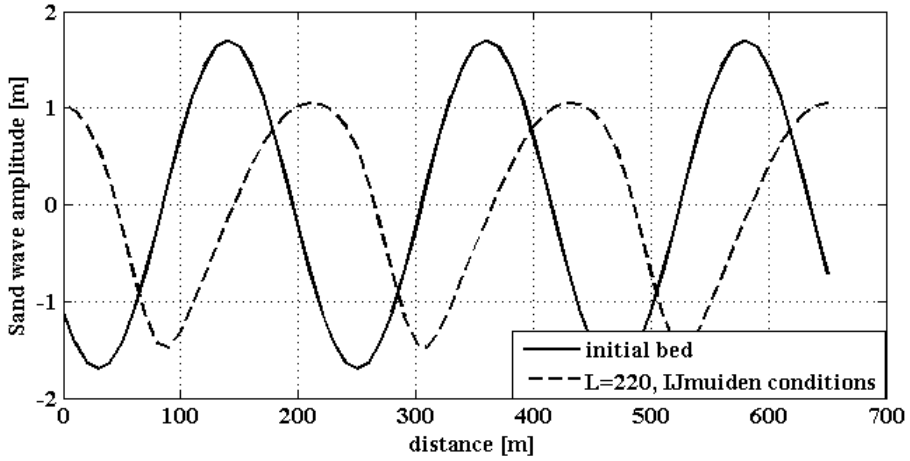

Figure 8.9 Model results after 10 morphological years for the IJmuiden conditions, when the sand wave length is decreased with a factor 2. The other parameters are set to their initial settings.

8.3 Dredging

The results for the bed evolution of a dredged sand wave is shown in Figure 8.10. Here, one crest is removed from the domain. Clearly, after ten years of modelling, the sand wave is not recovered. A small wave like pattern is visible over the cut sand wave. Considering the results of Katoh et al. (1998) and Knaapen et al (2002), it was expected that the sand wave would recover in about ten years. Since this result is not modelled, it is suggested that, considering the flat cut, no or too weak recirculating cells are excited initially. Without these currents, sand waves are not able to grow. In order to test the model's ability to simulate sand wave growth after dredging, the new profile obtained in Figure 8.10 is used for a second, consecutive, model run. In order to increase the possibility of growing sand waves, the amplitude of the none dredged sand waves is lowered to about 1 m. The results are shown in Figure 8.11. Note that sand wave growth is simulated and the dredged sand wave clearly takes the shape of a new sand wave. However, the sand wave is not regenerated to the size of the other sand waves. Similar results are obtained when more sand wave crests (e.g. three crests) are removed and when the sediment volume of one or more dredged crests is deposited in the sand wave troughs.

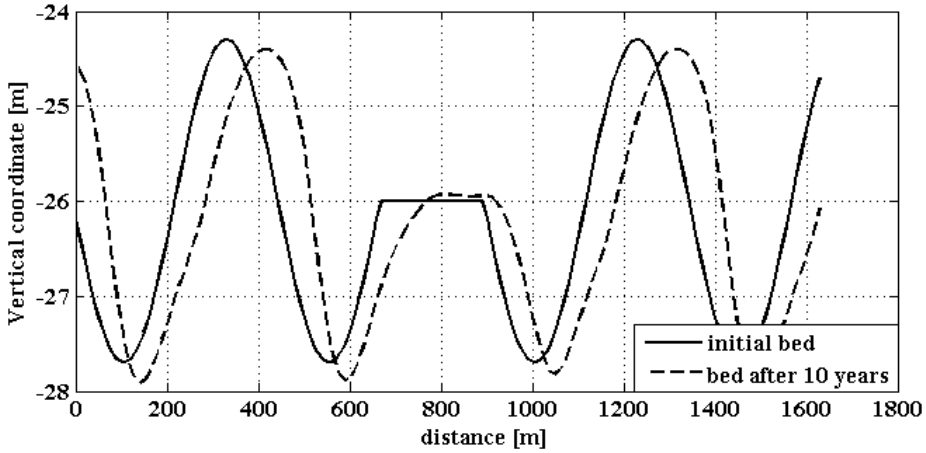

Figure 8.10 Model results of dredged sand wave after 10 morphological years for the IJmuiden initial conditions.

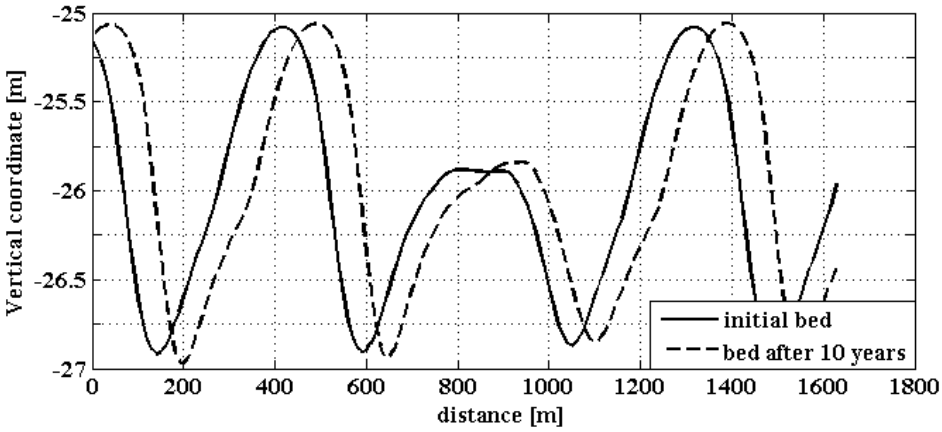

Figure 8.11 Model results of dredged sand wave after 10 morphological years for the IJmuiden initial conditions. The initial bed is obtained from the results of Figure 8.10, but the amplitude of the sand wave is decreased to about 1 m.

Chapter 9. Interpretation/ Discussion

The presented numerical model is able to simulate migrating sand waves. As was shown by e.g. Németh et al. (2002) and Besio et al. (2004), sand waves migrate because of asymmetries in the recirculation cell, which are induced by the relative phase shift between the M2 and M4 tidal constituents and the Z0 residual current. The relative phase shift induces a steady sand wave migration in the upstream or downstream direction. The strength of the residual background current, may enhance a downstream migration, or may counteract an upstream migration. So, even when an upstream migration is indicated from the relative phase shift, still a net downstream migration may be observed or modelled, for a sufficiently strong residual background current. It is suggested that the back and forth migration which may be observed for individual sand waves (see e.g. part I of this study or Van Dijk et al., 2011) is a consequence of (seasonal) variations in the residual background current. In addition to these two controlling parameters, it is indicated that the model is sensitive to changes in current strength of the M2 and M4 tidal constituents. Therefore, in order to model realistic sand wave characteristics, it is important that the flow structure is comparable to the real flow structure. In this study it was assumed that taking a two month flow record from MATROOS was sufficient to obtain realistic measures for the tidal constituents. Although the study of Buijsman & Ridderinkhof (2007) do not mention seasonal variability for the M2 and M4 constituents, it is worthwhile to test this statement by analysing a yearly flow record from MATROOS.

In general, it can now be concluded that the flow structure of the model is determined by the initial flow conditions. However, the results of varying the sand wave length, water depth or sand wave height, indicate that also these parameters may influence sand wave migration rates. Since recirculating current cells are needed to induce sand wave growth and migration, it is suggested that these environmental parameters have a, secondary, but possibly important effect on the flow structure and as a consequence on the sand wave evolution.

In order to improve the understanding of the complex interaction between the environmental parameter and sand wave behaviour, consider the difference in sand wave migration between crests and troughs, observed for the IJmuiden conditions in combination with the modelled sediment transport.

Figure 9.1 presents the sand wave evolution after 10 years of modelling for the initial conditions of IJmuiden, together with the time and depth averaged suspended load

transport and the time averaged bed load transport. The figure shows that at the crest and the lee side of the sand wave, sediment transported as suspended load, which causes smoothing of the crests and a decreasing lee length. Bed load is the dominant transport mechanism at the trough and stoss side of the sand wave, causing deepening of the troughs and growth of the stoss side. Figure 9.2 is the same as Figure 9.1 but for the Rotterdam initial conditions. The total sediment transport is lower than at IJmuiden and bed load is dominant over the entire sand wave. Recall that the crests and troughs migrate with the same rates at Rotterdam. Therefore, it is suggested that differences between crests and trough migration occur when suspended sediment transport is dominant over the crest and lee side of the sand wave, while bed load transport is dominant over the stoss site. Furthermore, it is indicated that different migration rates (both in magnitude as well as in differences between crest and trough migration) are obtained when other parameters, but the flow parameters, are changed. These parameters influence the flow structure and thereby the mechanism of sediment transport. For instance, it was shown that changing the sand wave length influences the difference between crest and trough migration. While for long sand waves a clear difference between bed load and suspended load transport is shown, this difference diminishes for short sand waves. This indicates that for long sand waves the near bed velocity at the lee side is higher than at the stoss side, enhancing the suspended load transport at the lee side.

The sediment transport mechanism is also important in damping or growth of the sand waves. Recall that sand waves are damped for the Rotterdam conditions. Since bed load transport is the most dominant transport mechanism, it is indicated that damping is caused by the bed load transport. However, Borsje et al. (2011), investigated the relative influence of bed load transport, suspended load transport and the slope effect. From this it is shown that bed load transport has a positive effect on the growth rate, while suspended load and the slope effect have a negative effect. Furthermore, it is shown that these effects are more pronounced for shorter sand waves. So, since sand waves at Rotterdam are relatively short, it is suggested that, despite the dominant bed load transport, the modelled damping results from the slope effect. This is confirmed by Figure 8.8 since these longer sand waves are not damped, while the same flow conditions hold.

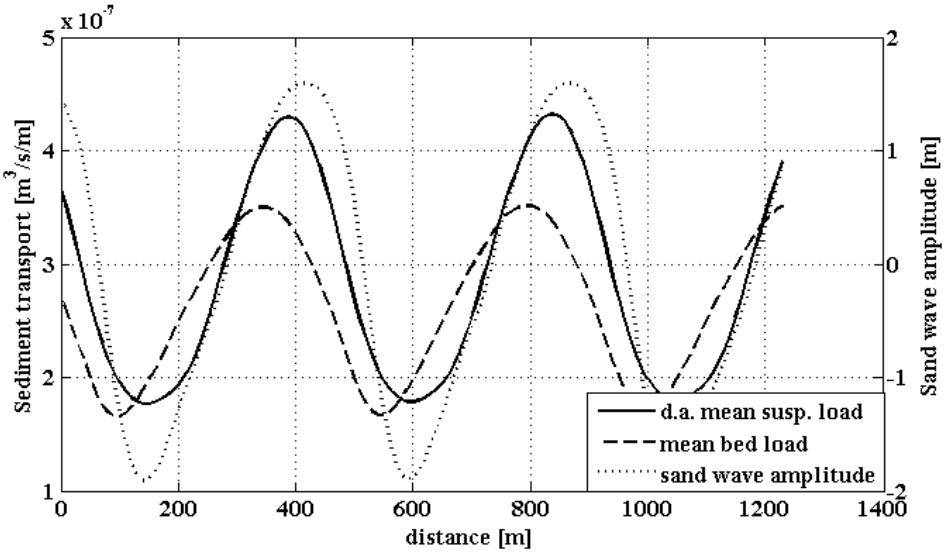

Figure 9.1 Mean depth averaged suspended load and mean bed load transport (left axis) for the IJmuiden conditions, plotted with the bed evolution, after 10 morphological years (right axis).

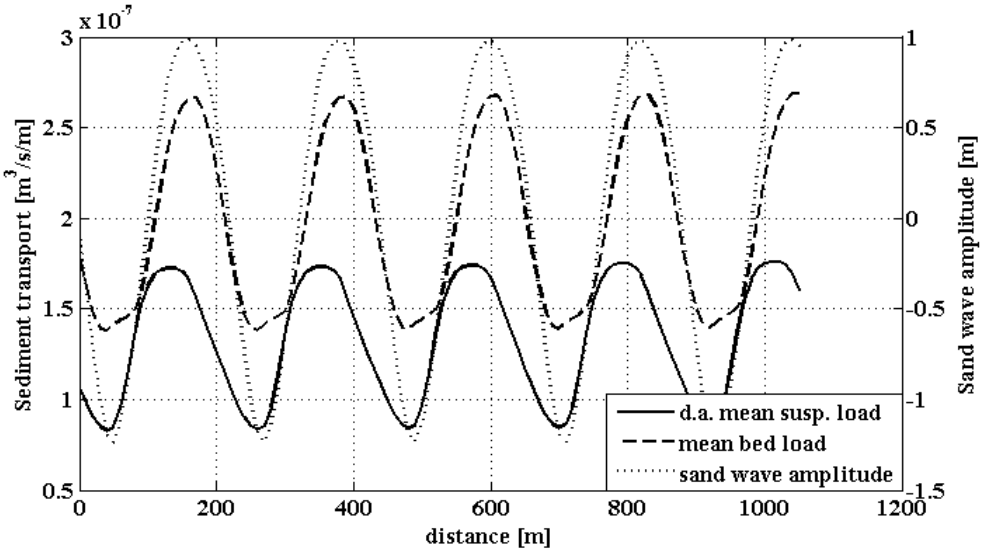

Figure 9.2 Mean depth averaged suspended load and mean bed load transport (left axis) for the Rotterdam conditions, plotted with the bed evolution, after 10 morphological years (right axis).

Chapter 10. Conclusions on model analysis

Objective 4

A validation of the obtained control parameters with help of a process-based numerical model is performed.

The model is able to simulate the horizontal bed evolution for both sites qualitatively to great extent. From this it is confirmed that the relative phase shift between the M2 and M4 tidal constituents is important in explaining the variation in migration rates between the Rotterdam and IJmuiden site. Furthermore it is shown that the background residual current Z0, may be an important tuning parameter in the model. Since this parameter may be seasonal depended, one has to be careful in making estimates for this parameter. Of the other parameters only the importance of the local water depth and median grain size is confirmed qualitatively by the model. The quantitative results however, remain a subject for further research.

Objective 5

Quantify the effects of dredging on the behaviour of sand waves with the help of a process-based numerical model.

From the model it is concluded that the dredged sand wave may recover in about 20 years to their original shape (simulated by two consecutive runs of 10 morphological years). However, since growth rates are small, the dredged sand wave did recover to the size of the surrounding sand waves. These results could not be confirmed by field observation, but considering other studies, it is suggested that the model did not perform well in regenerating sand waves after dredging.

Chapter 11. Synthesis on empirical and model results

The aim of this chapter is to relate the empirical and model conclusions and to present a perspective for further research. First, a short summary of the most important similarities between the results obtained from part I and part II will be presented, followed by the most important differences. After that, recommendations for further research will be presented.

One of the most important similarities between the model and empirical analysis is the difference in sand wave migration behaviour between the IJmuiden and Rotterdam study locations. In both analyses it was found that for IJmuiden the sand waves crests migrate faster than the sand wave troughs, while for Rotterdam the crests and troughs migrate with the same rates. Furthermore, it was found in both analyses that the sand waves at Rotterdam travel slower than the sand wave at IJmuiden. An examination was conducted to explain these differences, by means of environmental parameters. In part I, this was done by means of a PCR analysis, while in part II the sand wave migration sensitivity to the model parameters was tested by changing one parameter at a time, while the others were fixed to their initial values. From this, the influence of the relative phase shift between the M4 and M2 tidal constituents is indicated as one of the most important parameters to explain the differences in migration rates between the two study areas. Furthermore, within the IJmuiden area, variations in the sediment grain size and the water depth may effect sand wave migration behaviour, since similar effects for these parameters were obtained for both the data and model analysis. The same holds for changing the sediment grain size within the Rotterdam area. A final important result of this study is that a difference in sediment transport mechanism (i.e. bed load or suspended load transport) over a sand wave, is responsible for the differences in crests and troughs migration rates. Note that this result was obtained from the model analysis and could not be verified by the empirical analysis.

Although the qualitative sand wave migration was in good agreement between the empirical and model results, differences in quantitative migration was obtained. For both areas the modelled migration rates for the sand wave crests and troughs are overestimated by a factor four. Furthermore, the model showed damping sand wave heights for the Rotterdam conditions, while this was not observed. Possible explanations for these differences follow from a number of assumptions made to simplify the model analysis. First, a 2DV approach is used. This implies that all natural, three dimensional, effects,

like the tidal current ellipse, can not be represented by the model. It is expected that these effects influence the structure of the circulating cell and as a consequence the size and direction of sediment transport. Second, suspended sediment transport is not imposed at the lateral model boundaries. Therefore, suspended sediment will not enter the sand wave field by means of a background suspended sediment transport, which would be closer to natural conditions. It is expected that incorporating this mechanism in the model might decrease the high migration rates. Finally, it is suggested that the damping sand waves obtained for the Rotterdam conditions, might result from the chosen slope parameter λ_s. Since bed load transport is the dominant sediment transport mechanism for this area, it is suggested that the slope effect causes this damping. Increasing λ_s, will result in an increase of the slope correction factor, α_s (see equations 7.10 and 7.13), which will result in a larger bed load transport, hence less pronounced damping.

One of the most important difference between the results of the PCR and model analysis is the influence of the residual background current. From the PCR this parameter was not considered to be important, while the model results clearly showed that this parameter enhances downstream sand wave migration and as a consequence influences migration rates. Since it was indicated in part II that this parameter is seasonal dependent, it is suggested that the two month tidal current record (from May to July 2011) is not sufficient to provide a reliable measure for the residual background current strength, and may therefore have biased the results from part I and part II. Other contradictory results between the PCR and model analyses are obtained for the tidal current strength of the M2 constituent and the sand wave height. In part I it was indicated that decreasing the M2 strength, increases the sand wave migration. While the model part shows that decreasing the M2 strength, decreases the sand wave migration. The latter result can be understood by considering the recirculating cells, which are important for the sand wave behaviour, as discussed earlier. This cell is driven by the M2 tidal constituent, so decreasing the strength of this constituent will decrease the strength of the cell, hence less sediment will be transported. Considering this reasoning, the results obtained from the data part is unexpected especially since in the empirical analysis all parameters are uncorrelated, so this results can not be biased by other parameters. Therefore, this result from the data analysis remains suspicious and needs further attention. In contrast, from the data analysis it was suggested that decreasing the sand wave height will increase sand wave migration, while this result was not obtained from the model study. Since the relation obtained from the data part confirms the hypothesis on the influence of sand wave height, which was presented in chapter 1, the model sensitivity to sand wave height needs to be investigated.

A final comparison between the data and model results comprises the effects of dredging on sand wave behaviour. This study encountered problems in analysing these effects. In

the data part it was shown that some parts of the study areas are intensively dredged, which resulted in the complete destruction of the sand wave field. At these locations sedimentation rates could be provided, but it could not be concluded that this will result in the regeneration of sand waves. However, by inspection of the bathymetric map, a sand wave was identified from which only the crest was removed, at an individual location at the IJmuiden area. Here, it was indicated that the sand wave will not recover, although this is not certain because of the small number of available data sets after the dredging event. Also the model tests did not show any regeneration of dredged sand waves. It is possible that the model performs correctly, but this can not be verified by the empirical analysis.

The presented data and model analysis can be improved in several ways. In general, the two analyses can be improved by more accurate measures for the Z0 parameter. Improvements can be introduced by i) analyzing a longer tidal record in order to estimate a more accurate average or, ii) a seasonal depended residual background current is implemented in the model. It is expected that the latter change will result in a seasonal depended sand wave migration.

Improvements of the empirical analysis alone are twofold. First, note that, usually, a PCR analysis is performed on data sets with a ratio between the number of observations and the number of environmental parameters of at least 5:1, but a ratio of 10:1 is even better, this study uses a ratio of 9:10. The best solution to overcome this problem is to increase the number of observations. Within the considered sites, this can be done by considering the observations of individual sand waves, instead of the averages of the observations along a transect. The density of the sand waves that can be analysed, depends on the resolution with which the environmental data can be determined. Alternatively, the number of studied environmental parameters can be decreased, although this may result in the loss of some physical processes. Second, it is suggested that a priori physical knowledge is incorporated into the PCR analysis. For instance one can induce a non linear relation between the maximum tidal current strength and the sand wave length or a priori knowledge about the relative importance of the parameters can be used.

To improve the model analysis, it is suggested that first a more detailed analysis is performed on the important mechanisms in modelling small sand wave migration (sand wave amplitude ~0.5 m). When the most important mechanisms are analysed, the sand wave height can be increased, in order to investigate this influence. Furthermore, improvements should be made to model sand waves with small wave lengths (<200 m). From these analyses it is hypothesised that a more detailed explanation can be formulated for the overestimation of the migration rates. Additionally it can be tested whether a

background residual transport influences sand wave migration. Finally, in order to obtain a more physically realistic model, the model should be extended to 3D.

To improve the results for the data analysis on the effects of dredging on sand wave behaviour, a more comprehensive knowledge about the exact moments and locations of dredging activity needs to be obtained. Then, individual sand waves needs to be identified which are dredged to a certain level once, and for which data sets are available that span a considerable time length (e.g. ten years) after the dredging event. Only then sedimentation rates and possible sand wave regeneration can be monitored properly. When the exact natural behaviour of the sand waves after dredging is known, the outcome of the model results presented in this study can be verified properly. Additionally, the model results presented here can be improved by imposing environmental conditions typical for the dredged location (e.g. conditions for IJmuiden profile 7), instead of conditions typical for the entire study area. Alternatively to this, one can investigate whether the model is able to reproduce the results obtained from the results of regenerating sand waves in the Bisanseto Sea (Japan) (Katoh et al., 1998; Knaapen&Hulscher, 2002). Using conditions typical for this area should result in a sand wave regeneration of about ten years.

Appendix

Location / **Parameter**	**IJmuiden** *n=9*	Cross validation *n=9* av. β	Cross validation *n=9* σ	Cross validation *n=27* av. β	Cross validation *n=27* σ
Constant	0.00	0.00	0.00	0.00	0.00
Depth	-0.09	-0.09	0.04	-0.17	0.02
$\boldsymbol{U_{max\ M2}}$	-0.15	-0.15	0.04	0.02	0.01
$\boldsymbol{\varepsilon_{M2}}$	0.30	0.25	0.13	0.18	0.05
$\boldsymbol{U_{max\ M4}}$	-0.06	-0.07	0.05	0.02	0.01
$\boldsymbol{\varepsilon_{M4}}$	0.05	0.05	0.01	0.10	0.01
$\boldsymbol{\Phi_{M4\text{-}M2}}$	0.05	0.05	0.07	0.09	0.03
$\boldsymbol{Z_0}$	0.02	0.05	0.12	0.01	0.03
$\boldsymbol{D_{50}}$	-0.09	-0.09	0.06	-0.12	0.01
$\boldsymbol{\theta_w > \theta_{cr}}$	0.09	0.10	0.03	0.17	0.01
Height	-0.20	-0.19	0.06	-0.24	0.01
$\boldsymbol{R^2}$	0.52	0.54		0.58	

Table A.1 Results for the PCR with the sand wave migration rates as ouptut variables for the IJmuiden area; *n* denote the number of observations, av. β denote the average of the regression coefficients, which are averaged over *n* cross validation runs and σ is the correspondin standard deviations, Finally R^2 is the goodness of fit.

Location / **Parameter**	**Rotterdam** *n=9*	Cross validation *n=9* av. β	Cross validation *n=9* σ	Cross validation *n=27* av. β	Cross validation *n=27* σ
Constant	0.00	0.00	0.00	0.00	0.000
Depth	-0.17	-0.17	0.02	-0.25	0.004
$\boldsymbol{U_{max\ M2}}$	-0.16	-0.17	0.01	-0.10	0.004
$\boldsymbol{\varepsilon_{M2}}$	-0.09	-0.07	0.04	0.01	0.005
$\boldsymbol{U_{max\ M4}}$	0.04	0.04	0.04	0.03	0.007
$\boldsymbol{\varepsilon_{M4}}$	0.13	0.14	0.02	0.24	0.004
$\boldsymbol{\Phi_{M4\text{-}M2}}$	-0.16	-0.14	0.02	-0.12	0.005
$\boldsymbol{Z_0}$	0.02	0.03	0.04	0.05	0.009
$\boldsymbol{D_{50}}$	-0.12	-0.13	0.02	-0.18	0.004
$\boldsymbol{\theta_w > \theta_{cr}}$	0.19	0.17	0.02	0.21	0.004
Height	-0.15	-0.13	0.06	-0.13	0.007
$\boldsymbol{R^2}$	0.94	0.94		0.92	

Table A.2 Results for the PCR with the sand wave migration rates as ouptut variables for the Rotterdam area; *n* denote the number of observations, av. β denote the average of the regression coefficients, which are averaged over *n* cross validation runs and σ is the correspondin standard deviations, Finally R^2 is the goodness of fit.

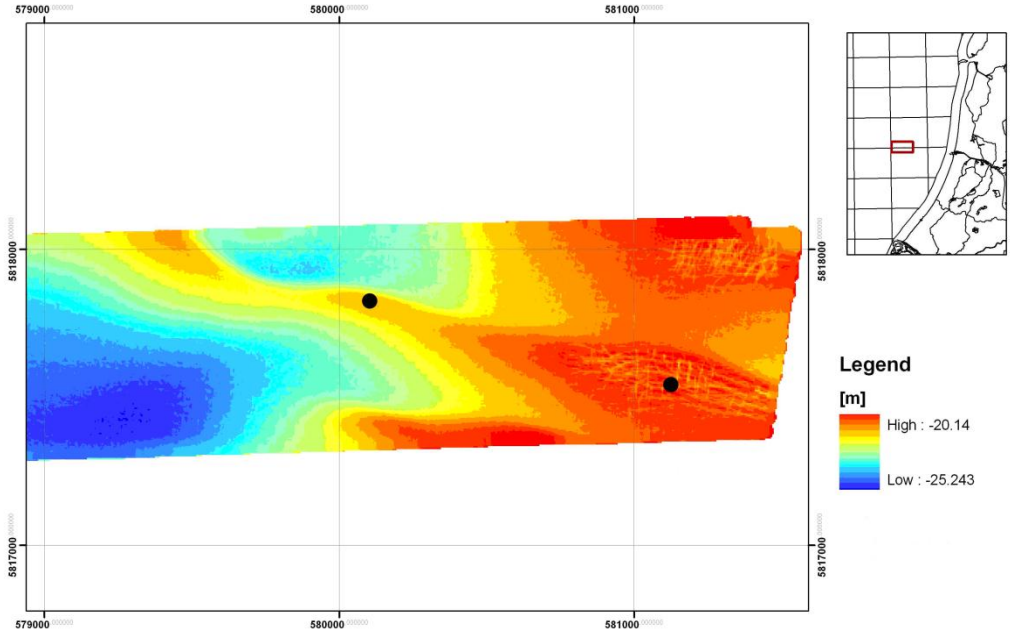

Figure A.1 Bathymetric map of study area for which a single crest is cut off. Left black dot denotes an area with no dredging acticvity, the right black dote is located at an area where clear dredging tracks are visible. The red rectangular in the insert shows the position of the study area in the Dutch coastal zone.

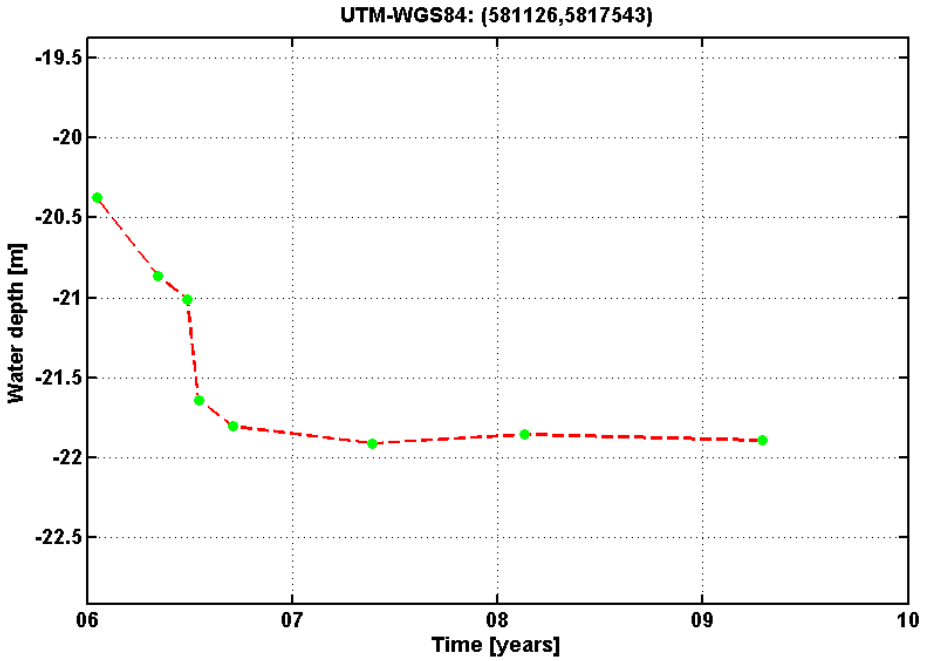

Figure A.2 Bed elevation in time at the right black dot in Figure A.1. The green points are measurement points. Between the years 2006 and 2007 a clear increase in water depth is visible. After that, the bed elevation hardly changes.

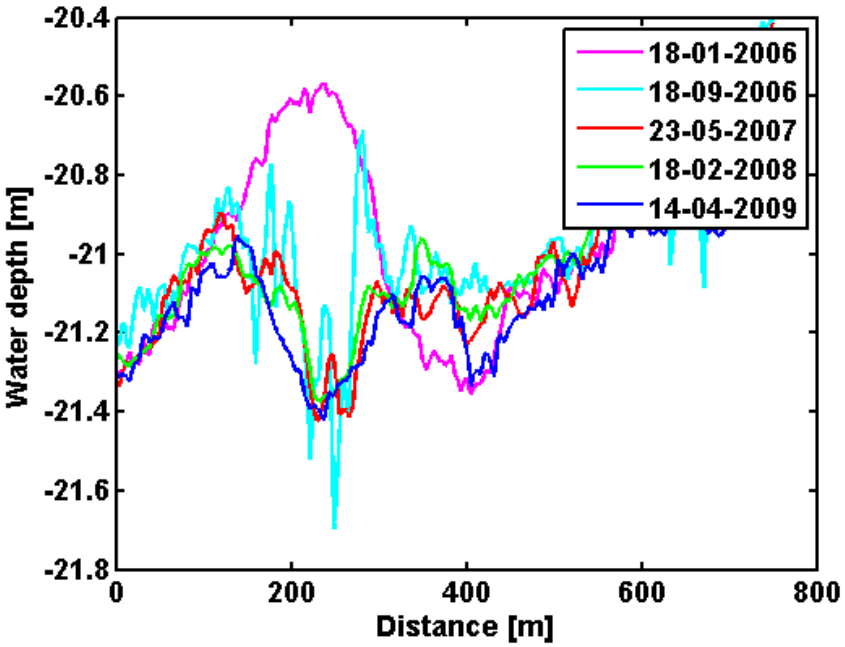

Figure A.3 Cross section through the dredged area presented in Figure A.1. The cross section runs from UTM-WGS84 (580810,5814700) to (581138,5818073). Only the first and the last data sets available for 2006 are presented. Note the spiky pattern between 100 m and 300 m for 18-09-2006, which is more smoothed for 23-05-2007. It is not known whether this is a result from forced or natural behaviour. This also holds for the sharp decrease in water depth between 18-01-2006 and 18-09-2006, between 300 m and 500 m.

References

Aliotta, S. & Perillo, G. M. E., 1987. A sand wave field in the entrance to Bahia Blanca estuary, Argentina. *Marine Geology,* 76, pp. 1-14.

Bagnold, R., 1966. *An approach to the sediment transport problem from general physics.* :US Goverment Print.

Barnard, P., Hanes, D., Rubin, D. & Kvitek, R., 2006. Giant sand wave at the mouth of San Francisco Bay. *Eos Trans. AGU,* 29, pp. 285-289.

Besio, G., Blondeaux , P. & Vittori, G., 2006. On the formation of sand waves and sand banks. *Journal of fluid mechanics ,* 557, pp. 1-27.

Besio, G., Blondeaux, P., Brocchini, M. & Vittori, G., 2004. On the modeling of sand wave migration. *Journal of geophysical research,* 109

Besio, G., Blondeaux, P. & Frisina, P., 2003. A note on tidally generated sand waves. *Journal of Fluid Mechanics,* 485, pp. 171-190.

Blondeaux, P., 1990. Sand ripples under sea waves: 1. Ripple formation. *Journal of Fluid Mechanics,* 218, pp. 1-17.

Blondeaux, P., De Swart, H. E. & Vittori, G., 2009. Long bed waves in tidal seas: an idealized model. *Journal of Fluid Mechanics,* 636, pp. 485-495.

Blondeaux, P. & Vittori, G., 1991. Vorticity dynamics in an oscillatory flow over a rippled bed. *Journal of Fluid Dynamics,* 226, pp. 257-289.

Blondeaux, P. & Vittori, G., 2011. A parameterization of the wavelength of tidal dunes. *Earth Surface Processes and Landforms,* DOI: 10.1002/esp.2137.

Boggs Jr., S., 1974. Sand wave fields in Taiwan Strait. *Geology* 2, pp. 251-253

References

Bokuniewicz, H. J., Gordon, R. B. & Kastens, K. A., 1977. Form and migration of sand waves in a large estuary, Long Island Sound. *Marine Geology* 24, pp. 185-199.

Borsje, B. W. et al., 2009. Modeling bio-geomorphological influences for offshore sandwaves. *Continental Shelf Research,* 29, pp. 1289-1301.

Borsje, B. W., Roos, P. C., Kranenburg, W. M. & Hulscher, S. J., 2011. Modelling sandwave formation in a numerical shallow water model . In: X. Shao, Z. Wang & C. Wang, eds. *RCEM 2011, Seventh LAHR Symposium on River Coastal and Estuarine Morphodynamics.* Beijing, China: s.n.

Buijsman, M. C. & Ridderinkhof, H., 2007. Long-term ferry-ADCP observations of tidal currents in the Marsdiep inlet. *Journal of Sea Research,* 57, pp. 237-256.

Buijsman, M. C. & Ridderinkhof, H., 2008a. Long term evolution of sand waves in the Marsdiep inlet. I: High-resolution observations. *Continental Shelf Research,* 28, pp. 1190-1201.

Calvete, D., Falques, A., De Swart, H. & Walgreen, M., 2001. Modelling the formation of shoreface-connected sand ridges on storm-dominated inner shelves. *Journal of Fluid Mechanics,* 441, pp. 169-193.

Davis, J. C., 1986. *Statistics and data analysis in geology.* 2 ed. New York: John Wiley & Sons, Inc..

Deltares, 2012. *User manual Delft-3D FLOW.* Delft, The Netherlands: Deltares (www.Deltares.nl).

Dodd, N. et al., 2003. Understanding coastal morphodynamics using stability methods. *Journal of Coastal Research,* 19, pp. 849-865.

Dorst, L. L., 2009. *Estimated sea floor dynamics in the southern North Sea to improve bathymetric survey planning.* Enschede, Netherlands: Published Ph.D. thesis, University of Twente.

Dyer, K., 1986. *Coastal and Estuarine Sediment Dynamics.* 1 ed. Bidstone, UK: John Wiley & Sons.

References

Fredsoe, J. & Deigaard, R., 1992. *Mechanics of Coastal Sediment Transport*: World Scientific.

Gerkema, T., 2000. A linear stability analysis of tidally generated sand waves. *Journal of Fluid Mechanics* 417, pp. 303-322.

Haan, C. T., 1977. *Statistical Methods in Hydrology.* Ames: The Iowa State University Press.

Hulscher, S., 1996. Tidal-induced large-scale regular bed form patterns in a three-dimensional shallow water model. *Journal of Geophysical Research* , 101, pp. 20,727-20,744.

Hulscher, S. J. M. H., De Swart, H. E. & De Vriend, H. J., 1993. The generation of offshore tidal sand banks and sand waves. *Continental Shelf Research,* 13, pp. 1183-1204.

Huthnance, J. M., 1982. On one mechanism forming linear sand banks. *Estuarine, Coastal and Shelf Science,* 14, pp. 79-99.

Ikehara, K. & Kinoshita, Y., 1994. Distribution and origin of subaqeous dunes on the shelf of Japan. *Marine Geology,* 14, pp. 75-87.

Jolliffe, I. T., 2002. *Principal Component Analysis, Second Edition.* 2nd ed. Aberdeen, UK: Springer.

Katoh, K., Kume, H., Kuroki, K. & Hasegawa, J., 1998. The development of sand waves and the maintenance of navigation channels in the Bisanseto Sea. In: *Coastal Engineering '98.* Reston, VA: ACSE, pp. 3490-3502.

Knaapen, M. A. F., 2005. Sandwave migration predictor based on shape information. *Journal of Geophysical Research,* 110, F04S11, doi:10.1029/2004JF000195.

Knaapen, M. A. F., Hulscher, S. J. M. H., De Vriend, H. J. & Stolk, A., 2001. A new type of sea bed waves. *Geophyiscal research letters,* 7, pp. 1323-1326.

Knaapen, M. & Hulscher, S., 2002. Regeneration of sand waves after dredging. *Coastal Engineering* 46, pp. 277-289.

References

Komarova, N. L. & Hulscher, S. J. M. H., 2000. Linear instability mechanisms for sand wave formation. *Journal of Fluid Mechanics* 413, pp. 219-246.

Lesser, G., Roelvink, J., Van Kester, J. & Stelling, G., 2004. Development and validation of a three-dimensional morphological model. *Coastal Engineering,* 51, pp. 883-915.

Ludwick, J. C., 1972. Migration of tidal sand waves in Chesapeake Bay entrence. In: D. Swift, ed. *Shelf Sediment Transport.* Stroudsburg, Pennsylvania: Dowden, Hutchinson and Ross, pp. 377-410.

Maljers, D. & Gunnink, J., 2007. *interpolation of measured grain-soze fractions*: TNO.

McCave, I., 1971. Sand waves in the North Sea off the coast of Holland. *Marine Geology,* 10, pp. 199-225.

Németh, A. A., Hulscher, S. J. M. H. & de Vriend, H. J., 2002. Modelling sand wave migration in shallow shelf seas. *Continental Shelf Research,* 22, pp. 2795-2806.

Németh, A. A., Hulscher, S. J. & Van Damme, R. M., 2007. Modelling offshore sandwave evolution. *Continental Shelf Research,* 27, pp. 713-728.

Ozasa, H., 1974. Field investigation of large submarine sand waves. *Coastal Engineering in Japan,* 17, pp. 155-184.

Passchier, S. & Kleinhans, M. G., 2005. Observations of sand waves, megaripples, and hummocks in the Dutch coastal area and their relation to currents and combined flow conditions. *Journal of Geophysical Research,* 110, F04S15, doi:10.1029/2004JF000215.

Perillo, G. M. E. & Ludwick, J. C., 1984. Geomorphology of a sand wave in lower Chesapeake Bay Virgina. *Geo-Marine Letters* 4, pp. 105-112.

Prandle, D., 1982. The vertical structure of tidal currents and other oscillatory flows. *Continental shelf research,* 2, pp. 191-207.

Reeder, D. B., Ma, B. B. & Yang, Y. J., 2011. Very large subaqueous sand dunes on the upper continental slope in the South China Sea generated by episodic, shoaling deep-water internal solitary waves. *Marine Geology* 279, pp. 12-18.

References

Rijkswaterstaat&Deltares, 2009. *Beschrijving Modelschematisatie simona-kuststrook-fijn-1999-v4*: RWS-Waterdienst&Deltares.

Rodi, W., 1984. *Turbulence models and their application in hydrodynamics-A state of the art review*. Karlsruhe, Germany: Univ. of Karlsruhe.

Schielen, R., Doelman, A. & De Swart, H. E., 1993. On the nonlinear dynamics of free bars in straight channels. *Journal of Fluid Dynamics*, 252, pp. 325-356.

Soulsby, R., 1997. *Dynamics of marine sands: a manual for practical applications.* London: Telford.

Sterlini, F., Hulscher, S. J. M. H. & Hanes, D. M., 2009. Simulating and understanding sand wave variation: A case study of the Golden Gate sand waves. *Journal of Geophysical Research* 114, pp. F02007, doi:10.1029/2008JF000999.

Stride, A., 1982. Offshore tidal sand:processes and deposits. *CRC Press.*

Tonnon, P. K., Van Rijn, L. C. & Walstra, D. J. R., 2007. The morphodynamic modelling of tidal sand waves on the shoreface. *Coastal Engineering*, 54, pp. 279-296.

Trowbridge, J. H., 1995. A mechanism fot the formation and maintenance of shore-oblique sand ridges on strom-dominated shelves. *Journal of Geophysical Research*, 100, pp. 16071-16086.

Van der Giessen, A., De Ruijter, W. & Borst, J., 1990. Three-dimensional current structure in the Dutch coastal zone. *Netherlands Journal of Sea Research* , 1-2, pp. 45-55.

Van Dijk, T. A. G. P. & Kleinhans, M. G., 2005. Processes controlling the dynamics of compound sand waves in the North Sea, Netherlands. *Journal of geophisical research* , 110, F04S10, doi:10.1029/2004JF000173.

Van Dijk, T. A. G. P., Lindenbergh, R. C. & Egberts, P. J. P., 2008. Separating bathymetric data representing multiscale rhythmic bed forms: A geostatistical and spectral method compared. *Journal of Geophysical Research*, 113, F04017, doi:10.1029/2007JF000950.

References

Van Dijk, T. A. G. P. et al., 2011. The scientific validation of the hydrographic survey policy of the Netherlands Hydrographic Office, Royal Netherlands Navy. pp. 165, Deltares.

Van Rijn, L. C., 1993. *Principles of Sediment Transport in Rivers, Estuaries and Coastal Seas*. Amsterdam: Aqua.

Van Rijn, L. C., 2007. Unified view of sediment transport by currents and waves. II: Suspended transport. *Journal of Hydraulogic Engineering,* Volume 133, pp. 668-689.

Van Rijn, L. C., Walstra, D. J. R. & Van Ormondt, M., 2004. *Description of TRANSPOR 2004 (TR2004) and implementation in DELFT3DDonline.* Delft, Netherlands: Rep. Z3748, Delft Hydraul..

Van Santen, R. B., 2009. Tidal sand waves in the North Sea: data analysis and modelling, Unpublished MSc dissertation thesis. *University of Utrecht, Utrecht, Netherlands.*

Van Santen, R. B., De Swart, H. E. & Van Dijk, T. A. G. P., 2011. Sensitivity of tidal sand wavelength to environmental parameters:A combined data analysis and modelling approach. *Continental Shelf Research,* 31, p. 966–978.

van Veen, J., 1935. Sand waves in the North Sea. *Hydrographical Review* 12, pp. 21-29.

Varfaillie, E., Van Lancker, V. & Van Meirvenne, M., 2006. Multivariate geostatistics for the predictive modelling of the surficial sand distribution in the shelf seas. *Continental Shelf Research,* 19, pp. 2454-2468.

Verboom, G. & Slob, A., 1984. Weakly-reflective boundary conditions for two dimensional shallow water flow problems. *Advances in water resources,* 7, pp. 192-297.

Xu, J. P. et al., 2008. Sandwave migration in Monterey Submarine Canyon, Central California. 248, pp. 193-212.

Zimmerman, J., 1981. Dynamics, diffusion and geomorphological significance of tidal residual eddies. *Nature,* 291, pp. 549-555.